Radioecological modelling of naturally occuring radiation at the Morupule-B Coal Thermal Power Station.

J Mudiwa

orcid.org 0000-0002-7339-6849

Thesis accepted in fulfilment of the requirements for the degree

Doctor of Philosophy in Physics

at the North-West University

Promoter: Prof MV Tshivhase

Co-supervisor: Dr LN Njinga

Co-supervisor: Mr PP Magampa

Graduation ceremony: July 2020

Student number: 29808243

Declaration

This serves as my declaration that this thesis from research undertaken by John Mudiwa at the Centre for Applied Radiation Science and Technology, Mafikeng Campus, North West University (South Africa), supervised by Prof. V.M. Tshivhase.

This study was never submitted in whole or in part anywhere else for any sort of award. In parts of this submission where other sources of information have been used, such sources have been cited in this work and acknowledged under references.

……. ……

John Mudiwa, ID 29808243 Date

(Student)

…… ……

Prof. Victor M. Tshivhase Date

(Principal Supervisor)

Dedication

First and foremost, I devote this work to my Lord and personal savior, Jesus Christ. I also devote this research work to my father Mr. Ben Buyen Barnabas Mudiwa, who always pushed me to do my best and also my wife Neo Daphne Mudiwa for her wonderful support, encouragement and positive attitude towards my life.

Acknowledgement

Firstly, I thank God for his blessings and favour upon my life that have enabled me to complete this thesis work. I sincerely show my genuine appreciation to my supervisor Prof. Victor M. Tshivhase.

My heartfelt appreciation also goes to the technical staff and officials of Morupule-B Coal Thermal Power Station for all the assistance they offered me in availing samples and other useful information used for this work.

Table of contents

List of Figures and Tables

Abbreviations

ARPANSA	Australian Radiation Protection and Nuclear Safety Agency
ATSDR	Agency for Toxic Substances and Disease Registry).
CARST	Centre for Applied Radiation Science and Technology
DOH	Department of Health
EC	Electron capture
EIA	Environmental Impact Assessment
FWHM	Full Width at Half Maximum
GPS	Global Positioning System
HPGe	High Purity Germanium Detector
IAEA	International Atomic Energy Agency
ICRP	International Commission on Radiological Protection
ICP-MS	Inductively Coupled Plasma Mass Spectrometry
MCA	Multi channel analyzer
MDA	Minimum detectable activity
nd	Not detectable
NNR	National Nuclear Regulator
NORM	Naturally Occuring Radioactive Material
NRC	National Research Council
RESRAD	Codes that analyzes potential human and biota radiation exposures
UNEP	United Nations Environment Programme
UNSCEAR	United Nations Scientific Committee on the Effects of Atomic Radiation
USDOE	United States Department of Energy
USEIA	United States Energy Information Administration
USEPA	United States Environmental Protection Agency

Abstract

The study was performed around the Morupule-B Coal Power Station in the central district of Botswana. A total of 99 water, soil, coal, bottom ash as well as fly ash samples were collected from the study area. Coal, bottom ash, soil and fly ash activity concentrations for natural radionuclides were measured through gamma spectrometry while ICP-MS was used to measure the concentrations of heavy toxic metals in water, soil, coal, bottom ash and fly ash samples.

The mean activity concentrations of ^{232}Th, ^{238}U and ^{40}K in soil samples in this study were 19.101 ± 2.140 Bq/kg, 14.149 ± 1.762 Bq/kg and 196.115 ± 4.392 Bq/kg respectively. For coal, bottom ash and fly ash samples, the mean ^{238}U activity concentrations were found to be 54.771 ± 4.460 Bq/kg, 97.311 ± 6.151 Bq/kg and 150.444 ± 9.595 Bq/kg respectively. The mean activity concentrations of ^{232}Th in coal, bottom ash and fly ash were found to be 27.319 ± 0.714 Bq/kg, 81.702 ± 1.030 Bq/kg and 116.674 ± 1.457 Bq/kg respectively. The mean ^{40}K activity concentrations for coal, bottom ash and fly ash samples were found to be 17.117 ± 3.831 Bq/kg, 37.265 ± 3.849 Bq/kg and 66.847 ± 10.107 Bq/kg respectively. The average fly ash activity concentration values for ^{238}U and ^{40}K from this study were generally lower than those from average world activity concentrations, while those of ^{232}Th were greater than the average world values by a factor of close to two. The average coal activity concentration values for ^{238}U and ^{232}Th from this study were generally higher than those from average world activity concentrations, while those of ^{40}K were lower than the average world values. From the current study results, it was observed that the activity concentrations of ^{238}U and ^{232}Th increased in ascending order from soil, coal, bottom ash to fly ash samples.

Radiological hazards assessment for soil, coal, bottom ash and fly ash samples were performed in this study. The estimated absorbed dose rate (D) for soil samples was 25.549 ± 9.026 nGy/h, which was lower than the worldwide absorbed dose rate of 57 nGy/h for soil. The estimated annual effective dose equivalent (AEDE) from soil samples was 31.333 ± 11.070 µSv/y, which was lower than the recommended worldwide value of 70 µSv/y for soils. The radium equivalent activity (Ra_{eq}) for soil was 54.435 ± 19.464 Bq/kg. The external hazard index (H_{ext}) for soil was 0.147 ± 0.053. The estimated absorbed dose rate (D) in coal was 42.519 ± 5.288 nGy/h. The estimated annual effective dose equivalent (AEDE) for coal was 52.146 ± 6.480 µSv/y, which was lower than the worldwide value of 406 µSv/y. The radium equivalent activity (Ra_{eq}) in coal samples was 95.156 ± 11.482 Bq/kg. The external hazard

index (H_{ext}) for coal was 0.257 ± 0.031. The estimated absorbed dose rate (D) for bottom ash samples was 95.859 ± 20.357 nGy/h, which was slightly higher than the worldwide absorbed dose rate of 60 nGy/h. The estimated annual effective dose equivalent (AEDE) for bottom ash was 117.563 ± 24.967 µSv/y, which was lower the recommended worldwide value of 460 µSv/y. The radium equivalent activity (Ra_{eq}) for bottom ash was 217.015 ± 46.052 Bq/kg. The external hazard index (H_{ext}) for bottom ash 0.586 ± 0.124. The estimated absorbed dose rate (D) for fly ash was 142.763 ± 46.278 nGy/h. The estimated annual effective dose equivalent (AEDE) for fly ash was 175.086 ± 56.756 µSv/y. The radium equivalent activity (Ra_{eq}) value for fly ash samples was 322.435 ± 104.923 Bq/kg. The mean Ra_{eq} values for soil, bottom ash, coal and fly ash were all below the worldwide accepted value of 370 Bq/kg. The external hazard index (H_{ext}) for fly ash was 0.871 ± 0.283. The average H_{ext} value for soil, coal, bottom ash and fly ash were all below the worldwide recommended value of one. Based on these findings, materials from the area under study can safely be used for building and construction.

The total carcinogenic risk from soil and water samples was found to be 1.04 such that soil samples contributed the most to the total cancer risk. RESRAD-OFFSITE computer code estimated the cancer risk from natural radionuclides ^{238}U, ^{232}Th and ^{40}K over a duration of 130 years to residents and other public members in the vicinity of the power station such that the maximum cancer risk with all pathways summed was found to be 3×10^{-3} from year 25, also depicting that the total cancer risks from year 0 to year 130 were higher than the acceptable South African and USEPA risk limits of 5×10^{-6} and 1×10^{-6} to 1×10^{-4} respectively.

Chapter 1: Introduction

This chapter will introduce the radioecological modelling of naturally occurring radiation at the Morupule-B Coal Thermal Power Station as well as the determination of heavy elements using Inductively Coupled Plasma-Mass Spectrometry (ICP-MS). It covers a background to this study, problem statement and objectives.

1.1 General background

The research discusses the radioecological determination of the naturally occurring radioactive material and heavy metals in fly ash, bottom ash, coal, soil and water [Heidrich, Brown and Collier, 2011] in and around Morupule-B Coal Thermal Power Station in the Southern African country of Botswana. Coal thermal power stations produce electricity through the combustion of coal fossil fuel. The produced heat then creates steam from water, which then turns a turbine that is connected to an electric current generator. The generated current eventually reaches the main electrical power grid. Figure 1-1 shows a typical coal thermal power station [Moazzem, Rasul and Khan, 2015].

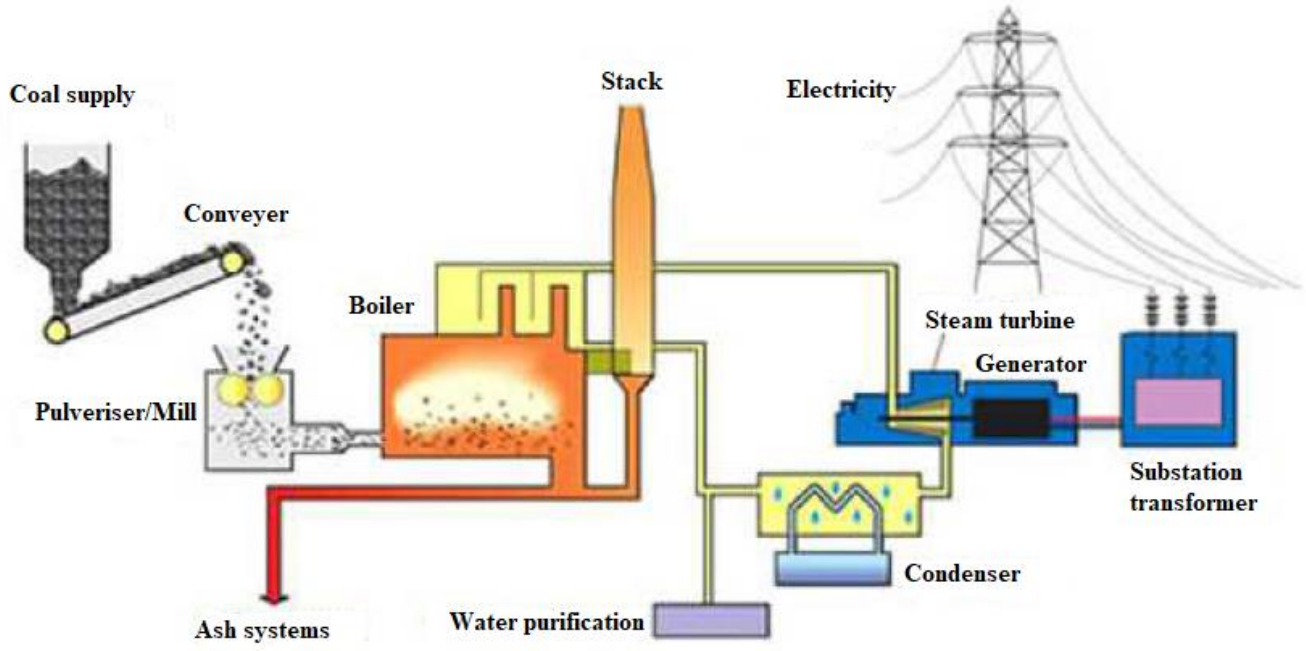

Fig. 1 - 1: Typical coal thermal power station [Moazzem, Rasul and Khan, 2015]

The combustion of coal occurs in the power station releasing gaseous products [Heidrich, Brown and Collier, 2011] through the smoke stack. The coal used contains some long-lived radionuclides [Chambers, 2013] that results in natural radioactivity including ^{232}Th, ^{238}U and ^{40}K and any of their decay products like ^{222}Rn or ^{226}Ra, normally referred to as NORM (naturally occurring radioactive material). Such radionuclides are found in all rocks or ground formations at different concentrations that also vary with different geological settings [Patra et al., 2013]. TENORM is usually used in reference to all naturally occurring radioactive materials in which anthropogenic activities have increased the possibility for radiation exposure. After combustion, some NORM will be concentrated in the resulting fly ash while some goes into the atmosphere through the stack gas pipe. The resulting fly ash should be securely stored to prevent contamination of bigger areas. The fly ash could also be utilized in the manufacture of cement and related products. The type of coal used (e.g. bituminous coal in this case) as well as the plant design greatly affects the activity that eventually discharges into the environment. Coal is categorized into four main groups being anthracite, bituminous, subbituminous and lignite with 86%-97% C, 45%-86% C, 35%-45% C and 25%-35% C respectively [USEIA, 2010].

1.1.1 Toxic heavy metals in the environment

There has been a continuous exposure of toxic heavy metals to humans for a very long time. Toxic heavy metals are found in all places due to anthropogenic and natural activities [Wang et al., 2017]. Most toxic heavy metals have a high atomic mass and number as well as a specific gravity larger than 5 g.cm^{-3}. This method of classification includes certain metalloids, actinides, lanthanides, transition metals, basic metals as well as metals from groups III to V in the Periodic Table. Some toxic heavy metals are arsenic (As), cadmium (Cd), chromium (Cr), cobalt (Co), copper (Cu), lead (Pb), manganese (Mn), mercury (Hg), nickel (Ni), selenium (Se) and zinc (Zn) [Tchounwou, 2012].

Organic pollutants gradually decompose to yield carbon dioxide and water, while toxic heavy metals tend to bio-accumulate since they cannot be broken down. Toxic heavy metals remain in the environment, being transferred from one medium to another. They are ingested daily by humans through air, food, soil or water [Atieh et al., 2017]. Human symptoms as well as the toxicity level depend on the type of metal, the absorbed dose and whether the exposure was acute, chronic or not. Certain toxic heavy metals have harmful effects to human body organs or tissues. Toxic heavy metals may be toxic to humans as well as animals even if present in very small quantities [Kamunda, 2017].

Fly ash is generally the major waste ash from coal power production, comprising up to 88% of total ash production from coal thermal power stations [Sandelin and Backman, 2001]. Some elements are preferentially retained in either the fly ash or bottom ash to variable degrees. It is also important to note that the relative enrichment also depends on the specific technologies that are used at the facility. Some elements, including copper and manganese, have been reported to display a small degree of selective retainment in bottom ash and fly ash. Elements such as arsenic, cadmium, chromium, lead, mercury and zinc have been reported to be selectively retained in fly ash. For mercury, the degree of enrichment is higher such that over 90% of the retained mercury is found in the fly ash [Brigden and Santillo, 2002]. However, certain elements show little or no selectivity between bottom ash and fly ash [Sandelin and Backman, 2001]. The storage or disposal of fly ash may result in the release of leached metals into soils, surface or ground waters leading to the build-up of most of these metals in soils or sediment. Some of these leached metals are very toxic to plants, animals and humans via soil, air and water mediums [Brigden and Santillo, 2002].

1.2 Problem statement and motivation

The human activity of coal combustion in coal thermal power stations has the potential to release vast amounts of natural radioactivity (NORM) into the environment [USEPA, 2006]. Fly Ash waste generated through this combustion contains NORM and may release even more natural radioactivity into the environment [ALNabhani, Khan, and Yang, 2015]. It is therefore crucial to securely store the fly ash waste produced in order to prevent the radionuclide contamination of larger areas. The cancer risk to the surrounding communities due to the natural radioactivity from the combustion should be determined. There is a need for forward-looking research since no similar studies have been done before.

The accrued radiation doses as well as reference levels as a result of these natural radionuclides within the coal power station and its surroundings must be established. Therefore, any possible need for area monitoring at the coal power station or fly ash storage should be looked into. Coal combustion thus yields natural radionuclides that may result in possible health, environmental and technological problems [Miller, 2016]. The combustion of coal, not only releases radionuclides into the environment but it has the potential to also release high levels of toxic heavy metals. There is therefore the need to determine

the concentration of such metals in the vicinity of the coal burning power plant to determine the potential health impacts on the population residing in this area.

Therefore, this study is important because it is looking at providing current data on the level of contamination due to the burning of coal for power generation. The study is also looking to provide forward guidance and potential problems that might arise in the future due to the burning of coal by determining the radiological risk using RESRAD radiation code.

1.3 Research aim and objectives

The aim of the study was to model the naturally occurring radiations and their variations with respect to time around the Morupule-B Coal Power Station in Botswana, using RESRAD radiation code.

The objectives of this study were to:

a. Determine the radiological risk due to the natural radioactive elements.
b. Determine the toxicological risk due to toxic heavy elements.
c. Model public radiation doses due to these natural radionuclides using RESRAD.
d. Evaluate the environmental impact from the coal combustion.
e. Determine if radioactive and toxic heavy elements monitoring at the Morupule-B Coal Power Station facility is necessary.
f. Provide recommendations to the regulatory authority and relevant organizations for the regulation of the coal power stations, based on the results.

Chapter 2: Literature review

This chapter introduces and outlines the available literature, involving natural radioactivity exposure to both the general public and occupationally exposed workers. Equations are also introduced on how to estimate natural radioactivity values and parameters coming from different samples in the study area. The interaction of gamma rays with matter as well as the biological effects of ionizing radiation are also discussed. Literature on the software RESRAD used in determining natural radioactivity is also outlined.

2.1 Radioactivity and radioactive decay

2.1.1 General

Around 3000 different nuclei have so far been discovered and most of them are unstable. Radioactivity is the spontaneous process through which unstable atomic nuclei, also known as the parent nuclei, decays into stable daughter nuclei [Podgoršak, 2014]. The unstable nuclei are referred to as radioactive. The radioactive atom attains stability by losing nucleons (protons or neutrons), other particles, or by the loss of energy [ARPANSA, 2015]. Radioactive atoms undergo spontaneous fission, alpha-particle (α), beta-particle (β) and electron capture (EC) with occasional gamma-ray emission (γ) in order to achieve stability [Saha, 2010]. Both the nucleons structural arrangement as well as binding energy govern the stability of a nuclide. The ratio of neutrons to protons (N/Z) is a criterion used for the stability of a nuclide. Radioactive decay caused by electron capture or particle emission causes changes in the atomic number for that radionuclide, while γ -ray emission does not [Saha, 2010]. Radioactive decay may be caused by any of the six processes being electron capture, spontaneous fission, isomeric transition (IT), α - decay, β^- decay and β^+ decay. Electron capture or particle emission may be trailed by isomeric transition. The mass, charge and energy of radionuclides must be conserved in all these decays [ARPANSA, 2015; Saha, 2010]. The rate of radioactive decay in a sample is better represented by the fundamental law of radioactive decay using equation 2.1 [Saha, 2010]:

$$N = N_0 e^{-\lambda t} \tag{2.1}$$

where N is the number of atoms present at time t, N_0 is the number of atoms that where initially present and λ is the radioactive decay constant. The radioactive decay constant is defined as the probability per unit time for the decay of a specific nucleus. The rate of decay of a sample gives its activity (A). Equation

2.2 gives the relationship between the activity, decay constant and number of atoms in a sample [Ali, 2008]:

$$A = \lambda N \tag{2.2}$$

where A is the activity (Bq/second), λ is the decay constant (s^{-1}) and N is the number of atoms of the nuclide present in the sample. The half life is the time required for half the number of radioactive nuclei to disintegrate as shown in equation 2.3 [Santawamaitre, 2012].

$$T_{1/2} = \frac{ln2}{\lambda} \tag{2.3}$$

where $T_{1/2}$ is the half life and λ is the decay constant (s^{-1}).

2.1.2 Serial radioactive decay

A simple radioactive decay shows the parent radionuclide decaying to a stable daughter. A typical example the ^{14}C radionuclide decaying to a stable ^{14}N product as seen in equation 2.4 [Saha, 2010]:

$$^{14}_{6}C \rightarrow {}^{14}_{7}N\,(stable) + \beta^{-} + \bar{\nu} \tag{2.4}$$

where β^{-} is a beta particle and $\bar{\nu}$ is an antineutrino. An antineutrino has no mass and charge. The beta particle is a fast and energetic electron [Saha, 2010]. Several radioisotopes decay in this manner including ^{1}H, ^{14}C, ^{32}P, ^{35}S, ^{36}Cl, ^{45}Ca and ^{131}I [L'Annunziata, 2007; Pressyanov, 2002]. In other cases, a decay sequence may take place forming a daughter product that is also radioactive, particularly in the natural radioactivity series. A complex decay chain starts with a radioactive parent nuclide *P* decaying into a daughter radionuclide *D* through a decay constant λ_P. Radionuclide *D* is radioactive and decays into a stable granddaughter nucleus *G*. The respective radioactive decay series for this process is represented by equations 2.5 to 2.7 [Santawamaitre, 2012]:

$$\frac{dN_P}{dt} = -\lambda_P N_P \tag{2.5}$$

$$\frac{dN_D}{dt} = \lambda_P N_P - \lambda_D N_D \tag{2.6}$$

$$\frac{dN_G}{dt} = \lambda_D N_D \tag{2.7}$$

Equation 2.5 gives the depletion rate of the number of radioactive parent radionuclide $\frac{dN_P}{dt}$. The rate of change in the number of daughter radionuclide, $\frac{dN_D}{dt}$, is given by the difference between the supply of new daughter nuclei through the decay of the parent nuclei as well as the loss of the daughter nuclei from its decay into a stable product. The stable end-product dN_G has a production rate that increases at the decay rate of the daughter nuclei [Santawamaitre, 2012]. In some instances, the granddaughter product of a radioactive decay is also unstable and therefore continues on producing another radioactive product, resulting in what is termed a radioactive decay chain or series [Krane, 1988]. There are three main limiting equilibrium conditions for these decay chain series namely secular equilibrium, transient equilibrium as well as the state of no equilibrium [L'Annunziata, 2007]. These three conditions are discussed in Sections 2.1.3.1, 2.1.3.2 and 2.1.3.3 respectively.

2.1.3 Radioactive equilibrium

Radioactive equilibrium describes the state at which members of a radioactive series decay at the same rate as they are produced [Prince, 1979]. The three most prevalent scenarios depicting the radioactive equilibrium states are described in sections 2.1.3.1 to 2.1.3.3.

2.1.3.1 Secular equilibrium

Secular equilibrium is the state in which the half life of the parent is very long relative to that of the daughter, such that $\lambda_p << \lambda_D$. $\lambda_P \approx 0$ yields $e^{-\lambda pt} \approx 1$. The number of the daughter nuclei is given by equation 2.8 [Santawamaitre, 2012].

$$N_D(t) = N_P(0)\frac{\lambda_P}{\lambda_D - \lambda_P}(e^{-\lambda_P t} - e^{-\lambda_D t}) \tag{2.8}$$

With the increase in time as the daughter grows, the number of daughter nuclei will eventually reach equilibrium after approximately seven half lives of the daughter [Krane, 1988; Santawamaitre, 2012]. At

equilibrium, the parent and daughter activities are equal as presented in equation 2.9 [Cember and Johnson, 2009].

$$\lambda_p N_p = \lambda_D N_D \tag{2.9}$$

In a radioactive decay chain, the number of nuclei of the various daughters present at equilibrium are inversely proportional to their decay constants and the formation rates as well as the decay rate for each radioactive daughter equals the decay rate of the parent [Santawamaitre, 2012]. An instance of secular equilibrium is the case where ^{226}Ra, having a half life of 1600 years, decays to ^{222}Rn having a half life of 3.82 days, establishing secular equilibrium for ^{222}Rn from its long-lived parent ^{226}Ra. Another example is the decay of ^{113}Sn, having a half life of 117 days, to ^{113m}In with a half life of 100 minutes [Saha, 2010] as presented in Figure 2-1.

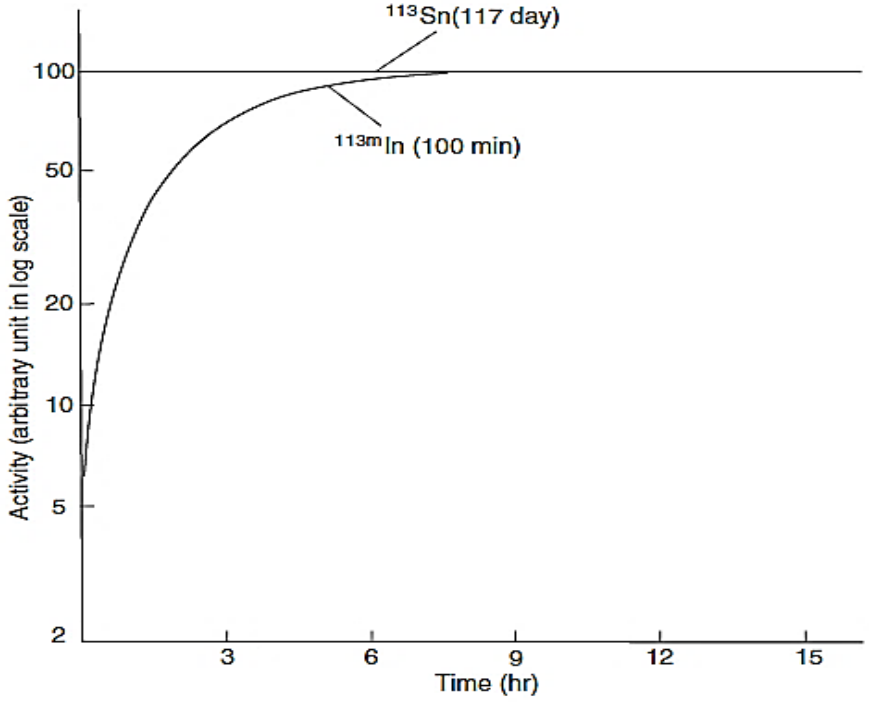

Fig. 2 - 1: Secular equilibrium between ^{113}Sn and ^{113m}In [Saha, 2010]

2.1.3.2 Transient equilibrium

Transient equilibrium occurs when the parent has a half life that is longer than that of the daughter but not significantly longer, such that $\lambda_p < \lambda_D$. It is important to note that in this case the approximation $\lambda_p = 0$ cannot be made. After a sufficiently long period of time, the exponential term of the daughter radionuclide becomes much smaller [L'Annunziata, 2007; Turner, 2007] depicting a transient equilibrium. After a transient equilibrium occurs, the ratio of the number of nuclei tends to become

constant. This occurs in relation to the parent as is characteristic of a transient equilibrium state [Cember and Johnson, 2009]. The daughter-product activity increases to ultimately surpass that of the parent, eventually attaining a maximum value. It then finally declines and follows the decay of the parent as shown in Figure 2-2. Figue 2-2 basically shows the growth and decay of a short-lived daughter ^{212}Bi from a slightly longe- lived parent ^{212}Pb in transient equilibrium.

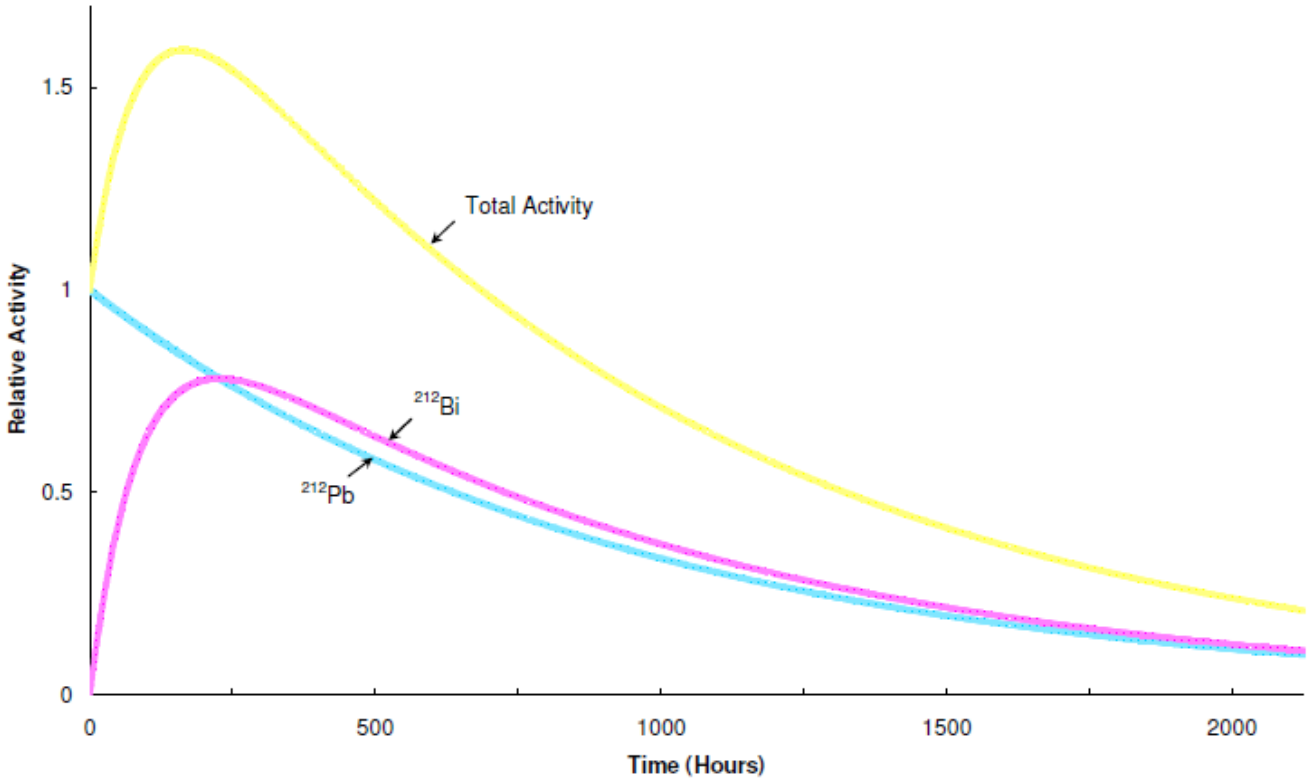

Fig. 2 - 2: Transient equilibrium between ^{212}Bi and ^{212}Pb [Santawamaitre, 2012]

2.1.3.3 No equilibrium

For the no equilibrium scenario, the parent has a half life that is shorter than that of the daughter. Since the parent has a half life that is shorter than that of the daughter, the daughter activity grows to a maximum and then decays with its half life [Magill and Galy, 2005] as shown in Figure 2-3.

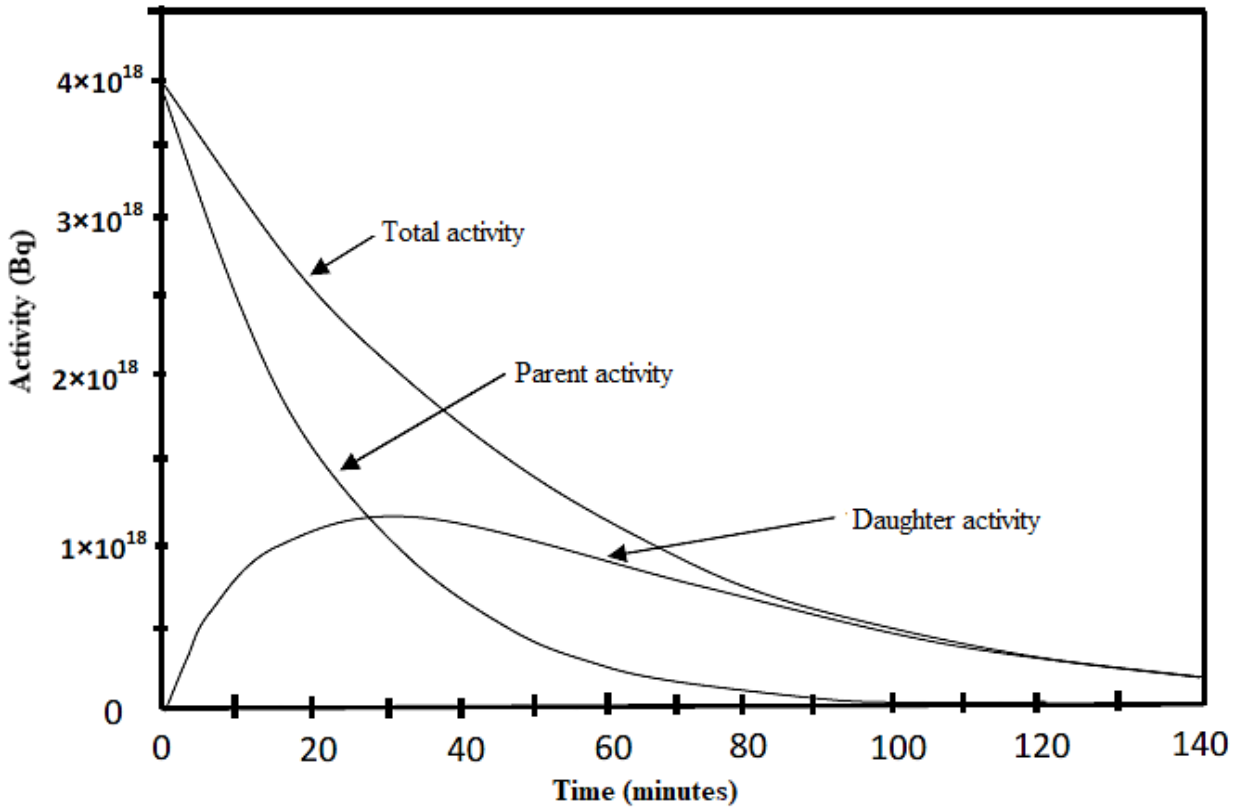

Fig. 2 - 3: No equilibrium incidence [Magill and Galy, 2005]

2.2 Types of decay

2.2.1 Spontaneous fission

Fission typically refers to when a heavy nucleus splits into two smaller fragments usually in the 60:40 ratio [Mohammed, 2014]. This is normally followed a release of two or three neutrons having a mean energy of 1.5 MeV as well as a release of approximately 200 MeV energy predominantly in the form of heat. In heavy nuclei, fission may occur spontaneously. Spontaneous fission has a low probability which rises with the mass number of the heavy nuclei. In the case of ^{235}U and ^{254}Cf, the half-lives for spontaneous fission are 2×10^{17} years and 55 days respectively [Saha, 2010].

2.2.2 Alpha decay

Heavy nuclei like neptunium, radon, uranium and others decay by alpha (α) particle emission. The alpha particle is simply the nucleus of the helium atom with two protons as well as two neutrons bound together

in the nucleus (${}^{4}_{2}He^{2+}$). In this type of decay, the atomic number of the parent nuclide reduces by 2 and the mass number by 4 [Saha, 2010]. Alpha decay is associated with high atomic number. An example of alpha (α) decay is shown in equation 2.10 [Mohammed, 2014].

$$^{235}_{92}U \rightarrow ^{231}_{90}Th + ^{4}_{2}He^{2+} \quad (2.10)$$

An alpha transition may be trailed by gamma-ray emission or beta particle emission or both. Alpha particles have a very short range in matter in the order of 10^{-6} cm, roughly 0.03 mm in body tissue.

2.2.3 Beta decay

A beta particle (β^-) has its origins from the nucleus of the neutron-rich and unstable nuclei [Lilley, 2001]. The beta particle essentially is a high energy and fast electron that is negatively charged as well as possessing the same mass as a normal electron [Cember and Johnson, 2009; L'Annunziata, 2007]. Beta decay processes occur through the emission of negative beta particles. In beta decay, a neutron (n) decays into a proton (p) as well as a beta (β^-) particle. An antineutrino ($\overline{\nu}$)is also produced in the beta decay as an entity that almost has no mass and charge and is mainly utilized to conserve energy during the decay process. The beta decay process increases the atomic number (*Z*) by one unit while the mass number (*A*) remains constant [Krane, 1988]. Equation 2.11 gives an example of beta decay [Lapp and Andrews, 1972].

$$^{131}_{53}I \rightarrow ^{131}_{54}Xe + \beta^- + \overline{\nu} \quad (2.11)$$

2.2.4 Positron emission

Nuclei that are rich in protons or deficient in neutrons, basically having a ratio of N/Z that is less than that of the stable nuclei, decay through positron (β^+) particle emission. This process is also accompanied by the emission of a neutrino (*v*), which basically is an opposite of the antineutrino [Saha, 2010]. Positron particles are positively charged electrons [L'Annunziata, 2007].

Positron particle emission results in a daughter n with an atomic number that is less than that of the parent by one. Positrons also have a short range in matter. At the end, positron particles combine with electrons and then become annihilated, such that each gives rise to two photons 511 keV that are emitted in

opposite directions [Gilmore, 2008; Kantele, 1995]. In positron emission, a proton basically transforms into a neutron through the emission of a positron. Positron emission can only happen when the difference in energy between the parent/daughter nuclides is ≥ 1.02 MeV [Saha, 2010]. An example of positron emission is given in equation 2.12 [Saha, 2010].

$$^{64}_{29}Cu \rightarrow ^{64}_{28}Ni + \beta^{+} + \nu \tag{2.12}$$

2.2.5 Electron capture

A nucleus with a smaller N/Z ratio as compared to a stable nucleus may, as an option to β^{+} decay, also undergo a process known as electron capture. In electron capture, the nucleus captures an electron from the k-shell, resulting in a proton being transformed to a neutron as well as a neutrino [Mohammed, 2014]. This normally leaves the daughter nucleus in an excited state. In order for this process to take place, there has to be an energy difference of less than 1.02 MeV between the parent and daughter nuclides [Faanu, 2011]. However, nuclides with an energy difference greater than 1.02 MeV may also decay by electron capture under conditions of statistical equilibrium. The probability of positron decay increases as the energy difference increases. This process reduces the parent's atomic number by one. A typical example of electron capture decay is shown in equation 2.13 [Faanu, 2011; Mohammed, 2014]:

$$^{67}_{31}Ga + e^{-} \rightarrow ^{67}_{30}Zn + \nu \tag{2.13}$$

In the EC process, the K-shell electrons are captured due of their closeness to the nucleus through a process known as K capture. An L shell electron is then captured through the L capture process and so on. The vacancy that results in the K-shell after electron capture is then filled by the transition of electrons from higher energy levels such as the L, M or N shells. The difference in the energies as electrons are transitioning from higher energy shells to lower ones will normally result in X-ray radiation that is characteristic of the daughter nucleus. Therefore, the resulting X-rays are named characteristic K X-rays, L X-rays or M X-rays and so on that belong to the daughter [Saha, 2010].

2.2.6 Isomeric transition

Quantum mechanics is helpful in describing the numerous excited energy states above the ground state in which a nucleus can remain. Such excited states are known as isomeric states that decay to the ground

state, having a lifetime from fractions of picoseconds to many years. Isomeric transition refers to the process when there is a decay from an upper excited state to a lower excited state [Saha, 2010]. In electron capture, β^- or β^+ decay, the parent nucleus could archieve the daughter nucleus'isometric states with respect to the ground state. The electron capture, β^- or β^+ decay process are therefore often complemented by isomeric transition. The variance in energy between the energy states might appear as gamma rays in isomeric transitions. Long-lived isomeric states are known as metastable states and they are detectable using suitable instruments. Isomeric transition basically occurs in long-lived metastable states or isomers of the parent nuclei such that the metastable state is represented by the letter m as in ^{99m}Tc [L'Annunziata, 2012; Mohammed, 2014]. Figure 2-4 represents the decay scheme of ^{99m}Tc . There is the possibility that instead of emitting a gamma-ray photon, the excited nucleus might transfer its excitation energy to an electron from the extra nuclear electron shell of its own atom, specifically the K shell, which is then ejected, on condition that the binding energy for the K electron < excitation energy [Beringer and Remington, 2005].

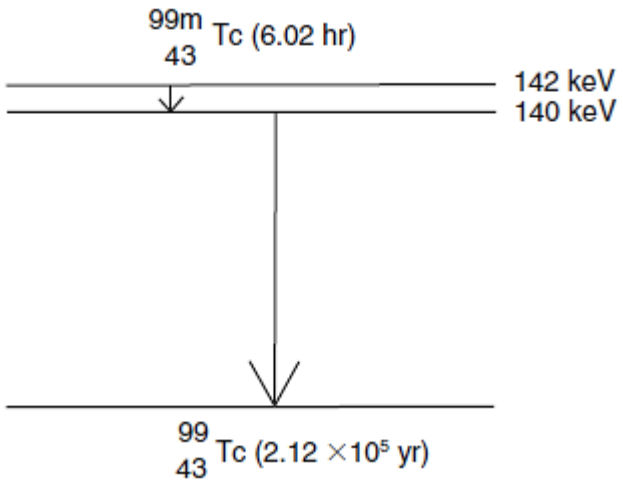

Fig. 2 - 4: Isomeric transition in ^{99m}Tc decay [Beringer and Remington, 2005]

2.3 Exposure due to natural sources of radiation

All living things are continuously being exposed to natural radiation from the earth [Desouky, Ding and Zhou, 2015]. The levels of these natural radiation exposures vary according to location and altitude. When dealing with human populations, it is necessary to consider external exposures from radionuclides that are naturally present in the environment or anthropogenic practices [Bal et. al., 2018]. The United Nations Scientific Committee on the Effects of Atomic Radiation (UNSCEAR) has publicized that

natural radiation sources account for over 98% of the total radiation dose on the population, excluding medical exposure [UNSCEAR, 2000]. Natural radiation is generally the largest contributor to the collective effective dose received by the world population. The two categories of natural radiation sources that human populations are continuously exposed to are:

a. Terrestrial radionuclides
b. Cosmic rays

Figure 2-5 shows the contributors to worldwide exposure to natural radiation sources. Natural radiation sources are inclusive of indoor gamma rays, outdoor gamma rays and radon gas.

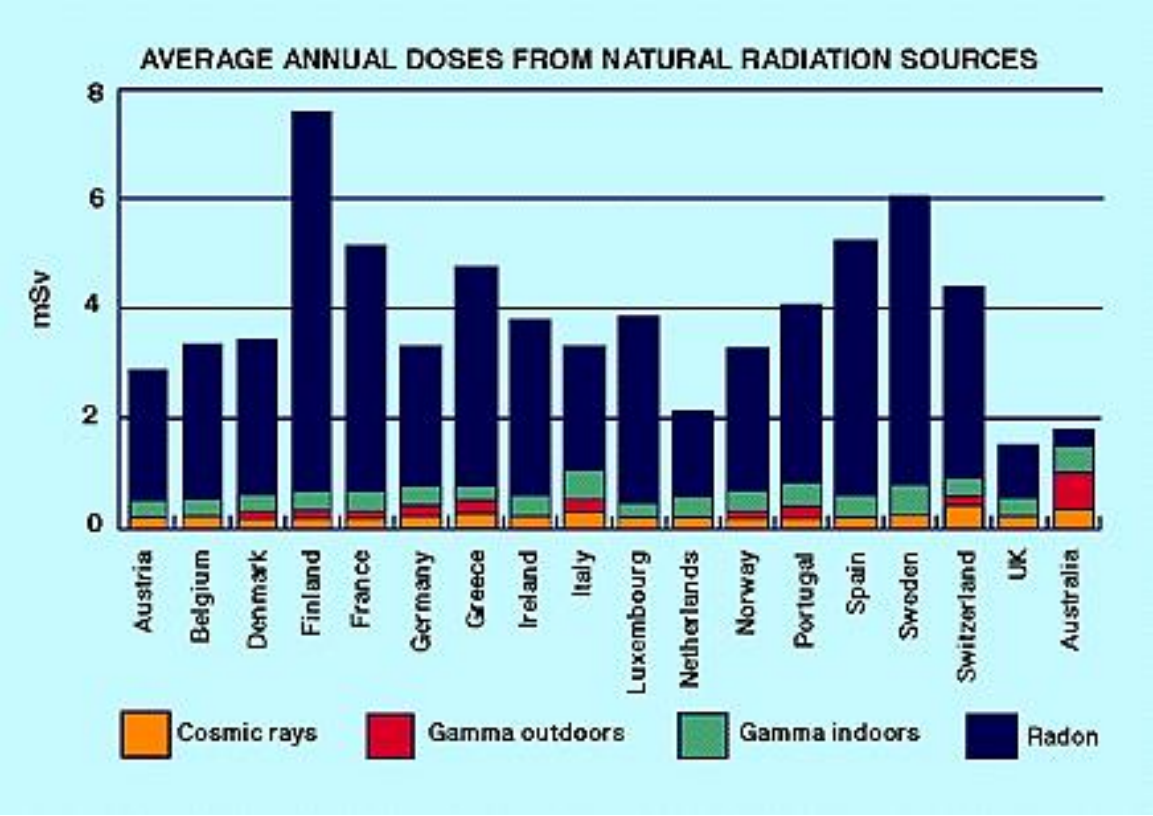

Fig. 2 - 5: World exposure chart to natural radiation [World Nuclear Association]

2.3.1 Terrestrial radiation

Naturally occurring radionuclides whose half-lives are comparable to the age of the earth are known as primordial radionuclides [UNSCEAR, 2008]. Primordial radionuclides are found in all environmental materials, including the human body. ^{238}U, ^{232}Th and ^{40}K are typical examples of primordial radionuclides with half-lives of 4.47×10^9 years, 1.41×10^{10} years and 1.28×10^9 years, respectively. Primordial radionuclides and their progeny contribute about 480 μSvy^{-1} of effective dose by external

irradiation. Natural uranium comprises of three isotopes being ^{238}U, ^{235}U and ^{234}U all of which are radioactive with very long half-lives. Natural Uranium has an average relative compositions by mass of 99.27% (^{238}U), 0.72% (^{235}U) and 0.0054% (^{234}U) [Thorne, 2003]. There are three naturally occurring radioactive decay series as well as the man-made Neptunium series.

The first series is the thorium decay series that basically consists of radionuclides such that all the mass numbers are evenly divisible by four (4n series). The thorium decay series has its origin in ^{232}Th existing at an isotopic abundance of 100%. ^{238}U is the parent of the uranium decay series (4n + 2 series) consisting of nuclides that give a remainder of 2 when their mass numbers are divided by 4 [Cember and Johnson, 2009]. ^{235}U is the parent of the actinium decay series (4n+3 series) consisting of nuclides that give a remainder of 3 when their mass numbers are divided by 4. ^{237}Np is the parent of the fourth long Neptunium decay series (4n+1 series) consisting of nuclides that give a remainder of 1 when their mass numbers are divided by 4 [Choppin, Liljenzin and Rydberg, 2002]. Tables 2-1 to 2-4 show the thorium decay series, neptunium decay series, uranium decay series and actinium decay series respectively.

Table 2 - 1: Thorium decay series [Cember and Johnson, 2009]

		Energy (Mev)		
Nuclide	**Half-life**	**Alpha**	**Beta**	**Gamma (Photons/ Trans.)**
$^{232}_{90}Th$	1.39 x 10^{10} yrs	3.98		
$^{228}_{88}Ra$	6.7 yrs		0.01	
$^{228}_{89}Ac$	6.13 h		Complex decay scheme Most intense beta group is 1.11 MeV	1.59 0.966 (0.2) 0.908 (0.25)
$^{228}_{90}Th$	1.91 yrs	5.421		0.084 (0.016)
$^{224}_{88}Ra$	3.64 d	5.681		0.241 (0.038)
$^{220}_{86}Rn$	52 s	6.278		0.542 (0.0002)
$^{216}_{82}Po$	0.158 s	6.774		
$^{212}_{82}Pb$	10.64 h		0.35, 0.59	0.239 (0.40)
$^{212}_{83}Bi$	60.5 min	6.086 (33.7%)	2.25 (66.3%)	0.04 (0.034 branch)
$^{212}_{84}Po$	3.04 x 10^{-7} s	8.776		
$^{208}_{81}Tl$	3.1 min		1.80, 1.29, 1.52	2.615 (0.997)
$^{208}_{82}Pb$	Stable			

Table 2 - 2: Neptunium decay series [Cember and Johnson, 2009]

Nuclide	Half-life	Energy (Mev)		
		Alpha	**Beta**	**Gamma (Photons/ Trans.)**
$^{241}_{94}Pu$	13.2 yrs		0.02	
$^{241}_{95}Am$	462 yrs	5.496		0.060 (0.4)
$^{237}_{93}Np$	2.2 x 10^6 yrs	4.77		
$^{233}_{91}Pa$	27.4 d		0.26, 0.15, 0.57	0.31 (very strong)
$^{233}_{92}U$	1.62 x 10^5 yrs	4.823		0.09 (0.02) 0.056 (0.02) 0.042 (0.15)
$^{229}_{90}Th$	7.34 x 10^3 yrs	5.02		
$^{225}_{88}Ra$	14.8 d		0.32	
$^{225}_{89}Ac$	10.0 d	5.80		
$^{221}_{87}Fr$	4.8 min	6.30		0.216 (1)
$^{217}_{85}At$	0.018 s	7.02		
$^{213}_{83}Bi$	47 min	5.86 (2%)	1.39 (98%)	
$^{213}_{84}Po$	4.2 x 10^{-6} s	8.336		
$^{209}_{81}Tl$	2.2 min		2.3	0.12 (weak)
$^{209}_{82}Pb$	3.32 h		0.635	
$^{209}_{83}Bi$	Stable			

Table 2 - 3: Uranium decay series [Cember and Johnson, 2009]

Nuclide	Half-life	Energy (Mev)		
		Alpha	**Beta**	**Gamma (Photons/ Trans.)**
$^{238}_{92}$U	4.51 x 10^9 yrs	4.18		
$^{434}_{90}Th$	24.10 d		0.193, 0.103	0.092 (0.04) 0.063 (0.03)
$^{234m}_{91}Pa$	1.175 min		2.31	1.0 (0.015) 0.76 (0.0063), I.T.
$^{234}_{91}Pa$	6.66 h		0.5	Many (weak)
$^{234}_{92}U$	2.48 x 10^5 yrs	4.763		
$^{230}_{90}Th$	8.0 x 10^4 yrs	4.685		0.068 (0.0059)
$^{230}_{90}$Ra	1.622 yrs	4.777		
$^{222}_{86}Em$	3.825 d	5.486		0.51 (very weak)
$^{218}_{84}Po$	3.05 min	5.998 (99.978%)	Energy not known (0.022%)	0.186 (0.030)
$^{218}_{85}At$	2 s	6.63 (99.9%)	Energy not known (0.1%)	
$^{218}_{86}Em$	0.019 s	7.127		
$^{214}_{82}Pb$	26.8 min		0.65	0.352 (0.036) 0.295 (0.020) 0.242 (0.07)
$^{214}_{83}Bi$	19.7 min	5.505 (0.04%)	1.65, 3.7 (99.96%)	0.609 (0.295) 1.12 (0.131)
$^{214}_{84}Po$	1.64 x 10^{-4} s	7.680		
$^{210}_{81}Tl$	1.32 min		1.96	2.36 (1) 0.783 (1) 0.297 (1)
$^{210}_{82}Pb$	19.4 yrs		0.017	0.0467 (0.045)
$^{210}_{83}Bi$	5.00 d		1.17	
$^{210}_{84}Po$	138.40 d	5.298		0.802 (0.000012)
$^{206}_{82}Pb$	Stable			

Table 2 - 4: Actinium decay series [Cember and Johnson, 2009]

Nuclide	Half-life	Energy (Mev)		
		Alpha	**Beta**	**Gamma (Photons/ Trans.)**
$^{235}_{92}U$	7.13 x 10^8 yrs	4.39		0.18 (0.7)
$^{231}_{90}Th$	25.64 h		0.094, 0.302 0.216	0.022 (0.7) 0.0085 (0.4) 0.0061 (0.16)
$^{231}_{91}Pa$	3.43 x 10^4 yrs	5.049		0.33 (0.05) 0.027 (0.05) 0.012 (0.01)
$^{227}_{89}Ac$	21.8 yrs	4.94 (1.2%)	0.0455 (98.8%)	
$^{227}_{90}Th$	18.4 d	6.03		0.24 (0.2) 0.05 (0.15)
$^{223}_{87}Fr$	21 min		1.15	0.05 (0.40) 0.08 (0.24)
$^{223}_{88}Th$	11.68 d	5.750		0.270 (0.10) 0.155 (0.055)
$^{219}_{86}Em$	3.92 s	6.824		0.267 (0.086) 0.392 (0.048)
$^{215}_{84}Po$	1.83 x 10^{-3} s	7.635		
$^{211}_{82}Pb$	36.1 min		1.14, 0.5	Complex spectrum, 0.065-0.829 MeV
$^{211}_{83}Bi$	2.16 min	6.619 (99.68%)	Energy not known (0.32%)	0.35 (0.14)
$^{211}_{84}Po$	0.52 s	7.434		0.88 (0.005) 0.56 (0.005)
$^{207}_{81}Tl$	4.78 min		1.47	0.87 (0.005)
$^{207}_{82}Pb$	Stable			

^{40}K is a naturally occurring radionuclide that is widely distributed in the environment and has a low atomic number [Cember and Johnson, 2009]. Potassium occurs in nature as a mixture of the isotopes ^{39}K, ^{40}K and ^{41}K such that ^{40}K is the only radioactive one among the three isotopes [Masarik, 2009].

2.3.2 Cosmic radiation

High energy cosmic rays from outer space continually bombard the earth such that the average worldwide exposure to cosmic rays makes up approximately 13% of the total annual effective dose to the population [UNSCEAR, 2008]. It is therefore important to assess the cosmic ray exposure on the ground level in order to better understand population exposures to ionizing radiation. Cosmic rays interact with nuclei in the atmosphere, producing a cascade of interactions as well as secondary reaction products that ultimately contribute to the decrease in cosmic ray exposure intensity with depth in the atmosphere: from

the stratosphere to aircraft altitudes as well as down to the ground level [Cinelli et. al., 2017, European Commission, 1996, Lockwood, 1960]. Cosmic ray interactions with nuclei in the atmosphere produce several radioactive nuclides known as cosmogenic radionuclides. Cosmogenic radionuclides [Beer, McCracken and Steiger, 2012] are shown in Table 2-5.

Table 2 - 5: Cosmogenic radionuclides [Beer, McCracken and Steiger, 2012]

Radionuclide	Half-life (years)	Decay type
^{3}H	12.26	Beta
^{7}Be	0.15	EC
^{10}Be	1.6×10^{6}	Beta
^{14}C	5.73×10^{3}	Beta
^{22}Na	2.6	EC
^{26}Al	7.4×10^{5}	EC
^{32}Si	280	Beta
^{32}P	0.04	Beta
^{33}P	0.07	Beta
^{35}S	0.24	Beta
^{36}Cl	3.01×10^{5}	Beta
^{39}Ar	269	Beta
^{81}Kr	2.29×10^{5}	EC

The prevailing component of cosmic rays at the ground level is the muons mostly with energies between 1 GeV to 20 GeV [UNSCEAR, 2008]. The three cosmogenic radionuclides ^{14}C, ^{3}H and ^{22}Na have metabolic functions in the human body. With exception of these three, cosmogenic radionuclides generally contribute minimally to radiation doses [UNSCEAR, 2000].

2.4 Interaction of gamma rays and X-rays with matter

Alpha and beta particles continue to lose their energies until all the energy has been transferred to the absorbing medium. The energies of X-rays and gamma rays on the other hand, allow them to travel

longer distances. Gamma rays and X-rays interact with matter via the photoelectric effect, Compton scattering and pair production [NRC, 1990].

2.4.1 Photoelectric effect

In photoelectric absorption, a gamma photon interacts with an absorber atom then completely disappears. In its place, an energetic photoelectron is ejected from one of the bound shells of the atom resulting in ionization and excitation. The photoelectron that is ejected has kinetic energy given by equation 2.14 [Cember and Johnson, 2009].

$$E_e = h\upsilon - E_b \tag{2.14}$$

where h is the Planck's constant, υ is the frequency of the incoming photon and E_b is the binding energy of the electron. In order to fulfil the conservation of momentum, the atom remains with minimal recoil energy [Nelson and Reilly, 1991]. Photoelectric absorption mostly happens for gamma photons less than 100 keV. Photoelectrons have their origins in the innermost shells such as K shells [Parks, 2015]. A free electron from a higher energy shell usually fills the vacancy created by a photoelectron. Energy is then released in the form of characteristic X-rays. Sometimes these characteristic X-rays may interact with outer shell electrons, thereby ejecting them from the atom in the form of low energy auger electrons. Materials with high Z (atomic number) such as lead are most likely to experience photoelectric effect [Kamunda, 2017]. The electron binding energy, the gamma-ray energy and Z affect the probability of photoelectric absorption. The probability increases for more tightly bound electrons [Nelson and Reilly, 1991]. and the relationship is given in equation 2.15.

$$\tau \propto Z^4/E^3 \tag{2.15}$$

where τ represents the mass attenuation coefficient, Z is the atomic number and E is the photon energy. Thus, photoelectric absorption is the major interaction for low-energy gamma rays, X-rays, and bremsstrahlung.

2.4.2 Compton scattering

Through the photoelectric effect, a gamma ray can transfer all of its energy to an electron as seen in section 2.4.1. Through the Compton Effect, a gamma ray may transfer only a portion of its energy to an electron. Whereas the transfer of gamma energy to an electron through the photoelectric effect is always nearly 100%, the transfer of energy through the Compton effect can vary from 0% to nearly 100%,

depending on the energy of the gamma ray as well as the angle that it is scattered [Parks, 2015]. The maximum kinetic energy given to an electron through Compton scattering is shown in equation 2.16 [Parks, 2015].

$$E_{eMax} = E\left[1 - \frac{1}{1 + 2\frac{E}{m_0 c^2}}\right] \tag{2.16}$$

where $E_{eMax} \approx E$ when $E >> mc^2$ and $E_{eMax} \approx 0$ when $E << mc^2$ m_o is the rest mass of an electron. The percentage of the maximum of the initial energy of the gamma ray that is transferred to the electron in Compton scattering is approximately 72% for a 0.662 MeV gamma ray [Parks, 2015]. This implies that a Compton scattering with 0.662 MeV gamma rays would yield scattered electrons with energies ranging between 0 MeV and 0.477 MeV.

2.4.3 Pair production

In pair production, a gamma ray with sufficient energy converts its energy into mass. The gamma ray creates an electron - positron pair of positive and negative particles each bearing a mass equal to the electron. To maintain the conservation of momentum and energy, this reaction only happens in the vicinity of a strong electric field near an atomic nucleus [Parks, 2015]. The energy that is provided to the atom is negligible when likened to the rest energies of the electron and positron and the kinetic energies they are given, such that there is a threshold energy of 1.02 MeV for pair production to occur [Hall and Giaccia, 2011].

2.5 Biological effects of ionizing radiation

Elevated levels of background radiation in some areas have not resulted in a significant increase of cancer in populations living in these areas. Therefore, the harmful effects due to exposure to ionizing radiation are linked to linear extrapolations from doses that are normally higher than the corresponding background radiations. The BEIR III 80 model has estimated that a single exposure to 100 mSv of radiation might cause approximately a maximum of 6000 excess cases of cancer deaths (other than leukemia and bone cancer) per million deaths, as compared to a natural incidence of about 250000 cancer deaths [NRC, 2002]. The linear extrapolation thus shows that 3 mSv of background radiation exposure over a time period of 70 years would yield approximately 12600 extra cancers per million deaths of people, or about

1 radiation-induced cancer per 20 cancers [NRC, 2002]. Other environmental factors such as drugs, smoking, bacterial, viral and fungal infections make it difficult to discern cancers caused by background radiations.

Health effects of ionizing radiation on living matter are better explained through interactions of radiations such as gamma rays and x-rays with matter. For x-rays and gamma rays, ionization and excitation mostly take place when fast electrons get knocked out of the atoms through the Compton effect and the photoelectric effect. The great numbers of ionizations affect the surrounding DNA structure in living matter, with the Auger effect likely to effect double strand breaks. On average, a DNA molecule in living matter is ionized about 0.9 times per year. Single DNA strand breaks in living matter are about 10 times higher [IAEA, 2002]. The biological effects of ionizing radiation are divided into stochastic effects and deterministic effects.

Deterministic effects are sometimes referred to as non-stochastic effects. They have a threshold dose under which there will be no effect and above which the severity of the effect increases. Basically, all the early radiation effects and most late tissue effects are deterministic. Examples of deterministic effects are acute radiation sickness and chronic radiation sickness. Such effects are dependent on the exposure duration, radiation type and amount of dose received [Choudhary, 2018].

Stochastic effects occur when an individual receives a high radiation dose. These effects are a probability such that their increased likelihood occurs with an increase in dose. There is therefore no threshold dose for stochastic effects and the severity of the effect does not increase with dose. The two types of stochastic effects are somatic stochastic effect and genetic effect [Choudhary, 2018].

2.6 Biological effects of heavy metals

Some metals like iron and copper are important to human life because of their irreplaceable functions in body organs. Varying quantities of heavy metals are required by every living organism. However, heavy metal quantities become toxic to these living organisms at elevated concentrations [Lane and Morel, 2009]. Toxic heavy metals like mercury, arsenic and lead add no value to the human body as well as in many other living organisms. Such metals might be toxic at low exposure levels. As per the heavy metal pollutants priority list, arsenic, lead and mercury appear as 1^{st}, 2^{nd} and 3^{rd} hazardous respectively [ATSDR, 2007].

Human mining activities may result in heavy metals contaminating water sources, agricultural lands and the environment. Excessive buildup of heavy metals in agricultural lands may also result in elevated heavy metal uptake by plants [Kamunda, 2017]. Involuntary ingestion of heavy metals may also take place through food and drink. Once absorbed, these heavy metals are distributed in body cells, tissues and organs. Despite the fact that excretion of unwanted substances occurs through the kidneys or digestive system, heavy metals may still remain stored in some parts including the bones, kidneys or liver for numerous years. This may result in serious health consequences [Kabata and Pendias, 1993; Kamunda, 2017].

Arsenic is a carcinogen to humans from very low levels of exposure [ATSDR, 2007]. After being absorbed, it is mainly spread in the liver, kidneys, lungs, spleen, aorta, and skin. Severe exposure to arsenic or its compounds might result in abdominal pain, diarrhea, nausea, muscle cramps, vomiting and burning of the mouth and throat [NRC, 1999]. Chronic exposure to lower levels of arsenic leads to rather unusual patterns of skin hyper-pigmentation, tingling, peripheral nerve damage manifesting as numbness and weakness in the feet and hands as well as causing diabetes [Kamunda, 2017; UNEP, 2002].

Due to its toxicity even at low concentrations, lead is therefore a human mutagen and probable carcinogen [Tchounwou, 2012]. Lead reduces cognitive development, induces renal tumours and also increases blood pressure in adults. Its toxicity results in the reduction of haemoglobin synthesis, thus disrupting the normal functioning of the kidneys, reproductive system, cardiovascular system and also causes chronic damage to the peripheral and central nervous systems [Ogwuegbu and Muhanga, 2005].

Mercury (Hg) occurs mainly in two forms being organic and inorganic mercury. Acute ingestion of inorganic mercury salts may lead to gastrointestinal disorders like abdominal pain, diarrhoea, hemorrhage and vomiting. Cadmium is still toxic at minute concentrations and is therefore viewed as a plausible carcinogen. Severe exposure to cadmium could lead to pulmonary problems including alveolitis and emphysema [Kamunda, 2017; UNEP, 2002].

Chromium (VI) compounds are toxic and are also known to be both carcinogenic and mutagenic and whereas chromium (III) is an essential element [Wang et al., 2017]. Inhaling high levels may cause

irritation on the lining of the nose leading to breathing problems. Long term exposure may result in circulatory disorders, nervous disorders, skin irritation as well as damage to the kidneys and liver. Nickel is known to cause cancer, depression, haemorrhages, kidney problems and heart attacks [NRC, 1999].

2.7 Application of RESRAD code in the determination of natural radioactivity

Environmental issues can be difficult to solve due to the complicated relationships among the numerous variables that exist [Avila, Broed and Pereira, 2003]. Therefore, RESRAD code plays an important role in solving and helping us to understand the complex relationships [Kamunda, 2017]. RESRAD is a software code that is very useful for environmental modelling and is particularly useful when radionuclides are involved. RESRAD (RESidual RADioactivity) is a frequently used computer software that was designed and implemented by Argonne National Laboratory at the U.S Department of Energy as well as the U.S Nuclear Regulatory Commission. It was designed to develop standards for assessing human radiation risk as well as doses in relation to radiological contamination [Kamunda, 2017]. RESRAD permits operators to specify the parameters of their specific location as well as to estimate the individual doses received anytime up to a hundred thousand years. The developers of RESRAD at Argonne have assigned a default value for each parameter which can be changed to the specific requirements of the site. RESRAD-OFFSITE is an addition to the RESRAD-ONSITE software that estimates the radiological effects on subjects on or out of the primary contamination zone [Mathuthu et al., 2016]. The RESRAD code computes the radiation dose plus excess cancer risk using the estimated radionuclide concentrations from the environs [USDoE, 2007].

RESRAD software assumes a pathway analysis process such that the soil radionuclide concentrations and the dose received by a critical population member are articulated as a pathway sum or summation of pathway factors that connect environmental compartments [Yu and Gnanapragasam, 1996]. It also assumes that these radionuclides are transportable between these compartments. The software further assumes and analyzes 9 possible exposure pathways being direct external radiation exposure due to contaminated soil, internal radiation exposure due to contaminated dust inhalation, internal radiation exposure due to radon inhalation, internal radiation exposure due to the intake of plants that grow on the contaminated soil that is irrigated with pond or well water, internal radiation exposure due to the intake of meat from livestock that has been fed with plant material grown on pond or well water and contaminated soil, internal radiation exposure due to milk intake from livestock that has been fed with

plant material grown on pond or well water and contaminated soil, internal radiation exposure due to intake of contaminated soil, internal radiation exposure due to aquatic food intake and lastly the internal radiation exposure due to drinking of pond or well water [Yu and Gnanapragasam, 1996].

Research and intercomparison of RESRAD-OFFSITE code with another commonly used code known as NORMALYSA has revealed that both codes generally yield very similar results quantitatively and qualitatively for radionuclide simulations contaminated with ^{210}Po, ^{210}Pb and ^{226}Ra with variations between both codes not more than 7 to 8 % [Koliabina et al., 2018]. However, RESRAD-OFFSITE operates with a more advanced plant root uptake model as compared to NORMALYSA. For RESRAD-OFFSITE root uptake model, the uptake of radionuclides is proportional to the root length present in the contaminated soil, whereas NORMALYSA assumes all plant roots are located in the topsoil. This results in higher and less accurate estimated crop radionuclide uptake values for NORMALYSA as compared to RESRAD-OFFSITE [Koliabina et al., 2018]. RESRAD-OFFSITE has the advantages of a very large radionuclide database of more than 1200 radionuclides, great uncertainty analysis and probabilistic capabilities, long application history with many supporting documents and the software code has been widely utilized by the IAEA for various model validations [Avila, 2019]. On the other hand, NORMALYSA has a relatively short application history with fewer supporting documents and a relatively smaller radionuclide database that requires more sophisticated training for the users [Avila, 2019]. Hence the decision to use RESRAD-OFFSITE for this work.

2.8 Radiation detection

Detection can take place whenever a nuclear particle enters a detector resulting in either excitation or ionization. Various types of detectors may be used based on either ionization or excitation. For example, a nuclear particle may cause excitation followed by fluorescent de-excitation upon interaction with a unique material [Bode, 1998]. For the type of detector whose operation is based on the principle of ionization, charge carriers are produced between the charged electrodes within the detector. Devices based on this principle can be solid semiconductor materials or gas filled devices whose function is based on this principle, are normally divided into ion chambers, proportional counters or Geiger-Müller tubes. Semiconductor detectors in the solid form have a p-n junction diode arrangement. Connecting a reverse bias voltage across the p-n diode increases the depletion region [Gruber, 2009]. When photons interact inside the depletion region, charge carriers, being negative electrons and positive holes, are released and

swept to their respective collecting electrodes by a voltage supply. The collected charge is then passed into a preamplifier before being converted to a voltage pulse whose amplitude is proportional to the initial photon energy. Silicon (Si) and germanium (Ge) are the most widely used materials for semiconductor detectors.

Semiconductor detectors are widely used for gamma spectrometry due to their properties such as good stability, excellent timing characteristics, simplicity of operation as well as high energy resolution. The energy gap, the mobility of the major carriers and atomic number constitute the three basic differences between Si and Ge detectors. Less energy is required to create an electron-hole pair in Ge than in Si, implying that some Si detectors can operate at room temperature while Ge detectors should first be cooled to 77 K in order to reduce the leakage current due to thermal generation of charged carriers to a suitable level. A Ge detector should therefore be cooled to liquid nitrogen temperatures and be operated inside a vacuum chamber [Cember and Johnson, 2009; Kamunda, 2017]. Gamma spectrometry is crucial as a non-destructive method for measuring activities of different radionuclides in various environmental samples. Radionuclide sources yield gamma rays of varying energies and emission probabilities. The resulting spectrum consisting of gamma lines is then analyzed with gamma spectrometry system. In this particular research, a High Purity Germanium detector (HPGe) was utilized.

2.9 High Purity Germanium detector (HPGe)

The High Purity Germanium detector (HPGe) detects gamma photons through the interaction properties of gamma rays with the absorbing material. Gamma rays interact with the HPGe detector through the photoelectric effect, compton scattering and pair production. These interactions produce charge carriers that move towards the electrodes under the influence of the electric field. The HPGe detector provides the best energy resolution for detection of radiation but with relatively low efficiency [Pallavicini, 2011]. It is therefore possible to design different kinds of detectors depending on the impurity dopant. HPGe detectors are made in various shapes for particular purposes of measurement with the planar or coaxial types being the most common [Santawamaitre, 2012].

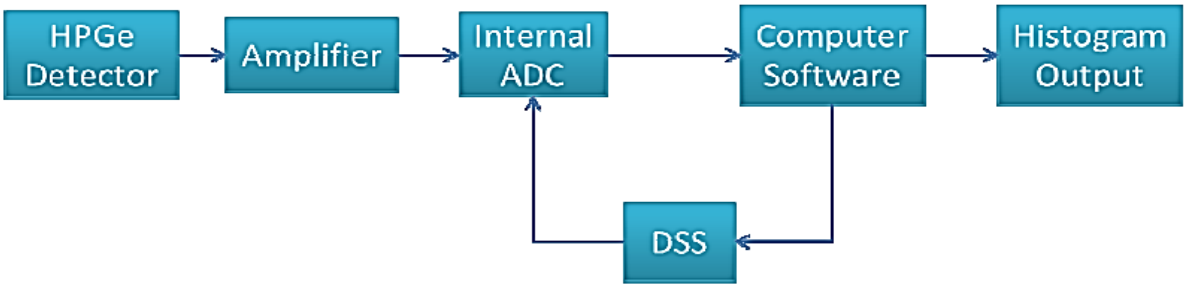

Fig. 2 - 6: Functional block diagram of HPGe gamma spectrometry system [Stratton, 2011]

Figure 2-6 shows a block diagram of a PC-based HPGe system consisting of a high purity germanium detector that is coupled to a high vacuum cryostat dewar system. The cryostat dewar system stores liquid nitrogen and also makes a path for the transfer of heat from the reservoir to the detector element. In order to reduce the background noise caused by natural radioactivity in the surroundings, the detector is shielded with lead [Mouchel and Wordel, 2000]. A high-voltage power supply provides the required high voltage for the detector as well as the essential voltages to all other system components. The HPGe system comprises of highly efficient electronic circuits containing a preamplifier that generates a response proportional to the amount of charge produced by the incident ray. This is then followed by an amplifier whose main function is to amplify the signal. Pulses are appropriately transformed into signals so as to maximize the ratio between the signal and background. The last section is the multichannel analyzer (MCA) that accumulates pulses of all voltage ranges at once and shows this data in real time as final results or as data for further analysis [Reguigui, 2006].

2.10 Energy resolution and efficiency

The average value at the full width at half maximum (FWHM) of the specific energy peak corresponds to its resolution. The resolution defines the ability of the detector to distinguish between two adjacent energy peaks, allowing for clear radionuclide identification. The resolution is directly proportional to the energy of the gamma rays. The HPGe detector has a very good resolution as compared to other detectors like the NaI (Tl) scintillation detector. The efficiency gives an indication of the radiation percentage that is detected by a particular detector from the total yield that is emitted from the source into a solid angle of 4π in the photo-peak [Keyser and Hensley, 2002]. The efficiency represents how well the detector counts all the gamma rays emitted from the source or how well the detector reads all the gamma rays that are incident on the detector. The intrinsic efficiency of the detector is given by equation 2.17 [Stratton, 2011].

$$\varepsilon_{int.} = \frac{\text{number of pulses recorded}}{\text{number of radiation quanta incident on the detector}} \quad (2.17)$$

where, $\varepsilon_{int.}$ is the detector's intrinsic efficiency. The sensitivity of the detector is dependent on its thickness and diameter. Its thickness also directly impacts the energy beyond which the efficiency sharply begins decreasing. It has been noted that efficiency decreases exponentially as the gamma ray energy increases. It has also been seen that the HPGe detector has a lower detection efficiency when compared to the NaI (Tl) detector. The HPGe is therefore efficient for detecting nuclides possessing lower energy but not nuclides possessing higher energy [Hossain, Sharip and Viswanathan, 2012].

2.11 Heavy metal detection instruments

Various analytical techniques may be utilized in heavy metal detection. Neutron Activation Analysis (NAA), Proton Induced X-Ray Emission Spectroscopy **(**PIXE), Inductively Coupled Plasma-Mass Spectrometry (ICP-MS) and X-Ray Fluorescence Spectroscopy (XRF) are some of the analytical techniques. The PIXE non-destructive technique utilizes a beam of energetic ions that are generated by an accelerator, producing protons within the 2-5 MeV range that generates vacancies in the inner electron shell. One of the inner shell electrons from the sample to be measured is ionized, yielding an inner shell vacancy [Mihalić et al., 2016]. Outer shell electrons would then fill the inner shell vacancies through the process of electron transition, leading to the emission of characteristic X-rays that identify with particular elements.

As a non-destructive technique, NAA may involve the irradiation of the sample with neutrons within a nuclear reactor for quantitative analysis of the major and trace elements. XRF is another non-destructive technique that yields characteristic X-rays when electrons from the outer shells of an atom fill in shell electron vacancies. X-rays knock off inner shell electrons to ionize the atom, thereby creating vacancies. By analyzing the resulting gamma rays based on the respective energies, this allows for the identification of heavy metal elements as well as their respective concentrations [Kamunda, 2017]. In this research, ICP-MS was used for the analysis of heavy metals in environmental samples.

2.12 Inductively Coupled Plasma-Mass Spectrometry

An ICP-MS system comprises two components being the ICP system and the MS system. The ICP system uses a nebulizer to atomize the liquid sample into plasma. The liquid sample is mixed with argon that rotates when it comes in contact with the sample. The primary use of the mass spectrometry (MS) system is the separation of different isotopes [Jarvis, 2006]. Figure 2.7 shows the various components of the ICP-MS system.

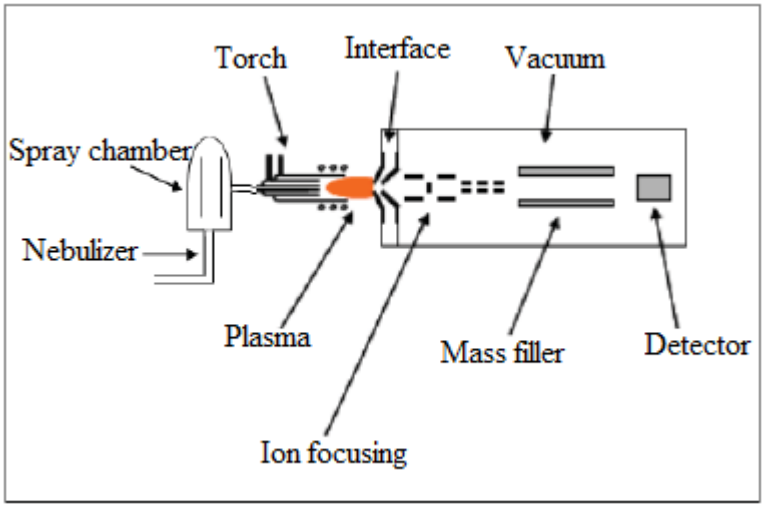

Fig. 2 - 7: ICP-MS system components [IAEA, 2005; Kamunda, 2017]

The sample introduction system is the first component of the ICP-MS. It comprises of a nebulizer as well as a spray chamber that turn liquid samples into argon plasma as fine aerosol droplets. The high velocity stream of argon gas functions by breaking the liquid sample into smaller droplets which are then injected into the spray chamber by the gas stream. The next component is the ICP torch with the RF coil, a combination that generates the argon plasma. The plasma produces a very high temperature (6000 K - 10000 K) environment for atoms, ions and electrons. Many elements transition from the atomic to the ionic states at these elevated temperatures as there is enough energy to completely dislodge their outer shell electrons [Jarvis, 2006]. The plasma dehydrates the aerosol, detaches the molecules as well as dislodges electrons from the components. This leads to the formation of singly-charged ions that are then directed into a mass-filtering unit known as the mass spectrometer. The Interface then links the ICP ion source to the high vacuum mass spectrometer. Within the interface, ions produced in the plasma are removed and introduced to the mass spectrometer as an ion beam. A high vacuum is required for the ion optics, quadrupole, and detector to operate [Johnson, Hadjar and Laskin, 2011].

The mass spectrometer functions as a mass sieve for sorting ions using their mass-to-charge ratios. The MS system has an electric field and magnetic field attached perpendicular to each other in order to bend the ions as they enter the system. As the ions exit the mass spectrometer, they first hit the dynode in an electron multiplier, which also functions as the detector. As individual ions exit the quadrupole, they are counted by the detector. The resulting stream of electrons gets amplified into a measurable pulse. The last section is the data handling and system controller whose function is to control all instrument control aspects and data handling to achieve concluding concentration results [Neetu, 2012].

Chapter 3: Materials and methods

This chapter presents information on the location and geology of the study area. The samples used, sample preparation, sample analysis using both gamma spectroscopy and ICP-MS are also explained. Radiological hazard assessment and related functions are also done in this section. Carcinogenic and non-carcinogenic risk assessment of heavy metals in samples from the study area is also explained.

3.1 Materials

Various equipment and resources were utilized for successful completion of this work. 1 litre plastic containers, polythene bags, hand auger, 1M HNO_3 as well as an instrument with Global Positioning System (GPS) functionality were particularly vital in carrying out this study. Natural radionuclides were analyzed using a gamma spectroscopy system at the Centre for Applied Radiation Science and Technology (CARST) based within North-West University (Mafikeng Campus). Heavy metal analysis was perfomed at Eco-Analytica Laboratories in Potchefstroom. RESRAD software was also a very useful tool.

3.2 The study area

The study area comprises of Morupule-B coal thermal power station and its surroundings. Morupule-B coal thermal power station is situated in the Botswana village of Morupule. Morupule-B coal thermal power station is a 600 MW coal plant situated approximately 5km from Palapye town and consisting of four (4) units each with a capacity of 150 MW. Figure 3-1 is a google map that shows the position of Morupule-B coal thermal power station in Botswana, located at the GPS coordinates 22.522˚S 27.050˚E. The power station lies approximately 280km to the north of Gaborone. Figure 3-2 presents an aerial view of Morupule-B coal power station. There are several farms within the study area that are utilized as grazing land for livestock such as goats, sheep and cattle. Some farms in the area also grow field crops like maize, beans and sorghum. Some residents and non-residents collect firewood from the study area for household use, while others sell it to earn income [Shumba Energy, 2017].

Fig. 3 - 1: Google map indicating the position of Morupule-B Coal Thermal Power Station [http://www.earth.google.com, Accessed April 26, 2019]

Fig. 3 - 2: Aerial view of Morupule-B Coal Thermal Power Station [http://www.earth.google.com, Accessed April 26, 2019]

3.2.1 Meteorology, geology and vegetation of the study area

The study area includes the upper catchment area of the Lotsane river, an ephemeral river that drains eastwards to Limpopo river. Lotsane river rises from Spring lines originating at the base of the sandveld escarpment and to the west is where the Lotsane river begins. The study area lies on an altitude of approximately 950m above sea level [Shumba Energy, 2017]. The study area has a southeast topographic gradient that is basically sloping towards Palapye, a town situated about 5 km away. Lotsane river begins about 30km away in Serowe running from west to east. The study area also includes Morupule river, which also is an ephemeral river. The typical climate in the study area is semi-arid regions with relatively cold and dry winters as well as hot and wet summers. The most prevalent wind directions at the power station are mostly in the eastern and north-eastern direction, while temperatures show major seasonal and daily variations [Shumba Energy, 2017].

The Morupule area geology comprises of the Ecca and Dwyka group strata from the Karroo Super group that consists predominantly of mudstone and shale, with subordinate amounts of siltstone, coal, sandstone and tillite. The structure of the area is relatively complex with a predominant fault pattern which trends

NNW-SSE and which is mimicked by the dolerite dyke pattern. Secondary faults with NW-SE and NE-SW orientation are also present [Shumba Energy, 2017]. The study area comprises mainly of two commonly widespread vegetation types being Burkea/ *Ochna savanna* and *Acacia erioloba savanna* [Ecosurv, 2016].

3.3 Sample collection

A very important point to understand in environmental sampling is that the collected samples should adequately represent the area being studied. The entire investigation site cannot be collected for analysis [Mouandza et al., 2018]. Representative sampling helps to safeguard the environment such that the generated data may be used as a reliable database encouraging compliance to regional and national laws or regulations and may be used for effective emergency response [IAEA, 2004]. There are two basic methods that are commonly used in environmental sampling namely random or probabilistic sampling and systematic sampling. The probabilistic method is done in a random manner with no prior knowledge of the research area while the systematic method requires prior knowledge of the radioactivity distribution in the study area [Mouandza et al., 2018]. Random sampling involves the arbitrary sample collection procedure within some defined boundaries from the study area possibly using a random number table such that all locations from the sampling area would have an equal probability of being chosen. In systematic sampling, the study area is divided utilizing triangular, square or herringbone grids such that samples are collected from the intersections of the grid lines [IAEA, 2004].

Representative water, soil, coal, bottom ash as well as fly ash samples were taken from the study area through the random sampling method since prior knowledge of the research area was unavailable. All sampling for this work was done at two different times in June 2017 and February 2018 respectively. Fifty-five (55) soil samples and eight (8) water samples were taken from the environs of Morupule-B Coal Thermal Power Station. Twelve (12) coal samples, twelve (12) bottom ash and twelve (12) fly ash samples were taken within the power station area such that coal samples were taken at the coal stockpile area while the bottom ash and fly ash samples were taken at the bottom ash and fly ash areas respectively. Figure 3-3 is a general sampling map for Morupule-B Coal Thermal Power Station and its surroundings, showing the area from which water, soil, coal, fly ash as well as bottom ash samples were collected. Figure 3-4 zooms into Figure 3-3 by showing the more detailed water sampling points on A1 road from Palapye to Gaborone. Figure 3-5 further zooms into Figure 3-3 by showing the more detailed water sampling points on A14 road from Palapye to Serowe. Figure 3-6 shows the various soil sampling points on A1 road along Lotsane river. Figure 3-7 shows the various soil samples collected along Morupule river. Figure 3-8 also zooms into Figure 3-3 by showing the aerial view of coal and bottom ash storage areas within the power station area. Each sample was properly labelled with a unique sample code and the respective GPS coordinates recorded in a log book. All samples were transported to the CARST laboratory for additional processing.

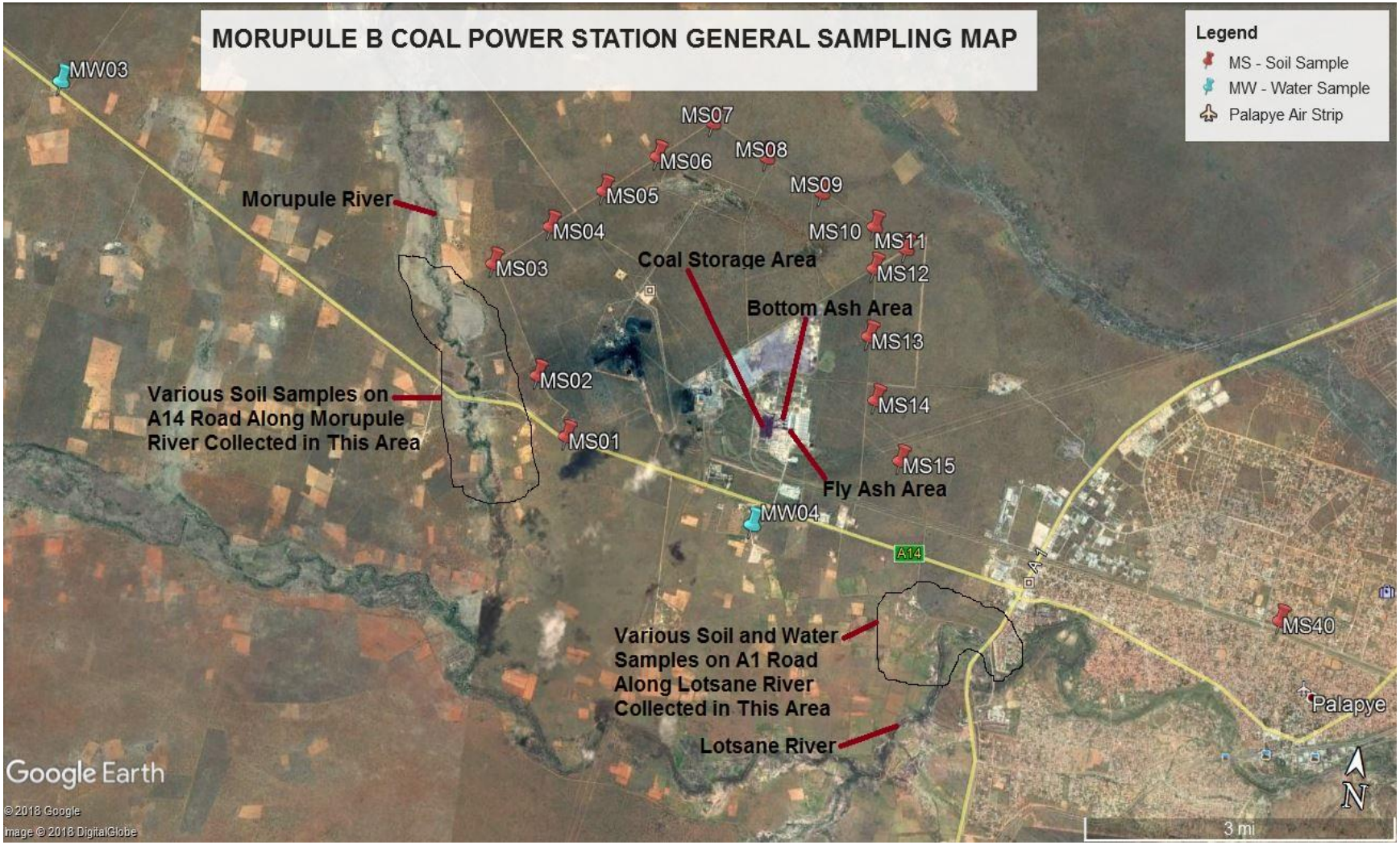

Fig. 3 - 3: General sampling map for Morupule-B Coal Thermal Power Station [http://www.earth.google.com, Accessed September 18, 2018]

Fig. 3 - 4: Water sampling points on A1 road from Palapye to Gaborone [http://www.earth.google.com, Accessed October 16, 2018]

Fig. 3 - 5: Water sampling points on A14 road from Palapye to Serowe [http://www.earth.google.com, Accessed November 26, 2018]

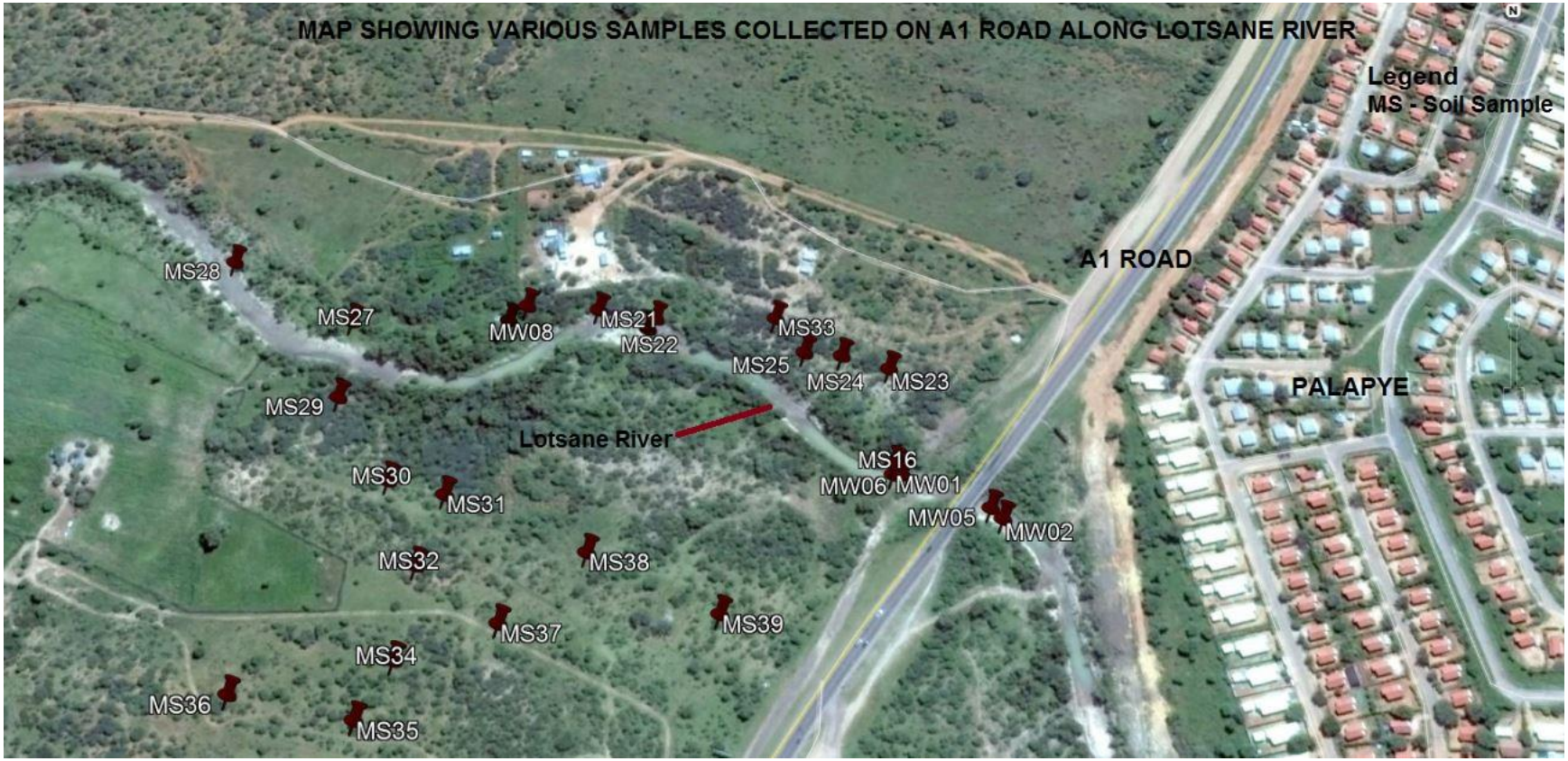

Fig. 3 - 6: Various soil sampling points on A1 road along Lotsane river [http://www.earth.google.com, Accessed November 26, 2018]

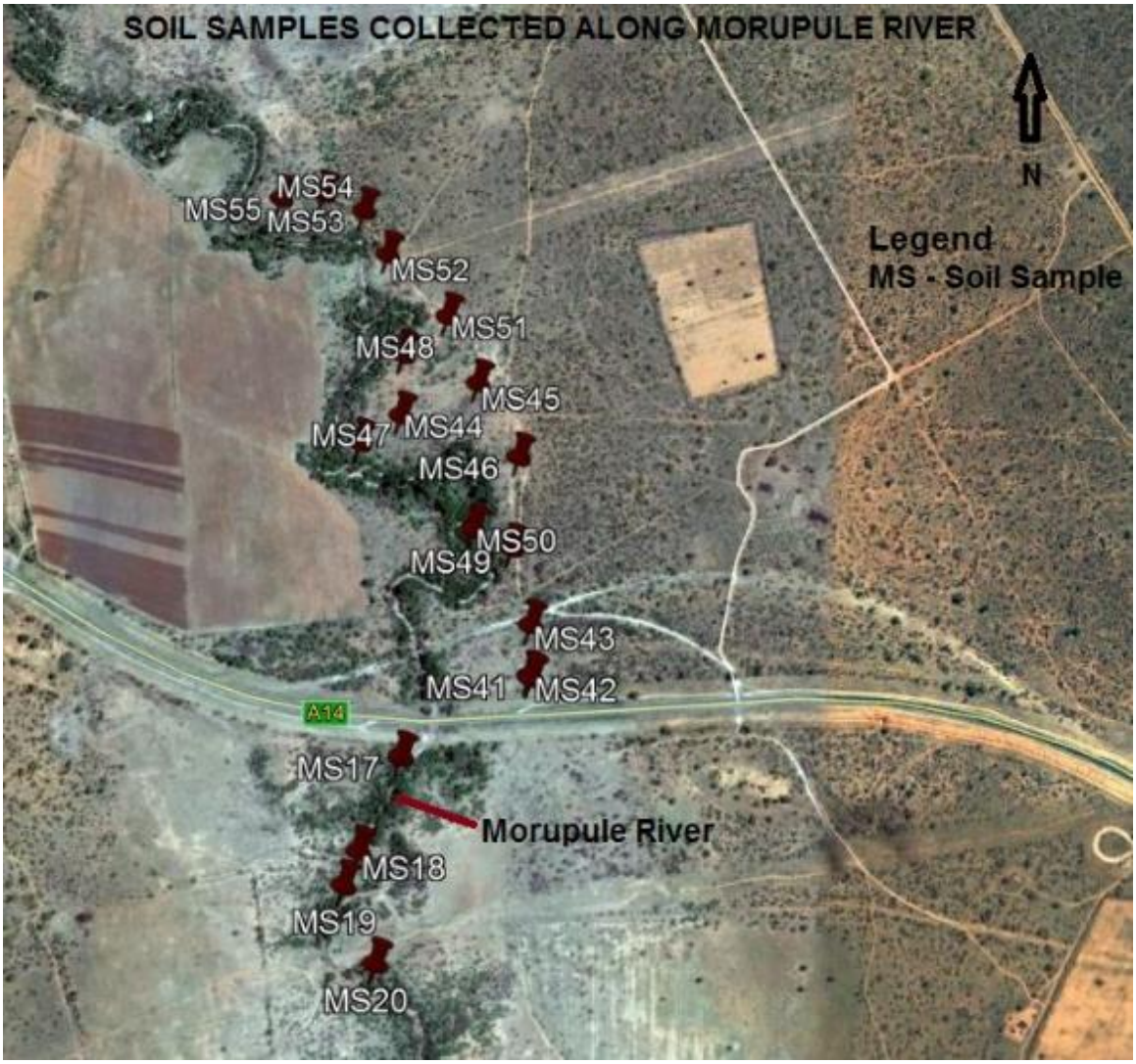

Fig. 3 - 7: Various soil samples collected along Morupule river [http://www.earth.google.com, Accessed November 15, 2018]

Fig. 3 - 8: Aerial view of the coal and bottom ash storage areas [http://www.earth.google.com, Accessed October 26, 2018]

3.3.1 Water sample collection

A total of eight (8) drinking and waste water samples from points in the study area were collected into polyethylene bottles. All the polyethylene bottles, each of approximately two litres volume, were then tightly sealed with a lid. The polyethylene bottles had been previously rinsed using a 0.1M dilute hydrochloric acid (HCl) to reduce contamination. Any suspended sediments and coarse material were removed by filtering the samples through a 0.45 µm filter paper. The collected water samples were then spiked with 1M HNO_3 before being sealed as a way to prevent the adsorption of radionuclides onto the internal surface of the polythene container walls [Martin and Hancock, 1992; Moulton-Meissner et al., 2015].

3.3.2 Soil, bottom ash, fly ash and coal samples collection

A total of fifty-five (55) soil samples from varying and undisturbed areas were collected by a hand auger from a 5cm depth and packaged into polythene bags. No soil samples were collected from inside the power station area. A total of twelve (12) coal samples from different points of the coal stockpile area within the power station were collected using a shovel and packaged into polyethylene bags. A total of twelve (12) bottom ash samples from different points of the bottom ash storage area within the power station were collected using a shovel and packaged into polyethylene bags. A total of twelve (12) fly ash samples from different points of the fly ash area within the power station were collected using a shovel and packaged into polyethylene bags [IAEA, 1989].

3.4 Samples preparation

Sample preparation is recognized as the major source of error and should be done properly, otherwise it may affect the final results [Plebani, 2012]. The sample preparation process was done carefully to avoid cross contamination, radionuclide loss and heavy metal loss. At CARST laboratory, the soil, coal, bottom ash as well as fly ash samples were initially spread onto clean plastic trays and air dried for several days as required. They were then dried to remove moisture and reduce to a constant weight in an oven at 105 °C for 3 hours [Faanu, 2011]. The soil and coal samples were only dried as above after being crushed into small grain sizes using mortar and pestle as well as an electric grinder.

The soil, coal, bottom ash as well as fly ash samples were subsequently sifted using a 2 mm sieve to attain a homogenous sample matrix [IAEA, 1989]. They were then transferred into previously weighed 1 L Marinelli beakers. The Marinelli beakers with the contents were then sealed for 28 days before gamma spectrometry measurements. This sealing was done to accomplish secular equilibrium between

the ^{226}Ra and its daughter nuclide ^{222}Rn [Faanu, 2011; Kamunda, 2017]. A small amount, about 1g of each of the above samples, was also packaged and sealed into a clean plastic vial for ICP-MS analysis. About 5ml for each of the collected eight (8) water samples was also packaged and sealed into clean plastic vials for ICP-MS analysis. After the 28-day period, radionuclide detection and measurements were performed on the sealed 1L Marinelli beakers. A gamma spectroscopy system consisting of a High Purity Germanium detector (HPGe) was utilized for this purpose.

3.5 Analytical methods

Activity concentration measurements in soil, coal, bottom ash as well as fly ash samples were performed using gamma spectrometry coupled to an HPGe detector. ICP-MS was utilized to perform heavy metal concentration measurements in water, coal, bottom ash, soil and fly ash.

3.5.1 Gamma spectrometry

The High Purity Germanium detector was supplied by Canberra Industries. Before any sample measurements were done, energy and efficiency calibration of the HPGe detector were carried out. Each soil, coal, bottom ash and fly ash sample was measured for 12 hours. The counting as well as analysis of spectra was computer-controlled utilizing GENIE 2000 software from Canberra Industries [Kamunda, 2017]. The activity concentration of ^{238}U can not be determined directly from its own gamma emissions and therefore, its daughter nuclides, ^{234}Th and ^{234m}Pa were used. The activity concentration was determined from the weighted mean of the activities determined from the 63 keV and 92.6 keV gamma lines of ^{234}Th and the 1001 keV gamma line of ^{234m}Pa. The activity concentration of ^{226}Ra was determined through the weighted mean of the 295.2 keV and 351.9 keV gamma-ray energies of ^{214}Pb and 609.6 keV, 1120.3 keV and 1764.5 keV gamma-ray energies from ^{214}Bi. The activity concentration of ^{232}Th was estimated using the weighted mean activity concentrantrations from 238.6 keV of ^{212}Pb and 338.3 keV, 911.6 keV and 969.1 keV for ^{228}Ac. The activity concentration of ^{40}K was determined from its 1460.8 keV gamma-ray line [Kamunda, 2017]. All these measurements were performed at CARST laboratories located within the premises of North West University (Mafikeng Campus).

3.5.1.1 Energy calibration for gamma spectrometry

Calibration was performed on the high resolution gamma spectrometry system using an HPGe (High Purity Germanium Detector) for energy and efficiency using a mixed radionuclides standard in 1L Marinelli beaker. To perform the daily HPGe detector energy calibration, the gamma-ray energy peaks from the reference standard spectrum and spectrometer channel number were matched [Baum et al.,

2002; Wahl, 2007]. Details of the energy calibration source are given in Appendix 1. At lower energies, the HPGe detector material mostly interacts with gamma rays through photoelectric absorption giving full energy peaks. Compton scattering and pair production are also very significant when gamma rays interact with the detector material [Santawamaitre, 2012]. A calibration curve featuring Energy vs. Channel Number was produced from the recorded centroid channels and their corresponding radionuclide energy peaks. A calibration curve in polynomial format was generated using the least square curve fitting method as shown in equation 3.1 [Yücel et al., 2003].

$$E_i = \sum_0^N a_n C_i^{\,n} \tag{3.1}$$

where, E_i denotes the calibration energy of the ith channel number, the summation runs from n = 0 to n = N, C_i denotes the ith channel number and a_n denotes the calibration constant [Yücel et al., 2003]. To perform the calibration, counting of standard radionuclides shown in Appendix 1 as well as gamma-ray energy peaks from 60 keV to 2000 keV was done. The standard was counted for 12 hours using the HPGe detector. The energy calibration resulted in the fitted polynomial shown in Figure 3-9.

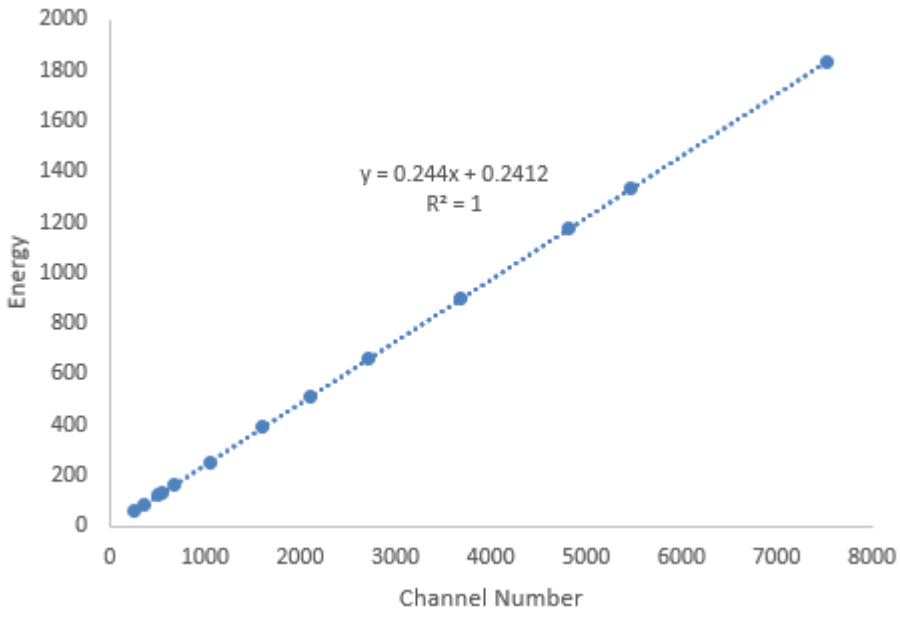

Fig. 3 - 9: Energy calibration curve

3.5.1.2 Efficiency calibration for gamma spectrometry

Section 2.10 has earlier on given a preview on detector efficiency. The HPGe detector was calibrated for efficiency so as to ensure the correct quantification of radionuclides that were present in the collected samples [Barrera et al., 2017]. For the efficiency calibration, Efficiency was plotted against Energy giving rise to polynomial. During the efficiency calibration, the peak search algorithm was useful to find

and quantify peaks before associating them with decay-corrected emission rates for each line. An efficiency plot and equation were therefore determined through the process, yielding an efficiency curve as high as a polynomial of the third order. It was important to ensure that all detector adjustments are done before determining the efficiencies and this was maintained until a new calibration was carried out [Faanu, 2011]. The general HPGe detector trend shows that its efficiency increases to a maximum and then decreases with energy [Kshetri, 2012]. The same radionuclides standard shown in Appendix 1 was used to perform the energy and efficiency calibration of the HPGe detector, such that the standard was counted at a number of calibration points between 60 keV to 2000 keV [Luca et al., 2012]. Figure 3-10 shows the efficiency calibration curve.

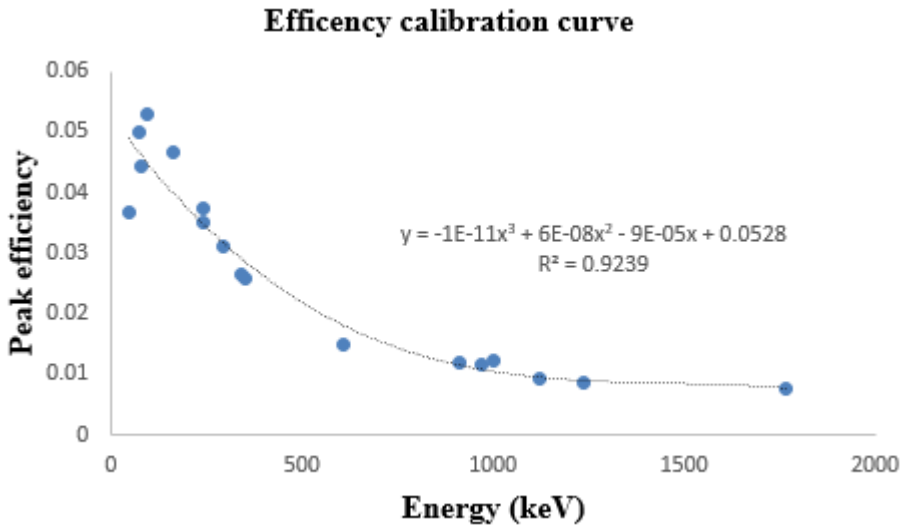

Fig. 3 - 10: Efficiency calibration curve

3.5.1.3 Activity concentration calculations

Equation 3.2 was used to determine the activity concentrations of ^{40}K, ^{238}U and ^{232}Th in soil, coal, bottom ash as well as fly ash samples [IAEA, 2004].

$$A = \frac{N}{\varepsilon_f P_\gamma t_s m\ K} \tag{3.2}$$

such that,

N = corrected net peak area for the analogous full energy peak

$N = N_S - N_B$

N_S = net peak area from the spectrum of the sample

N_B = analogous net peak area from the background spectrum

ε_f = the efficiency corresponding to the photo peak energy

t_S = lifetime (seconds) corresponding to the sample spectrum collection

m = mass corresponding to the measured sample in kg

P_γ = respective peak energy analogous to a specific gamma-ray emission probability

K = correction factor

$$K = K_1 . K_2 . K_3 . K_4 . K_5 \tag{3.3}$$

K_1 is the correction factor [IAEA, 2004] for the nuclide decay from the sample collection time to the commencing of the measurement as seen in equation 3.4:

$$K_1 = exp\left[-\frac{ln2\Delta t}{T_{1/2}} \right] \tag{3.4}$$

where Δt denotes the elapsed time since the commencing of the measurement and $T_{1/2}$ denotes the half-life.

K_2 signifies the correction factor [IAEA, 2004] corresponding to the nuclide decay within the duration of counting as seen in equation 3.5:

$$K_2 = \frac{T_{1/2}}{ln2.t_s}\left[1 - exp\left[-\frac{ln2.t_s}{T_{1/2}} \right] \right] \tag{3.5}$$

where t_S (seconds) denotes the real time corresponding to the sample spectrum collection.

K_3 is the correction factor due to self-attenuation within the measured sample in relation to the calibration sample. K_3 signifies a quotient of the full energy peak efficiency $\varepsilon\,(\mu, E)$ for a sample with the linear attenuation coefficient μ to the full energy peak efficiency $\varepsilon\,(\mu_{ref}, E)$ for a sample with the linear attenuation μ_{ref}.

$$K_3 = \frac{\varepsilon(\mu, E)}{\varepsilon(\mu_{ref}, E)} \tag{3.6}$$

K_3 = 1 for a scenario in which the matrices for both the measured sample as well as the calibration sample are similar. For a pulse sampling cycle in which the detector absorbs two or more photons, the

summation of at least two energies is documented in place of at least two unlike signals. Full energy photons that are added to additional pulses are not documented as part of the single photon peak thus signifying a loss in efficiency or counts such that any loss count is determined by the rate. Random summation results in a correction factor (K_4) for pulses loss as shown in equation 3.7 [IAEA, 2004]:

$$K_4 = exp(-2R\tau) \tag{3.7}$$

where τ the resolution time of the measurement system and R is the mean count rate. For low count rates this correction factor could be taken as 1. K_5 is the coincidence correction factor for those nuclides decaying through a range of successive photon emissions. If the nuclide has no cascade of gamma-rays then, K_5 =1. The corresponding propagated uncertainty for the activity concentration is given by the formula in Appendix 29.

3.5.1.4 Uncertainty estimation

There is an uncertainty associated with each measurement that has to be identified and quantified [Faanu, 2011]. Systematic and random uncertainties quantify the doubts associated with measurements. Factors such as environmental conditions contribute to these uncertainties. For every measurement, random uncertainties are always present. Random uncertainties are detectable through repeat measurements, but it is impossible to eliminate them. Systematic uncertainty remains constant for a series of measurements and may be difficult to detect. Systematic uncertainty may be due to an instrument being out of calibration, or due to an experimental setup differing from actual theory. Therefore, it is crucial to quote every measurement with its uncertainty and confidence level [Bell, 1999]. Equations from Appendix 29 are used to calculate the uncertainties for quantities such as activity concentration in this work.

3.5.1.5 Lowest level of detection

The lowest radioactivity quantity that can be measured at specific conditions is known as the lowest level of detection (LLD) [Faanu, 2011]. The Detection limit is the minimum number of counts that should be measured from a sample in order to ensure a 95% probability for the true net counts to reach the critical level [Santawamaitre, 2012]. According to Currie, the detection limit (L_D) is represented by equation 3.8.

$$L_D = 2.706 + 4.653\sigma_{N_B} \tag{3.8}$$

where σ_{N_B} denotes the standard deviation of the number of counts for a blank sample. The minimum or lowest detectable activity (MDA) is a performance criterion for gamma spectrometry [Currie, 1968] such

that its value depends on both the L_D as well as the efficiency of a counting system. Equation 3.9 calculates the MDA.

$$MDA = \frac{L_D}{\varepsilon_f P_\gamma T} \tag{3.9}$$

where ε_f denotes the absolute efficiency, $P\gamma$ represents the gamma ray yield while T is the measurement time in seconds. The minimum detectable activities (MDA) in Table 3-1 were estimated for ^{238}U, ^{232}Th and ^{40}K with values obtained as 0.13 Bq, 0.13 Bq and 0.12 Bq respectively at the 95% confidence level.

Table 3 - 1: Lowest detectable activities for ^{40}K, ^{232}Th and ^{238}U

Nuclide	Lowest level of detection
^{238}U	0.13
^{232}Th	0.13
^{40}K	0.12

3.5.2 Inductively Coupled Plasma-Mass Spectrometry

ICP-MS analysis was utilized to perform toxic heavy metal analysis for water, bottom ash, soil, coal and fly ash. ICP-MS is useful in the quantitative determination of several elements [Helaluddin et al., 2016]. Prior to being analyzed by the ICP-MS system, the soil, bottom ash, coal and fly ash samples were initially digested by means of a microwave system as explained in the next section.

3.5.2.1 Microwave digestion

Digestion is performed so as to extract the toxic heavy metals from the soil, fly ash, coal and bottom ash samples. A gram of individually measured dry soil samples as well as 9 mL hydrochloric acid and 3 mL nitric acid were all mixed in a rotor container, with approximately 1 mL hydrogen peroxide being subsequently added to the reaction vessel. The contents were subsequently digested for 45 minutes at 120 ^{o}C. After cooling, the digested contents were then added into 100 mL volume volumetric flasks containing 2 % nitric acid. Distilled water was subsequently utilized in topping up the 100 mL volumetric flask [Kamunda, 2017; Mathuthu et al., 2016]. After sedimenting overnight, the digested contents were sieved using No. 40 whatman filter paper.

Each 5 mL nitric acid, 1 mL hydrochloric acid as well as 5 mL water sample were poured into a rotor vessel containing 1 mL hydrogen peroxide [Kamunda, 2017]. The mixture was again digested following the same procedure as that of fly ash, coal, soil and bottom ash samples.

3.5.2.2 ICP-MS measurements

The TotalQuant method was utilized in enabling drift and contamination detection while also simultaneously increasing the results accuracy. The Perkin Elmer Pure Plus NexION Dual Detector Calibration Solution standard was used. The TotalQuant calibration was attained utilizing 200 micrograms per litre of Ce, Cu, Mn, Al, Ba, Co, U, Ni, In, Li, Mg, Zn, Tb, and Pb [Kamunda et al., 2016]. The standard, blank solution and replicate samples were analyzed simultaneously in adherence to the quality control process. Arsenic, lead, mercury, cadmium, chromium, cobalt, nickel, copper and zinc were the toxic heavy metals of interest. With the use of equation 3.10, the ICP-MS heavy metal concentration results of mg/L were subsequently changed to mg/kg for solid samples [Kamunda et al., 2016].

$$\frac{(a-b)*v}{w} mg/L \tag{3.10}$$

where

a = toxic heavy metal concentration for the sample in mg/L;

b = toxic heavy metal concentration for the blank in mg/L;

v = total volume of the digest in mL

w = weight of soil sample (g).

Some major elements used for the blank (background, distilled water) in this work were As, Pb, Hg, Cd, Cr, Cu, Zn, Co and Ni. Samples were basically analyzed using the ICP-MS system for the determination of heavy metals. The PerkinElmer NexION Dual Detector comprises of various elements including Bi, Cd, Pb, As, Cr, Co and others that were utilized in calibrating the ICP-MS system. This was achieved through the addition of similar amounts of different elements into different vials. The various vials were then analyzed through ICP-MS to subsequently generate a calibration curve. Unknown concentrations of samples for each sample were subsequently estimated through the comparison of measured counts for a specific isotope to an external calibration that was previously generated for that element [O'Sullivan et al., 2013].

3.6 Radiological risk assessment

In this section, the radiation dose is assessed. This section focuses on the absorbed dose rate in air (D), the annual effective dose equivalent (AEDE), the radium equivalent activity $\left(Ra_{eq}\right)$ and the external hazard index $\left(H_{ex}\right)$.

3.6.1 Absorbed dose rate in air (D)

For the assessment of any radiological hazard, the radiation exposure due to radionuclides present in the soil, coal, bottom ash and fly ash samples can be determined in terms of many parameters. The direct link between activity concentrations of natural radionuclides and their exposure is referred to as the absorbed dose rate in air at a height of 1 metre above the ground [Alashrah and El-Taher, 2016]. The mean activity concentrations of ^{232}Th, ^{40}K and ^{226}Ra in soil, fly ash, coal and bottom ash were utilized to determine the absorbed dose rate in air at a height of 1m using equation 3.11 [Chang et al., 2008].

$$D(nGyh^{-1}) = 0.462 \times A_{Ra} + 0.604 \times A_{Th} + 0.0417 \times A_K \quad (3.11)$$

where D is the absorbed dose rate in $nGyh^{-1}$; A_{Ra}, A_{Th} and A_K are the activity concentrations of ^{226}Ra, ^{232}Th and ^{40}K respectively. All dose coefficients, in units of $nGyh^{-1}$ per $Bq.kg^{-1}$ were extracted from the UNSCEAR 2000 report [UNSCEAR, 2000].

3.6.2 Annual effective dose equivalent (AEDE)

The absorbed dose rate in air at 1 metre above the ground does not directly give the radiological risk that an individual is exposed to [Ndontchueng et al., 2014]. The absorbed dose can be deliberated in terms of the annual effective dose equivalent (AEDE) from outdoor terrestrial gamma radiation which is converted from the absorbed dose by taking into account the conversion coefficient from absorbed dose in air to effective dose as well as the outdoor occupancy factor. Equation 3.12 gives the annual effective dose equivalent [UNSCEAR, 2000].

$$AEDE\left(\mu Sv.y^{-1}\right) = D\left(nGy.h^{-1}\right) \times 8760h \times 0.2 \times 0.7\left(Sv.Gy^{-1}\right) \times 10^{-3} \quad (3.12)$$

UNSCEAR 2000 report gives 0.7 $Sv.Gy^{-1}$ for the conversion coefficient from absorbed dose in air to effective dose received by adults and 0.2 for the outdoor occupancy factor.

3.6.3 Radium equivalent activity (Ra_{eq})

The activity levels of the natural radionuclides ^{226}Ra, ^{40}K and ^{232}Th in soil, coal, bottom ash and fly ash samples can be evaluated using a radiological index known as the radium equivalent activity (Ra_{eq}). This is also possible since there is a non-uniform distribution of natural radionuclides in soil, coal, bottom ash and fly ash samples. (Ra_{eq}) is the most widely used index to assess radiation hazards and is computed using equation 3.13 [Beretka and Mathew, 1985]. It estimates that 370 $Bq.kg^{-1}$ of ^{226}Ra, 259 $Bq.kg^{-1}$ of ^{232}Th and 4810 $Bq.kg^{-1}$ of ^{40}K produce the same gamma-ray dose rate.

$$Ra_{eq}\,(Bq.kg^{-1}) = A_{\mathrm{Ra}} + 1.43A_{\mathrm{Th}} + 0.077A_{\mathrm{K}} \tag{3.13}$$

The maximum allowed value of the radium equivalent activity is 370 $Bq.kg^{-1}$, corresponding to an effective dose of 1 mSv for the general public [Nguelem, Ndontchueng and Motapon, 2016].

3.6.4 External Hazard Index (H_{ex})

The external hazard index (H_{ext}), as shown in equation 3.14 [Faanu, 2011], was introduced so as to limit the radiation exposure from natural radionuclides to the maximum allowed value of 1 $mSv.y^{-1}$.

$$H_{ext} = A_{\mathrm{Ra}}/370 + A_{\mathrm{Th}}/259 + A_{\mathrm{K}}/4810 \leq 1 \tag{3.14}$$

To keep the radiation hazard insignificant, the value of the external hazard index must not exceed unity, value of H_{ext} corresponds to the upper limit of radium equivalent activity of 370 $Bq.kg^{-1}$ [Abdel-Rahman and El-Mongy, 2017].

3.7 Determination of radiation dose and risk using RESRAD code

Several parameters in this study were used as inputs to the RESRAD-OFFSITE (3.2). Residents (public members) in the vicinity of the power station were selected as a critical receptor for this particular assessment of risk. Parameters were cautiously chosen with the viewpoint of yielding representative risk and dose estimates. As and when necessary, some site-specific parameters were used to replace the default parameters. Some of the input parameters for the model included ^{238}U, ^{232}Th and ^{40}K as well as meteorological data such as wind direction and speed. Hydrogeological parameters such as the hydraulic conductivity and soil density were also considered. Other hydrological data including precipitation rate, irrigation rate, field capacity, erosion rate, total porosity, runoff coefficient as well as other soil-specific factors were determined according to the condition of the site under study [Yu et al., 1993]. The major

exposure pathways include dust inhalation, direct contact with the soil radionuclides as well as the intake of contaminated water, soil and vegetables. Dietary data for soil, vegetables and water as well as the soil ingestion rate, inhalation rate and distribution coefficient for radionuclides from the South African National Nuclear Regulator [NNR, 2013] were used. The in-built RESRAD radionuclides library was used in this assessment. Table 3-2 presents a synopsis of some parameters that were utilized.

Table 3 - 2: RESRAD summary of input parameters

Quantity	**Value**	**Details**
Contaminated area in m^2	78×10^6	Mean estimated area
Contaminated area thickness in m	0.150	Mean estimated area
Mean ^{238}U, ^{40}K and ^{232}Th soil activity concentrations	From Table 4-1	Data from measurements
Contaminated area erosion rate in m/y	0.001	Default value for RESRAD [Yu et al., 1993]
Contaminated area density in g/m^3	1.440	Sandy loam soil [Yu et al., 1993]
Depth of cover in m	0.000	Zero cover depth for radionuclides
Contaminated area field capacity	0.200	Default value for RESRAD [Yu et al., 1993]
Overall porosity for contaminated area	0.430	Sandy loam soil [Yu et al., 1993]
Evapotranspiration factor	0.500	Default value for RESRAD [Yu et al., 1993]
Rainfall rate in m/y	1.000	Comparatively humid location [Yu et al., 1993]
Contaminated area hydraulic conductivity in m/y	1.090×10^3	Sandy loam soil [Yu et al. 1993]
Irrigation rate	0.200	Default value for RESRAD [Yu et al., 1993]
Exponential b factor specific to soil	4.900	Sandy loam soil [Yu et al., 1993]
Rate of inhalation rate in m^3/y	8059.2	Republic of South Africa [NNR, 2013]
Runoff coefficient	0.650	Moderately steep residential region
Rate of leaching	0.000	Default value for RESRAD [Yu et al., 1993]
Mean yearly speed of wind in m/s	5.000	For particular area [Hagemann, 2013]
Ingestion rate for soil in g/y	37	Republic of South Africa [NNR, 2013]
Period of exposure in years	30	Default value for RESRAD [Yu et al., 1993]
Fraction of time spent onsite Indoor Outdoor	 0.000 0.100	For South Africa [NNR, 2013]
Fraction of time spent offsite Indoor Outdoor	 0.800 0.100	For South Africa [NNR, 2013]
Uranium distribution coefficient, K_d, in cm^3/g	-200	Republic of South Africa [NNR, 2013]
Potassium distribution coefficient, K_d, in cm^3/g	5.500	Default value for RESRAD [Yu et al., 1993]
Thorium distribution coefficient, K_d, in cm^3/g	-60000	Default value for RESRAD [Yu et al., 1993]
Rate of drinking water in L/y	600	Republic of South Africa [NNR, 2013]

3.8 Risk assessment due to heavy toxic metals

Heavy metals pose a potential risk through contaminated water, soils and plants. The risk is calculated according to recommendations from several publications [Kamunda, 2017; USEPA, 1989; USEPA, 1991; USEPA, 2001; USEPA, 2004; USEPA, 2007; USEPA, 2011a]. The average daily intake (ADI) through different pathways in mg/kg-day was determined using equations 3.15 to 3.18 as recommendedby USEPA [USEPA, 1989]. For the ingestion of heavy metals through soil and water and plants, the average daily intake ADI_{ing} (mg/kg-day) is calculated through equation 3.15 [Kamunda, 2017].

$$ADI_{ing} = \frac{C \text{ x } IR_{ing} \text{ x } EF \text{ x } ED}{BW \text{ x } AT \text{ x } 10^6} \tag{3.15}$$

where C represents the toxic heavy metal concentration (mg/kg) for soil and plants and in mg/L for water. IR_{ing} denotes the ingestion rate in mg/day, EF represents the frequency of exposure (days/year), ED represents the duration of exposure (years), BW denotes the body weight for the exposed person (kg), AT denotes the duration for averaging the dose (days) and the conversion factor (kg/mg) is 10^6. For the toxic heavy metal inhalation through soil particulates, the average daily intake is calculated using equation 3.16 [Kamunda, 2017].

$$ADI_{inh} = \frac{C_s \text{ x } IR_{inh} \text{ x } EF \text{ x } ED}{BW \text{ x } AT \text{ x } PEF} \tag{3.16}$$

such that the average daily intake (ADI_{inh}) for heavy metals that are inhaled from soil has the units of mg/kg-day, C_S represents the toxic heavy metal concentration for soil (mg/kg), the inhalation rate is IR_{inh} (m^3/day) while the particulate emission factor (PEF) is in the units of m^3/kg. Equation 3.15 defines BW, ED, EF, and AT. For dermal contact with water, the average daily intake is calculated through equation 3.17 [Kamunda, 2017].

$$ADI_{demw} = \frac{C_w \text{ x } SA \text{ x } PC \text{ x } ET \text{ x } EF \text{ x } ED \text{ x } CF}{BW \text{ x } AT} \tag{3.17}$$

where the average daily intake of toxic heavy metals (ADI_{demw}) through dermal contact with water is in the units mg/kg-day. C_W (mg/L) represents the metal concentration in water, the exposed skin area is SA in cm^2, the dermal permeability coefficient is PC in cm/h, ET (hour/day) denotes the exposure time for taking a bath or shower, the unit conversion factor is CF (L/cm^{-3}). Equation 3.15 defines BW, ED,

EF, and AT. For dermal contact with soil, the average daily intake is calculated using equation 3.18 [Kamunda, 2017].

$$ADI_{dems} = \frac{C_s \text{ x } SA \text{ x } FE \text{ x } AF \text{ x } ABS \text{ x } EF \text{ x } ED}{BW \text{ x } AT \text{ x } 10^6} \quad (3.18)$$

where ADI_{dems} is the average daily intake through dermal contact with soil (mg/kg-day). The toxic heavy metal concentration in soil is C_S (mg/kg) , FE is the fraction of the dermal exposure ratio to soil, AF (mg/ cm^2) is the soil adherence factor, ABS is the fraction of the applied dose absorbed across the skin, 10^6 is the conversion factor in kg/mg. Equation 3.15 defines BW, ED, EF, and AT. Table 3-3 gives the exposure quantities that were utilized in performing the health risk assessment for the study [Kamunda, 2017].

Table 3 - 3: Risk assessment parameters for various exposure pathways [Kamunda, 2017]

Parameter	**Media**	**Unit**	**Individual**	**Reference**
Body weight (BW)	all	kg	70	[DEA, 2010]
Exposure frequency (EF)	all	days/year	350	[DEA, 2010]
Exposure duration (ED)	all	years	30	[DEA, 2010]
Ingestion rate (IR_{ing})	soil	mg/day	100	[DEA, 2010]
	water	L/day	2	[USEPA, 2004]
	plants	mg/day	200	
Inhalation rate (IR_{inh})	soil	m^3/day	20	[DEA, 2010]
Skin surface area (SA)	soil & water	cm^2	5800	[DEA, 2010]
Soil adherence factor (AF)	soil	mg/cm^2	0.07	[DEA, 2010]
Dermal absorption factor (ABS)	soil		0.1	[DEA, 2010]
Dermal exposure ratio (FE)	soil	none	0.61	[USEPA, 2004]
Particulate emission factor (PEF)	soil	m^3/kg	1.3 x 10^9	[DEA, 2010]
Mean time (AT)	all	days		
For carcinogens			365 x 70	[DEA, 2010]
For non-carcinogens			365 x ED	[DEA, 2010]
Exposure period for shower and bath (ET)	water	hours/day	0.3	[USEPA, 2004]
Dermal permeability coefficient (PC)	water	cm/h	0.001	[USEPA, 2004]
Unit conversion factor (CF)	water	L/cm^{-3}	0.001	[USEPA, 2004]

3.8.1 Non-carcinogenic risk of toxic heavy metals

The hazard quotient (HQ) is a unitless number that basically describes the non-carcinogenic risk and gives the probability of an individual suffering an adverse effect. HQ is the quotient of the average daily intake divided by the toxicity threshold value, normally defined as the reference dose (RfD) for a specific chemical [Kamunda, 2017; USEPA, 1989] as shown in equation 3.19.

$$HQ = \frac{ADI}{RfD} \tag{3.19}$$

where RfD denotes the chronic reference dose for the heavy metal (mg/kg-day). For *n* heavy metals, the non-carcinogenic effect on the population is the sum of all the HQs from individual heavy metals and is normally known as the Hazard Index (HI). HI is represented in equation 3.20 [USEPA, 1989].

$$HI = \sum_{k=1}^{n} HQ_k = \sum_{k=1}^{n} \frac{ADI_k}{RfD_k} \tag{3.20}$$

such that the values of the toxic heavy metak k are HQ_k , ADI_k . For an HI value below one, the exposed population is not likely to experience adverse health effects. If it exceeds one, then there is a possibility for non-carcinogenic effects [Kamunda, 2017; USEPA, 1989].

3.8.2 Carcinogenic risk assessment due to toxic heavy metals

Carcinogenic risk is determined in terms of the rising possibility for an individual developing cancer as a result of exposure to a potential carcinogen during their lifetime. Equation 3.21 calculates the lifetime cancer risk [Bello, Muhammad and Bature, 2017].

$$Risk = ADI \times CSF \tag{3.21}$$

where Risk is the probability for an individual developing cancer during their lifetime and has no units. ADI denotes the average daily intake or dose and CSF represents the cancer slope factor in $(mg/kg/day)^{-1}$. CSF changes the computed daily toxic metal intake averaged over a lifetime of exposure directly to incremental risk for an individual developing cancer [Bello, Muhammad and Bature, 2017; Yang et al., 2018]. The mean contribution from the individual toxic heavy metals for different media through all pathways calculates the total lifetime cancer risk using equations 3.22 and 3.23 [Bello, Muhammad and Bature, 2017].

$$\text{Risk}_{\text{total}} = \text{Risk}_{\text{ing}} + \text{Risk}_{\text{inh}} + \text{Risk}_{\text{dermal}} \quad (3.22)$$

where Risk_{ing}, Risk_{inh} as well as $\text{Risk}_{\text{dermal}}$ are the risk contributors for different media such as water, soil and plants. Equation 3.23 calculates the risk for the particular pathway due to n number of toxic heavy metals [Bello, Muhammad and Bature, 2017].

$$\text{Risk}_{\text{pathway}} = \sum_{k=1}^{n} \text{ADI}_{\text{K}}\ \text{CSF}_{\text{K}} \quad (3.23)$$

where ADI_{K} and CSF_{K} represent the ADI and CSF for the k^{th} toxic heavy metal. Both non-carcinogenic and carcinogenic risk assessment of heavy metals are estimated from the RfD and CSF values largely derived from the Department of Environmental Affairs (DEA), South Africa and USEPA [Kamunda, 2017] as shown in Table 3-4.

Table 3 - 4: Reference doses in mg/kg-day and cancer slope factors for various metals [Kamunda, 2017]

Heavy metal	Ingestion RfD	Dermal Rfd	Inhalation Rfd	Ingestion CSF	Dermal CSF	Inhalation CSF	Source
As	0.003×10^{-1}	0.003×10^{-1}	0.003×10^{-1}	1.500	1.500	15.000	[DEA, 2010; USEPA, 2002]
Pb	0.036×10^{-1}	-	-	0.085×10^{-1}	-	0.042	[DEA, 2010]
Hg	0.003×10^{-1}	0.003×10^{-1}	0.086×10^{-3}	-	-	-	[DEA, 2010]
Cd	0.005×10^{-1}	0.005×10^{-1}	0.057×10^{-3}	-	-	6.300	[DEA, 2010; USEPA, 1991]
Cr(VI)	0.003	-	0.030×10^{-3}	0.500	-	41.000	[DEA, 2010; USEPA, 2007]
Co	0.020	0.057×10^{-4}	0.057×10^{-4}	-	-	9.800	[USEPA, 2011a]
Ni	0.020	0.056×10^{-1}	-	-	-	-	[DEA, 2010; IRIS, 2007]
Cu	0.037	0.024	-	-	-	-	[DEA, 2010; USEPA, 2011a]
Zn	0.300	0.075	-	-	-	-	[DEA, 2010; USEPA, 2011a]

Chapter 4: Results and discussion

The aim of this work was to determine NORM and heavy elements in and around the Morupule-B Coal Power Station in order to determine the risks to the workers and the public using the RESRAD radiation code. Water, soil, coal, bottom ash and fly ash samples were collected from the study area, prepared and then stored prior to analysis [Santawamaitre, 2012]. Radioactivity measurement in the samples was performed by using gamma spectrometry while toxic heavy metal determination was performed using ICP-MS. This chapter discusses the study results. Other aspects such as dose rate, annual effective dose, hazard assessment, natural radionuclide activity concentrations, RESRAD modelling and radiation dose reconstruction are also discussed. Experimental results for the study area are compared with those from similar studies.

4.1 Activity concentrations in the study area

Detailed results showing activity concentrations of ^{214}Pb and ^{214}Bi from the ^{226}Ra series, ^{234}Th and ^{234m}Pa from the ^{238}U series, ^{228}Ac and ^{212}Pb from the ^{232}Th series, ^{210}Pb, ^{40}K, ^{212}Bi and ^{208}Tl for all samples (soil, coal, bottom ash and fly ash samples) from the study area are listed in Appendices 8 to 23. All activity concentrations are expressed in units of Bq/kg dry weight [Santawamaitre, 2012]. Figures 4-1, 4-2, 4-3 and 4-4 shows the overall activity concentration of ^{238}U, ^{40}K and ^{232}Th for soil, coal, bottom ash and fly ash samples respectively.

Based on results from Figures 4-1, 4-2, 4-3 and 4-4, it can be seen that the activity concentrations of ^{238}U and ^{232}Th increase in ascending order from soil, coal, bottom ash to fly ash samples. The highest activity concentrations of ^{238}U were found to be 47.152 ± 3.591 Bq/kg, 69.737 ± 4.673 Bq/kg, 144.001 ± 7.601 Bq/kg and 221.495 ± 11.784 Bq/kg for soil, coal, bottom ash and fly ash samples respectively. The lowest activity concentrations of ^{238}U were found to be 7.932 ± 2.969 Bq/kg, 40.257 ± 4.605 Bq/kg, 67.956 ± 4.313 Bq/kg and 109.529 ± 6.095 Bq/kg for soil, coal, bottom ash and fly ash samples respectively. The highest activity concentrations of ^{232}Th were found to be 33.105 ± 0.605 Bq/kg, 29.834 ± 0.737 Bq/kg, 117.772 ± 1.012 Bq/kg and 196.864 ± 2.320 Bq/kg for soil, coal, bottom ash and fly ash respectively. The lowest activity concentrations of ^{232}Th were found to be 5.367 ± 0.238 Bq/kg, 22.666 ± 0.665 Bq/kg, 65.814 ± 0.772 Bq/kg and 77.937 ± 1.253 Bq/kg for soil, coal, bottom ash and fly ash samples respectively. The highest activity concentrations of ^{40}K were found to be 352.900 ± 7.397 Bq/kg, 25.670 ± 2.587 Bq/kg, 68.860 ± 2.440 Bq/kg and 123.900 ± 4.769 Bq/kg for soil, coal, bottom ash and fly ash respectively. The lowest activity concentrations of ^{40}K were found to be 88.150 ± 2.241 Bq/kg, 9.126 ±

4.442 Bq/kg, 27.870 ± 3.667 Bq/kg and 37.170 ± 5.953 Bq/kg for soil, coal, bottom ash and fly ash samples respectively. Figure 4-1 clearly shows that soil samples from the study area have the highest measured values of ^{40}K activity concentrations, as compared to coal, bottom ash and fly ash samples. The average mean activity concentrations of ^{238}U, ^{232}Th and ^{40}K for soil samples in this study are 19.101 ± 2.140 Bq/kg, 14.149 ± 1.762 Bq/kg and 196.115 ± 4.392 Bq/kg respectively which are comparable to mean worldwide activity concentrations. The slight differences between soil activity concentrations of ^{238}U, ^{232}Th and ^{40}K to worldwide values could be due to geology and geochemical states of various sampling sites [Faanu, 2011].

4.1.1 Activity concentration in soil samples

Potassium-40 had the highest concentration in all soil samples from the study area. The concentration of the potassium did not follow any specific pattern with some isolated sampling areas showing higher activity concentrations than others. The most likely explanation for the high levels of potassium in some sampling areas compared to others is the general variation in terms of land use and agriculture, with potassium being applied heavily in farm lands. Also low lying sampling areas where sediments eroded from farming areas were deposited could explain the high levels in some areas. The concentration of ^{238}U in all sampling areas never exceeded 50 Bq/kg. The mean activity was below the world activity concentration measured in soil. The soil from the study area shows very little sign of extensive contamination in terms of ^{238}U. The activity concentration of ^{226}Ra which is a daughter nuclide of ^{238}U is much lower than that of the parent nuclide as seen in Figure 4-1. This suggests that the soil has been standing undisturbed and unpolluted in terms of the ^{238}U series radionuclides for a while. Radium is much more mobile under natural conditions compared to uranium and therefore, it is expected to leach through the soil at a much faster rate. This explains the lower activity concentration observed when compared with the parent nuclide. A comparison of the activity concentrations of the three main radionuclides with findings from other study areas in the world, shown in Table 4-1, confirms that the area is not polluted from the burning of coal from a radionuclide perspective.

Table 4 - 1: ^{232}Th, ^{40}K and ^{238}U activity concentrations for soil compared to published data [Faanu, 2011; UNSCEAR, 2000]

	Soil activity concentration (Bq/kg)					
	^{238}U		**^{232}Th**		**^{40}K**	
Country of study	**Range**	**Mean**	**Range**	**Mean**	**Range**	**Mean**
Botswana (Morupule-B)	7-47	19	5-33	14	88-352	196
Ghana (Tarkwa mine)	8-26	15	27	60 -249		157
Algeria	2-110	30	2-140	25	66-1150	370
Egypt	6-120	37	2-96	18	29-650	320
United States	4-140	35	4-130	35	100-700	370
India	7-81	29	14-160	64	38-760	400
Malaysia	49-86	66	63-110	82	170-430	310
Lithuania	3-30	50	9-46	25	350-850	600
United Kingdom	2-330		1-180		0-3200	
Hungary	12-66	29	12-45	28	79-570	370
Spain			2-210	33	25-1650	470
World average		33		45		420

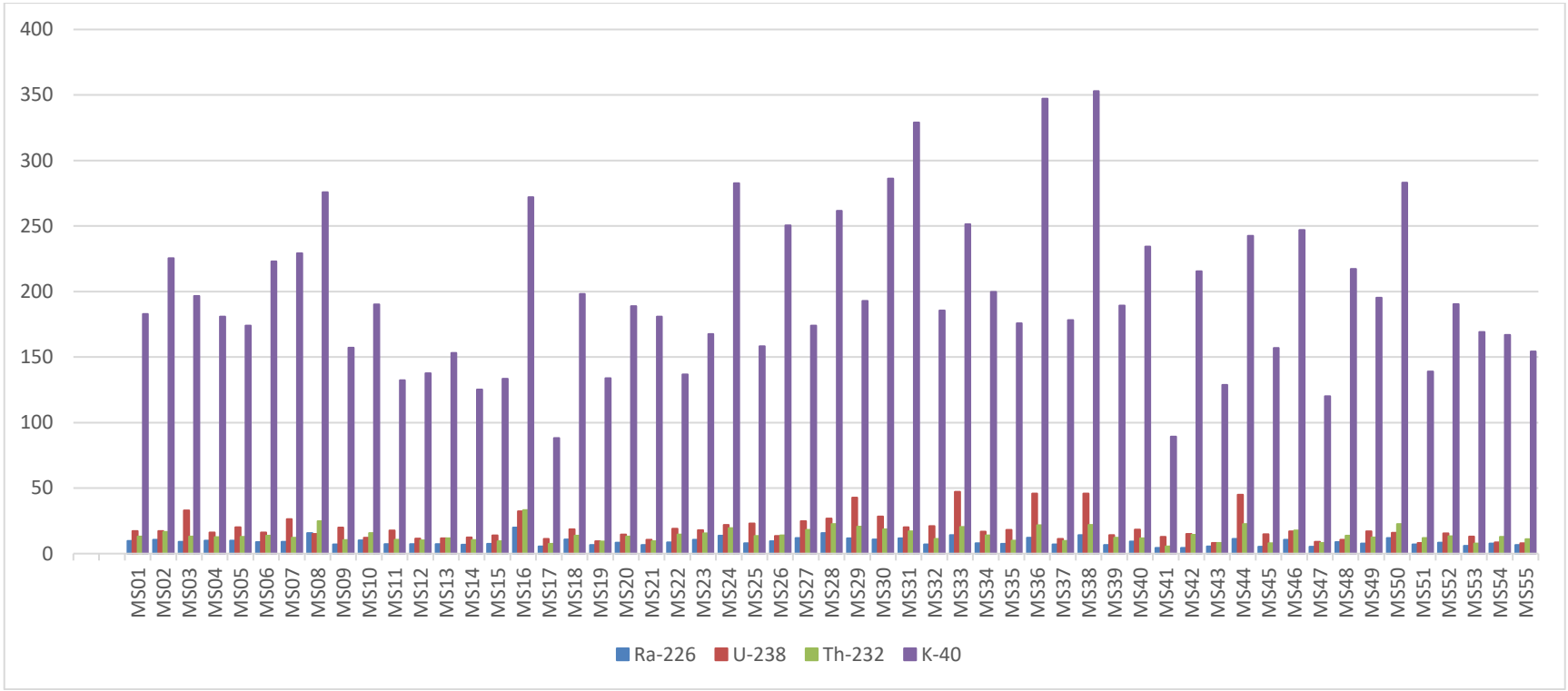

Fig. 4 - 1: Overall activity concentration of ^{238}U, ^{232}Th and ^{40}K in soil samples

4.1.2 Activity concentration in coal samples

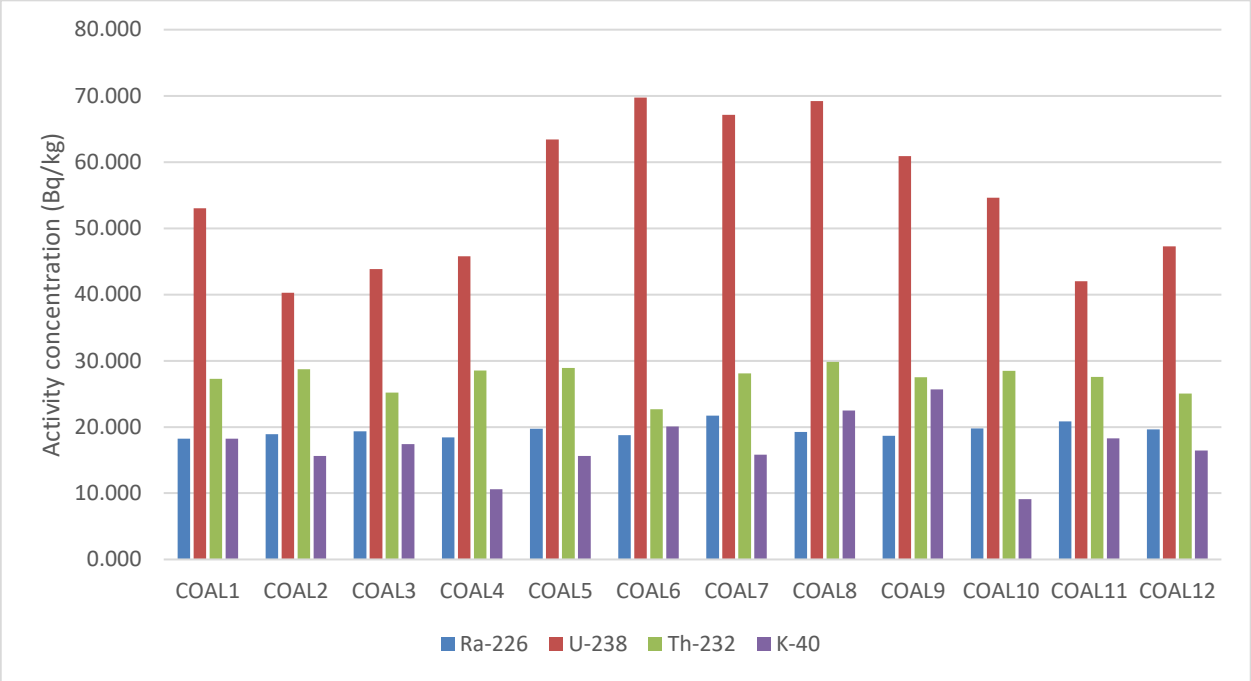

Fig. 4 - 2: Activity concentration of ^{238}U, ^{232}Th and ^{40}K in coal samples

Uranium-238 is the most dorminant radionuclide in all the analysed coal samples from the study area. The concentration of the radionuclides in the coal was not epected to reflect the concentration in the surrounding soil as the coal is being mined from underground and its formation is different from the formation of the soil. The activity concentration of ^{238}U in all samples is the highest, ranging between 40 Bq/kg and 70 Bq/kg. Minerals dug from underground usually have low concentrations of potassium compared to the surface soil and the coal from this study shows the same trend. The activity concentration of ^{40}K is consistently the lowest in all the samples that were analysed, which is contrary to the observation made in the soil samples that were analysed. Due to the fact that the coal has higher concentrations of the radionuclides, ^{238}U and ^{232}Th and ^{226}Ra there exists a possibility of contamination of the soil which contains these radionuclides in low concentrations. Radium-226 is a daughter nuclide of ^{238}U and under normal undisturbed conditions would be expected to be in equilibrium with its parent nuclide. However, from this study, the concentration in the coal samples of the ^{226}Ra radionuclide is much less than the uranium, exceeding 3 times in some samples. The reason for the disequilibrium is most likely due to the fact that the coal deposits were exposed to water, which caused the leaching of the radium at a much faster rate than the uranium. The concentration of ^{232}Th in the samples is consistenty higher than the concentration observed in the soil. The possible explanation for this higher activity is mostly due to the

retardation of the thorium that was being leached from the surface as it reached the coal deposits. The concentration of the radionuclide is almost homogeneous within the samples analysed.

4.1.3 Activity concentration in bottom ash samples

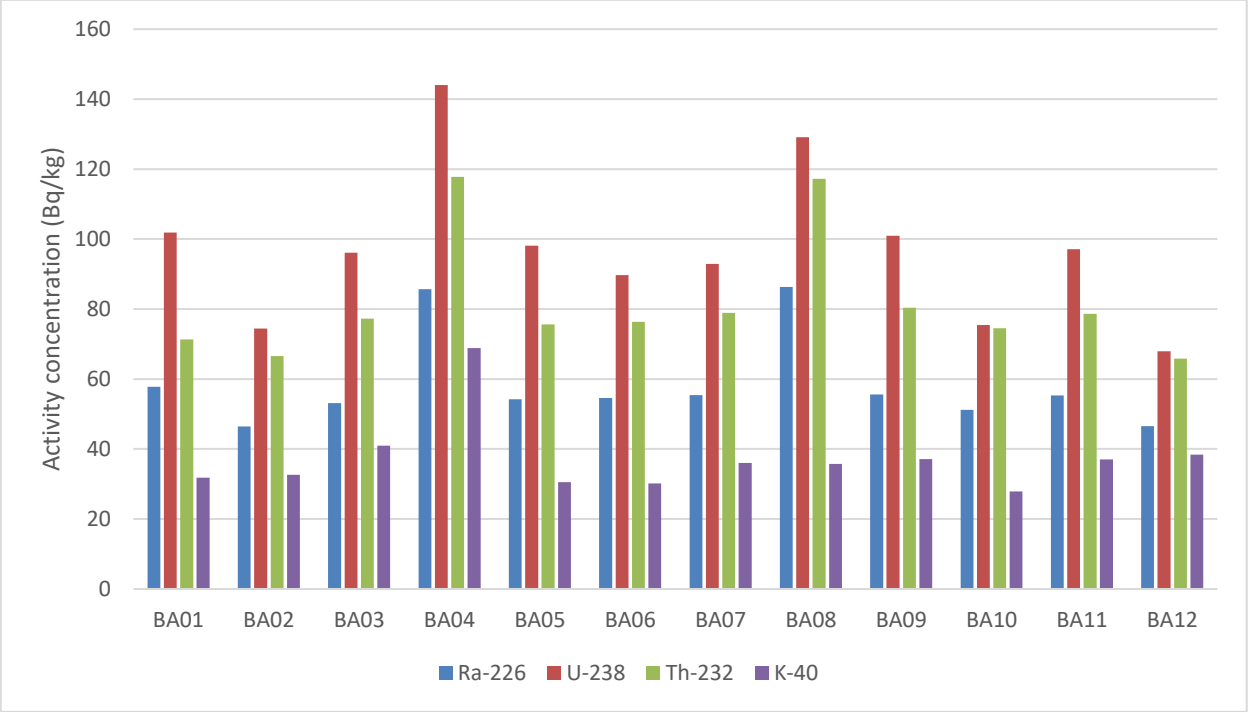

Fig. 4 - 3: ^{238}U, ^{232}Th and ^{40}K activity concentration in bottom ash

Bottom ash comes from the heavy remains of burning coal. It forms a huge bulk in terms of mass of the waste generated from the burning of coal. In this study, the activity concentration in bottom ash samples had activity concentrations of the three main radionuclides under consideration higher than the concentration in the coal from which it is generated. The increase in activity concentration is mainly due to the reduction is mass with the burning of coal, especially with the loss of volative organic materials found in the coal. The activity concentration of ^{238}U was the highest in all the bottom ash samples that were analysed in this study as seen in Figure 4-3. However, the bottom ash samples have much higher concentrations of ^{232}Th as a percentage of the total activity. The percentage increase in the radionuclides were 200%, 118% and 80% for ^{232}Th, ^{238}U and ^{40}K respectively. Thus coal samples with high contents of ^{232}Th will always see the highest concentration off the contaminant in the bottom ash of the coal burning process.

Table 4 - 2: Average world activity concentration of ^{238}U, ^{40}K and ^{232}Th in fly ash and coal in Bq/kg [UNSCEAR, 1982]

Nuclides	Nuclides	Coal	Fly Ash
Morupule-B (this study)	^{40}K	17	67
Morupule-B (this study)	^{238}U	55	150
Morupule-B (this study)	^{232}Th	27	117
Average world value	^{40}K	50	265
Average world value	^{238}U	20	200
Average world value	^{232}Th	20	70

4.1.4 Activity concentration in fly ash samples

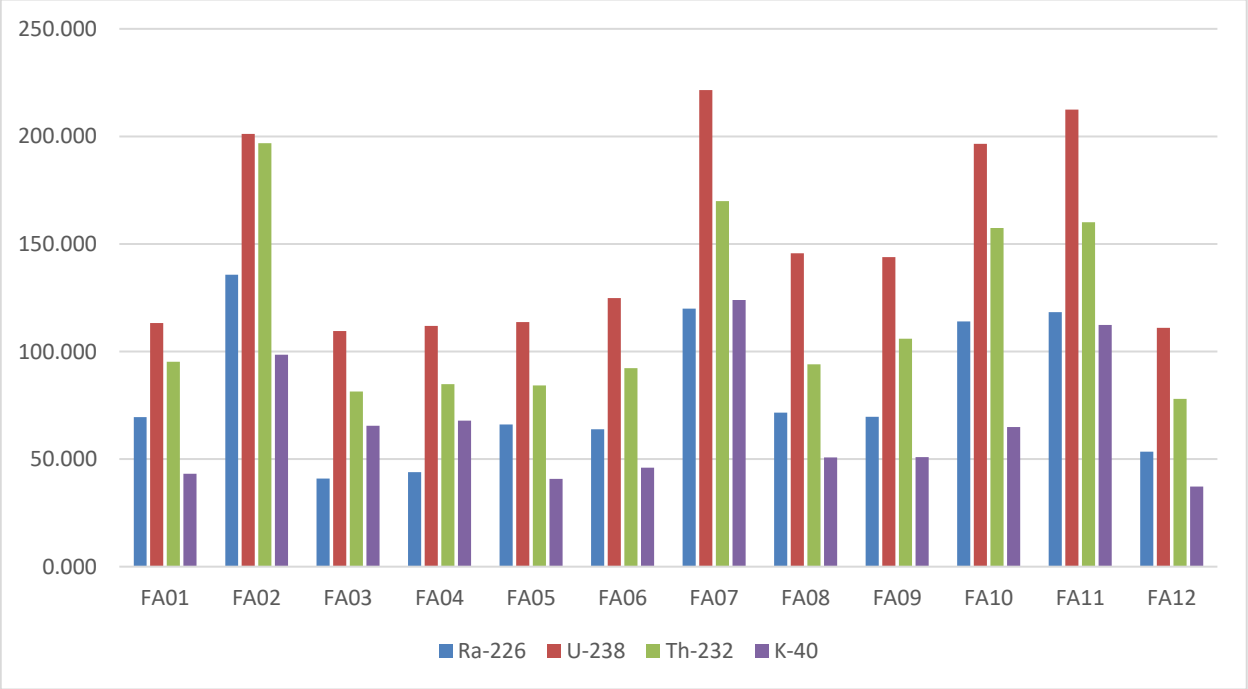

Fig. 4 - 4: ^{238}U, ^{40}K and ^{232}Th activity concentration for fly ash

Fly ash is the lowest density waste generated when coal burns during electricity generation. It is the lighest in weight as well and therefore has a higher probability of being blown into the surrounding environment and causing possible contamination. The activity concentration of all the radionuclides considered in this study were the highest in fly ash samples. This is mainly due to the low density and

light nature of the waste. Fly ash is also widely used in the construction industry for the manufacture of cements and therefore, the concentration of the radionuclides in it are of importance. The percentage increase of ^{232}Th, ^{40}K and ^{238}U from the burning of the coal in the fly ash was 333%, 235% and 172% respectively. The percentage increase follows the same trend observed in the bottom ash samples. ^{232}Th is actually concentrated to a value that is above the world average for the radionuclide measured in fly ash samples and presents the second highest risk in terms of contamination after ^{238}U, which even though it was not enhanced as much as the ^{232}Th still had the highest activity concentration.

4.1.5 Summary of activity concentrations in all particulate samples

Table 4-2 shows a comparison of the worldwide coal and fly ash activity concentrations to those from this study. Based on the results for coal samples from Figure 4-2, it was noted that ^{232}Th and ^{238}U activity concentrations increased in the order coal < bottom ash < fly ash. The mean ^{238}U activity concentrations were found to be 54.771 ± 4.460 Bq/kg, 97.311 ± 6.151 Bq/kg and 150.444 ± 9.595 Bq/kg for coal, bottom ash and fly ash respectively. The mean ^{232}Th activity concentrations were found to be 27.319 ± 0.714 Bq/kg, 81.702 ± 1.030 Bq/kg and 116.674 ± 1.457 Bq/kg for coal, bottom ash and fly ash respectively. The mean ^{40}K activity concentrations were found to be 17.117 ± 3.831 Bq/kg, 37.265 ± 3.849 Bq/kg and 66.847 ± 10.107 Bq/kg for coal, bottom ash and fly ash respectively. The average world activity concentration shows that the NORM content of fly ash is greater than that of coal as depicted in Table 4-2 [UNSCEAR, 1982]. Average fly ash activity concentration values for ^{238}U and ^{40}K from this study are generally lower than those from average world activity concentrations, while those of ^{232}Th are greater than the average world values by a factor of close to 2 as depicted in Table 4-3 [UNSCEAR, 1982]. Average coal activity concentration values for ^{238}U and ^{232}Th from this study are generally higher than those from average world activity concentrations, while those of ^{40}K are lower than the average world values [UNSCEAR, 1982]. The average bottom ash activity concentration values were 683.500 ± 76.000 Bq/kg and 83.000 ± 5.000 Bq/kg for ^{238}U and ^{232}Th respectively from Figueira Thermoelectric Power Plant in Brazil, which are greater than those from this study. On the other hand, the average bottom ash concentration from Figueira Thermoelectric Power plant in Brazil was 597.000 ± 39.000 Bq/kg, which is much greater than the activity concentration of ^{40}K in bottom ash samples from this study [Fungaro et. al., 2017]. Differences between the ^{40}K, ^{232}Th and ^{238}U activity concentrations and the worldwide values could be due to the nature of the coal deposits in this study.

4.2 Correlation between ^{232}Th and ^{40}K; ^{238}U and ^{40}K; ^{238}U and ^{232}Th

^{232}Th, ^{40}K and ^{238}U activity concentrations may be represented as elemental concentrations in ppm or µg.g^{-1} of thorium or uranium as well as the percentage of ^{40}K by means of equation 4.1 [Santawamaitre, 2012]:

$$F_E = \frac{M_E C}{\lambda_E N_A f_{A,E}} A_E \tag{4.1}$$

F_E denotes the elemental concentration due to the presence of nuclide E in the sample: M_E, λ_E, $f_{A,E}$ as well *as* A_E denotes the atomic masses (kg.mol^{-1}). N_A is Avogadro's constant being 6.023 x 10^{23} atoms.mol^{-1} , C is a constant with values of 10^6 for ^{238}U and ^{232}Th as well as 10^2 for ^{40}K [Santawamaitre, 2012]. The measured activity concentrations of ^{40}K (Bq.kg^{-1}), ^{232}Th (Bq.kg^{-1}) and ^{238}U (Bq.kg^{-1}) can be utilized in the calculation of the respective elemental concentrations of potassium, thorium (ppm) and uranium (ppm) by means of conversion factors [Christodoulides et al., 2003; IAEA, 2003]:

1 ppm Th = 4.06 Bq.kg^{-1} of ^{232}Th (4.2)

1 ppm U = 12.35 Bq.kg^{-1} of ^{238}U (4.3)

1% K = 313 Bq.kg^{-1} of ^{40}K (4.4)

Calculating the elemental concentrations of potassium, uranium and thorium by means of equation 4.1 is consistent with the IAEA methodology for calculating conversion factors. The calculated soil elemental concentrations for U, Th and K from this research range from 0.642 ± 0.240 ppm to 3.818 ± 0.291 ppm for ^{238}U, 1.322 ± 0.059 ppm to 6.099 ± 0.168 ppm for ^{232}Th and 0.282 ± 0.007 % to 1.127 ± 0.024 % for ^{40}K with arithmetic means of 1.547 ± 0.811 ppm, 3.485 ± 1.273 ppm and 0.630 ± 0.190 % respectively. Figures 4-5, 4-6 and 4-7 present the correlations between U and Th, U and K as well as Th and K activity concentrations respectively. Figure 4-5 presents positive relationship between U and Th as seen from the correlation coefficient of 0.62 (R^2 = 0.42). Th/U elemental ratios normally have theoretical values roughly equal to 3.0 under normal conditions of continental crust [Christodoulides et al., 2003; Santawamaitre, 2012]. In this study, the soil elemental ratios of Th/U range from 0.392 ± 0.023 to 1.650 ± 0.198, having an arithmetic mean and standard deviation of 0.827 ± 0.192. This arithmetic mean is much lower than the theoretical value of 3.0 [Faanu, 2011]. This low value can be attributed to the depletion of thorium or an enrichment of uranium by natural processes in the area [Santawamaitre, 2012; UNSCEAR, 2000]. However, in this study the activity concentration of ^{238}U is much higher than

the activity concentration of ^{232}Th which is not usually the case under natural conditions. The lower ratio in this case was not due to the depletion of thorium but rather due to a high ^{238}U concentration. The value of Th/U gives the relative depletion or enrichment of radionuclides for various types of soil and rock samples, [Faanu, 2011]. K/U and K/Th ratios range from 4.028 ± 0.344 to 20.545 ± 4.244 and 8.055 ± 0.211 to 20.12 ± 0.741 having arithmetic means and standard deviations of 11.721 ± 4.113 and 14.413 ± 2.995 respectively. Figure 4-6 presents rather a moderate uphill positive relationship between U and K as seen from the correlation coefficient of 0.60 (R^2 = 0.36), while figure 4-7 indicates a relatively strong positive relationship between the K/Th radionuclide pairs with the correlation coefficient value of 0.77 (R^2 = 0.59).

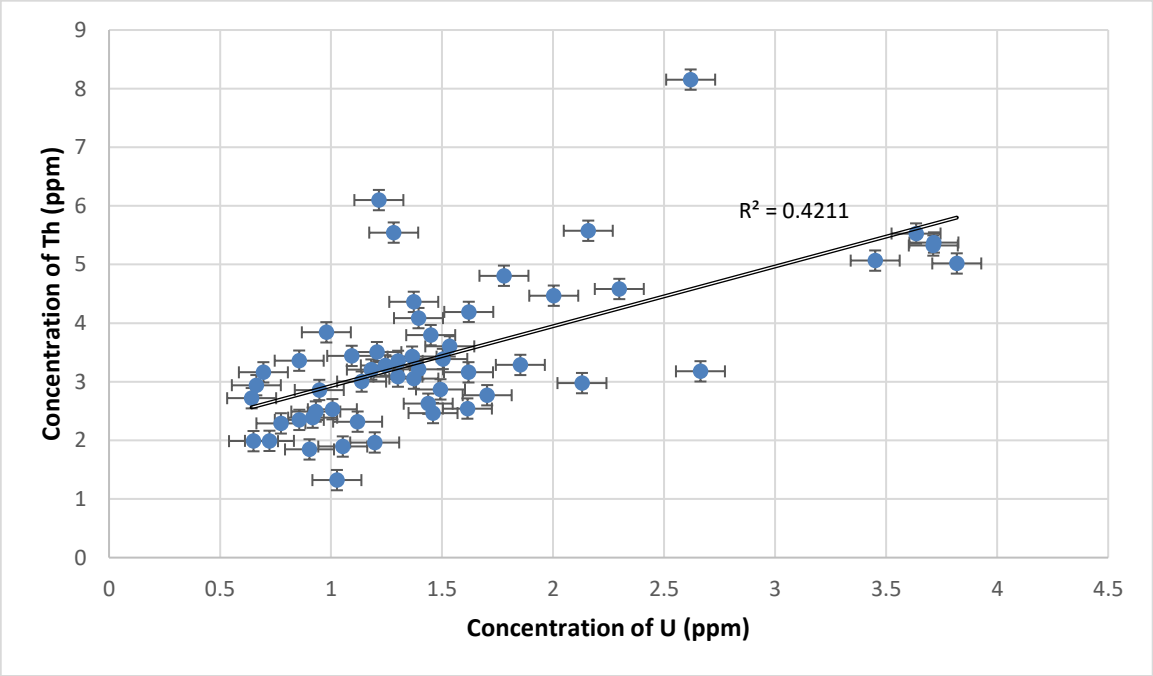

Fig. 4 - 5: Correlation between U and Th soil activity concentration

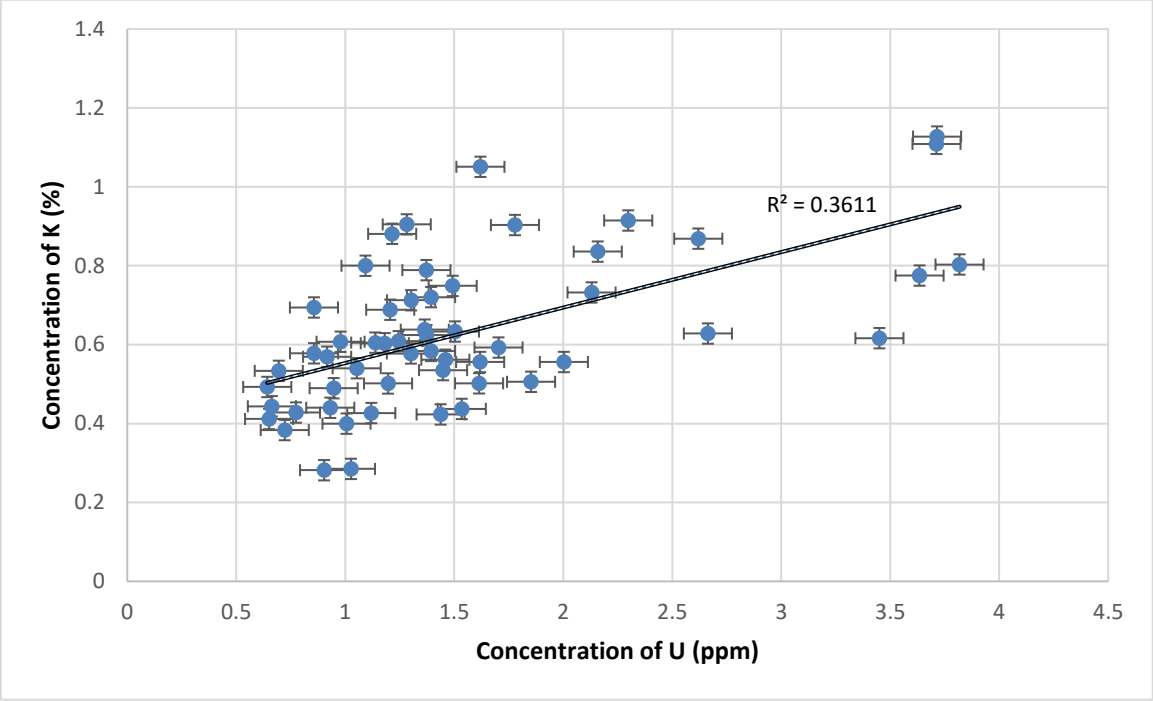

Fig. 4 - 6: Correlation between U and K soil activity concentration

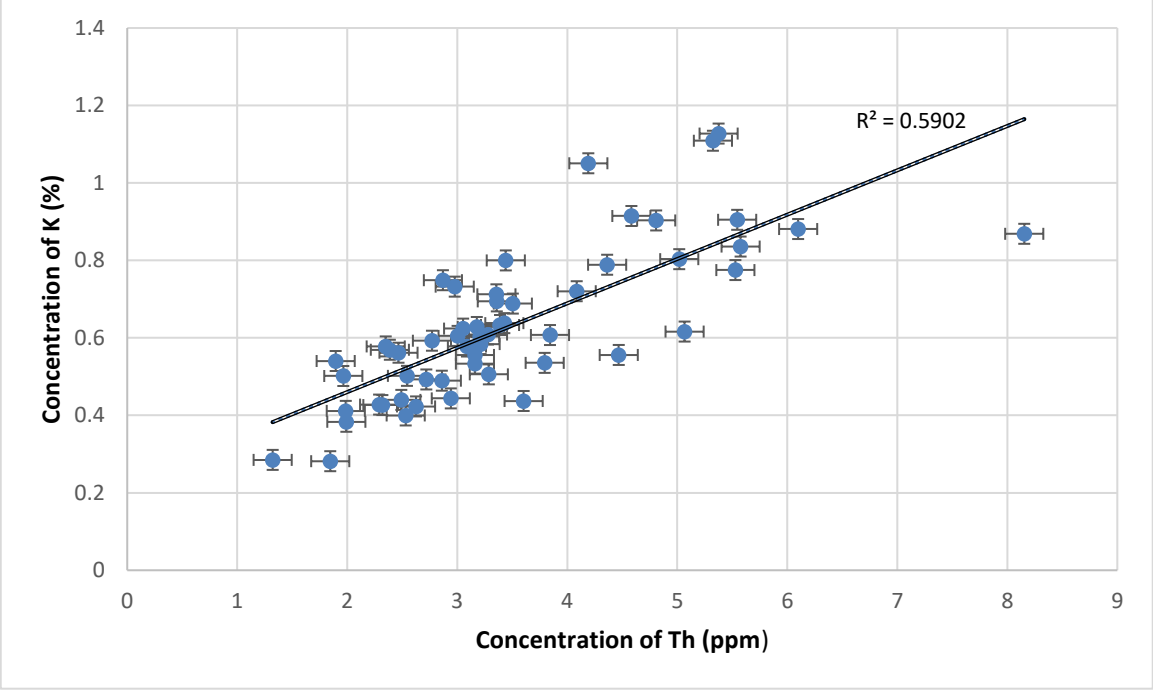

Fig. 4 - 7: Correlation between Th and K soil activity concentration

4.3 Radiological hazard assessment

A fundamental objective when performing radioactivity measurements from environmental samples is to estimate the radiation dose and effects on humans [ARPANSA, 2015]. Radiological risk may be assessed in several ways. In this research, four quantities were calculated to assess the radiological risk being (a) absorbed dose rate (D) in air at 1m above the ground, (b) annual effective dose equivalent (AEDE) (c) radium equivalent activity (Ra_{eq}) and (d) external hazard index (H_{ext}). Tables 4-3 to 4-6 show the quantities linked to natural radionuclides for soil, coal, bottom ash and fly ash samples respectively. It is therefore imperative to estimate the gamma radiation hazards on human subjects linked to the use of any of the above samples as building material by calculating the values of the four quantities above for all samples [Harb et al., 2008]. For instance, fly ash is normally utilized in making cement or can be used as a lightweight filler for concrete [Penfold et al., 1998]. The values of the radiological parameters from (a) to (d) above can be calculated using equations 3.9 to 3.10 from Sections 3.6.1 to 3.6.4. Appendices 30 to 33 show the actual estimated values of these parameters for each of the soil, coal, bottom ash and fly ash samples from this study.

4.3.1 Soil

From Table 4-3, the estimated absorbed dose rates (D) from soil samples ranged from 12.817 ± 1.716 nGy/h to 49.095 ± 1.187 nGy/h, with a mean of 25.549 ± 9.026 nGy/h. These values are lower than the worldwide average absorbed dose rate of 57 nGy/h [Santawamaitre, 2012]. Table 4-3 shows that the estimated annual effective dose equivalent (AEDE) for soil samples ranges from 15.719 ± 2.105 µSv/y to 60.210 ± 1.456 µSv/y with a mean of 31.333 ± 11.070 µSv/y. These values of annual effective dose equivalent (AEDE) are within the worldwide mean value of 70 µSv/y [Santawamaitre, 2012]. From Table 4-3, the radium equivalent activity (Ra_{eq}) ranges from 27.217 ± 3.736 Bq/kg to 104.263 ± 2.567 Bq/kg, with a mean of 54.435 ± 19.464 Bq/kg. These values are below the recommended limit of 370 Bq/kg [Faanu, 2011]. From Table 4-3, the external hazard index (H_{ext}) ranges from 0.073 ± 0.010 to 0.282 ± 0.007, with a mean of 0.147 ± 0.053. The average H_{ext} value is less than one, meaning that there is insignificant external exposure risk due to NORMs in the soil [Ademola and Onyema, 2014].

Table 4 - 3: Radiological risk assessment parameters for soil in this study

	D (nGy/h)	AEDE (µSv/y)	Ra_{eq} (Bq/kg)	H_{ext}
Min	12.817 ± 1.716	15.719 ± 2.105	27.217 ± 3.736	0.073 ± 0.010
Max.	49.095 ± 1.187	60.210 ± 1.456	104.263 ± 2.567	0.282 ± 0.007
Mean ± S.D.	25.549 ± 9.026	31.333 ± 11.070	54.435 ± 19.464	0.147 ± 0.053
Worldwide Ref. value [Santawamaitre, 2012]	57	70	< 370	< 1
Range	18 - 93	-	-	-

4.3.2 Coal

From Table 4-4, the estimated absorbed dose rates (D) from coal samples ranged from 36.188 ± 2.199 nGy/h to 50.947 ± 2.144 nGy/h, with a mean of 42.519 ± 5.288 nGy/h. These values are all below the recommended worldwide mean value of 60 nGy/h [UNSCEAR, 2000; Faanu, 2011]. Table 4-4 shows that the estimated annual effective dose equivalent (AEDE) ranges from 44.381 ± 2.697 µSv/y to 62.481 ± 2.629 µSv/y with a mean of 52.146 ± 6.480 µSv/y. These values of annual effective dose equivalent (AEDE) are within the worldwide mean value of 460 µSv/y [Pandit, Sahu and Puranik, 2011]. Table 4-4 further shows that the radium equivalent activity (Ra_{eq}) in coal samples ranges from 81.186 ± 4.773 Bq/kg to 113.635 ± 4.656 Bq/kg, with a mean of 95.156 ± 11.482 Bq/kg. These values are below the recommended limit of 370 Bq/kg [Faanu, 2011]. Table 4-4 also shows that the external hazard index (H_{ext}) ranges from 0.219 ± 0.013 to 0.307 ± 0.013, with a mean of 0.257 ± 0.031. The average H_{ext} is below one, implying that there is no significant external exposure risk due to the coal [Ademola and Onyema, 2014].

Table 4 - 4: Radiological risk assessment parameters for coal in this study

	D (nGy/h)	AEDE (µSv/y)	Ra_{eq} (Bq/kg)	H_{ext}
Min	36.188 ± 2.199	44.381 ± 2.697	81.186 ± 4.773	0.219 ± 0.013
Max.	50.947 ± 2.144	62.481 ± 2.629	113.635 ± 4.656	0.307 ± 0.013
Mean ± S.D.	42.519 ± 5.288	52.146 ± 6.480	95.156 ± 11.482	0.257 ± 0.031
Worldwide Ref. value	60	460 µSv/y	< 370	< 1
Range	-	-	-	-

4.3.3 Bottom ash

From Table 4-5, the estimated absorbed dose rates (D) ranged from 72.748 ± 2.914 nGy/h to 140.530 ± 3.004 nGy/h, having a mean of 95.859 ± 20.357 nGy/h. These values are higher than the worldwide absorbed dose rate of 60 nGy/h [Pandit, Sahu and Puranik, 2011; UNSCEAR, 2000]. Table 4-5 shows that the estimated annual effective dose equivalent (AEDE) ranged from 89.218 ± 3.573 µSv/y to 172.351 ± 3.684 µSv/y with a mean of 117.563 ± 24.967 µSv/y. These values of annual effective dose equivalent (AEDE) are lower than the worldwide value of 460 µSv/y [UNSCEAR, 1993]. The radium equivalent activity (Ra_{eq}) ranged from 165.026 ± 6.298 Bq/kg to 317.718 ± 6.528 Bq/kg, with a mean of 217.015 ± 46.052 Bq/kg. These values are below the recommended limit of 370 Bq/kg [Faanu, 2011]. Table 4-5 also shows that the H_{ext} varied from 0.446 ± 0.017 to 0.858 ± 0.018, with a mean of 0.586 ± 0.124. The average H_{ext} is below one, meaning that the area is safe for human occupation with insignificant risk due to external exposure from NORMs in the bottom ash [Ademola and Onyema, 2014].

Table 4 - 5: Radiological risk assessment parameters for bottom ash in this study

	D (nGy/h)	AEDE (µSv/y)	Ra_{eq} (Bq/kg)	H_{ext}
Min	72.748 ± 2.914	89.218 ± 3.573	165.026 ± 6.298	0.446 ± 0.017
Max.	140.530 ± 3.004	172.351 ± 3.684	317.718 ± 6.528	0.858 ± 0.018
Mean ± S.D.	95.859 ± 20.357	117.563 ± 24.967	217.015 ± 46.052	0.586 ± 0.124
Worldwide Ref. value	60	460 µSv/y	< 370	< 1
Range	-	-	-	-

4.3.4 Fly ash

From Table 4-6, the estimated absorbed dose rates (D) ranged from 102.540 ± 4.025 nGy/h to 215.940 ± 4.210 nGy/h, with a mean of 142.763 ± 46.278 nGy/h. These values are lower than the worldwide absorbed dose rate of 60 nGy/h [UNSCEAR, 2000]. Table 4-6 shows that the estimated annual effective dose equivalent (AEDE) ranged from 125.751 ± 4.937 µSv/y to 264.833 ± 5.163 µSv/y with a mean of 175.086 ± 56.756 µSv/y. These values of annual effective dose equivalent (AEDE) are lower than the worldwide value of 460 µSv/y [UNSCEAR, 1993]. Radium equivalent activity (Ra_{eq}) values for fly ash samples ranged from 231.062 ± 8.744 Bq/kg to 490.247 ± 9.136 Bq/kg, with a mean of 322.435 ± 104.923 Bq/kg. The mean value is less than the recommended limit of 370 Bq/kg [Faanu, 2011]. It is important to note that Ra_{eq} values that exceed 370 Bq/kg may increase radiation hazards [Ahmed, Mohammed and Abdaljalil, 2018].

Table 4-6 further shows that the external hazard index (H_{ext}) ranged from 0.624 ± 0.024 to 1.324 ± 0.025, with a mean of 0.871 ± 0.283. The average H_{ext} value is below one, indicating a low risk from external exposure from the NORMs in the fly ash [Ademola and Onyema, 2014]. There is a notable increase in these radiological hazard quantities in fly ash relative to the normal soil fom the study area. There is therefore still an increased risk due to the fly ash, though it is not a significant risk. Due to the stochastic nature of ionizing radiation risk, any addition to the background radiation increases the risk [Thomas and Symonds, 2016].

Table 4 - 6: Radiological risk assessment parameters for fly ash in this study

	D (nGy/h)	**AEDE (µSv/y)**	**Ra_{eq} (Bq/kg)**	**H_{ext}**
Min	102.540 ± 4.025	125.751 ± 4.937	231.062 ± 8.744	0.624 ± 0.024
Max.	215.940 ± 4.210	264.833 ± 5.163	490.247 ± 9.136	1.324 ± 0.025
Mean ± S.D.	142.763 ± 46.278	175.086 ± 56.756	322.435 ± 104.923	0.871 ± 0.283
Worldwide Ref. value Range	60 -	460 µSv/y -	< 370 -	< 1 -

4.3.5 Summary of radiological parameters for all samples

All estimated values for D, AEDE, Ra_{eq}, and H_{ext} in this study were generally highest for fly ash, followed by bottom ash, coal and soil samples in descending order as shown in Figure 4-8. The relatively high fly ash and bottom ash values for D, AEDE, Ra_{eq}, and H_{ext} could be attributed to the reasoning that during the combustion of coal, most of the non-combustible material, including the natural radionuclides, concentrate in both the bottom ash as well as fly ash thus enhancing the D, AEDE, Ra_{eq}, and H_{ext} values [Penfold et al., 1998].

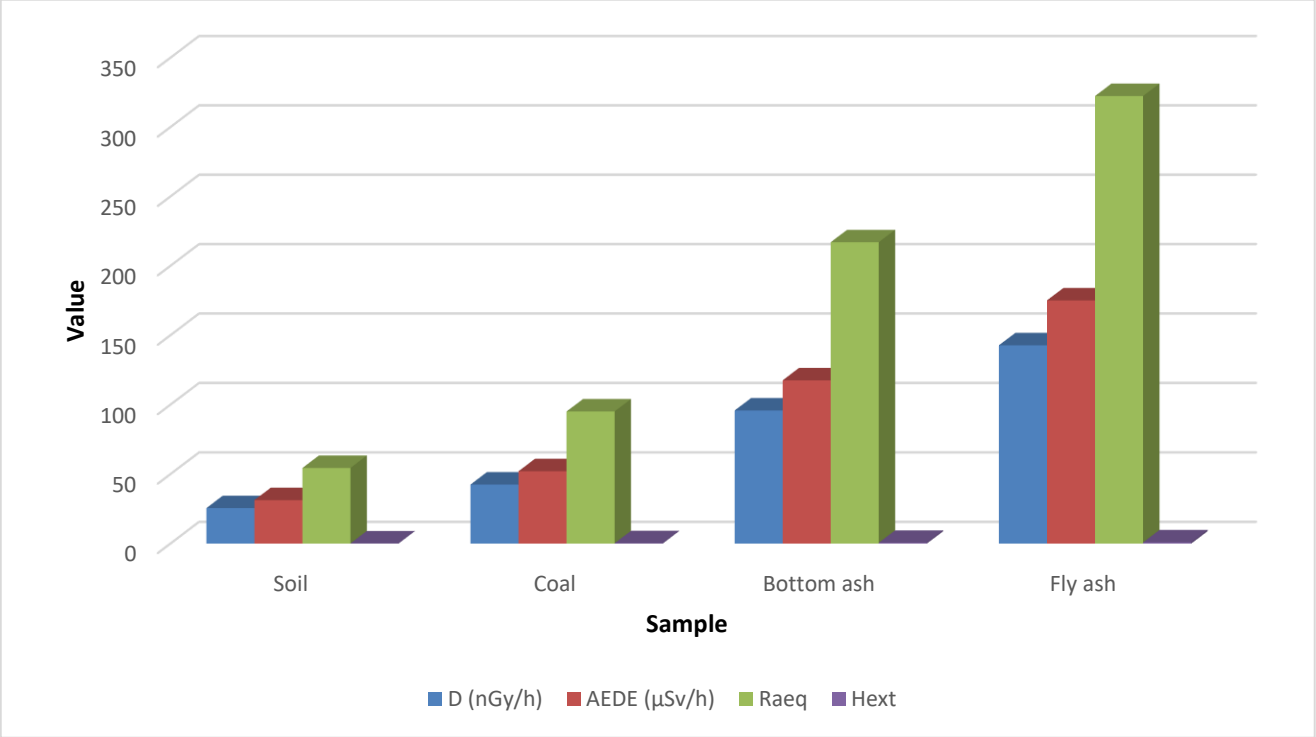

Fig. 4 - 8: Comparison of radiological parameters for all samples

Results from this study illustrate that all calculated annual effective dose averages of the soil, bottom ash, coal and fly ash samples are below the recommended limit of 1 mSv/year for members of the public [UNSCEAR, 2000]. Based on these findings, materials from the area under study can safely be used for building and construction.

4.4 Toxic heavy metal concentrations for soil, water, fly ash, coal and bottom ash

The respective concentrations of toxic heavy metal concentrations for water and soil in the vicinity of the power station as well as for coal, bottom ash and fly ash within the power station are presented in this section.

4.4.1 Toxic heavy metal concentrations in water samples

The mean toxic heavy metal concentrations for water samples in mg/L from various locations in the vicinity of the power station are shown in Table 4-7. These mean concentrations were also used to compute the mean daily intakes for residents in the study area resulting in carcinogenic and non-carcinogenic risk assessment for individual members of the public. Botswana has a mostly semi arid climate with a scarcity of water. Due to this water shortage, water from both rivers and boreholes is

therefore consumed by humans. The mean toxic heavy metal concentrations in water from the power station vicinity presented in descending order are Zn > Cu > Ni > Pb > Cr > Co > As. Toxic heavy metal concentrations below the detection limit (BDL) were written as 0.000. The ranges of these toxic heavy metals in mg/L were: Zn (0.036 to 5.271, averaging 0.871); Cu (0.031 to 1.362, averaging 0.451); Ni (0.001 to 0.212, averaging 0.056); Pb (0.001 to 0.083, averaging 0.029); Cr (0.000 to 0.025, averaging 0.006); Co (0.000 to 0.004, averaging 0.002); As (0.000 to 0.002, averaging of 0.001) respectively.

Table 4 - 7: Heavy metal concentrations in water samples

Sample Code	**Toxic heavy metals concentration (mg/L)**						
	As	**Pb**	**Cr**	**Cu**	**Zn**	**Co**	**Ni**
MW01	0.000	0.025	0.004	0.853	0.459	0.000	0.125
MW02	0.000	0.083	0.000	1.362	0.137	0.000	0.078
MW03	0.000	0.040	0.000	0.570	5.721	0.000	0.003
MW04	0.000	0.060	0.000	0.658	0.451	0.000	0.212
MW05	0.002	0.007	0.025	0.044	0.036	0.004	0.011
MW06	0.001	0.003	0.010	0.039	0.066	0.003	0.008
MW07	0.001	0.013	0.005	0.054	0.054	0.004	0.012
MW08	0.001	0.001	0.000	0.031	0.047	0.001	0.001
Average	0.001	0.029	0.006	0.451	0.871	0.002	0.056
Minimum	0.000	0.001	0.000	0.031	0.036	0.000	0.001
Maximum	0.002	0.083	0.025	1.362	5.721	0.004	0.212

The results were then compared to the available South African as well as international guidelines of acceptable limits of toxic heavy metals in drinking water shown in Table 4-8.

Table 4 - 8: Recommended toxic heavy metal limits for drinking water [DOH, 2004; USEPA, 2011b; WHO, 2004]

Country	**Concentration limit of toxic heavy metals (mg/l)**								
	As	**Pb**	**Hg**	**Cd**	**Cr**	**Cu**	**Zn**	**Co**	**Ni**
WHO	0.010	0.010	0.006	0.003	0.050	2.000	n.a	n.a	0.070
South Africa	0.010	0.010	0.001	0.003	n.a	1.000	n.a	n.a	n.a
USEPA	0.010	0.015	0.002	0.005	0.100	1.300	0.500	0.100	n.a
This work	0.001	0.029	n.a	n.a	0.006	0.451	0.871	0.002	0.056

n.a: not available

The results indicated that the average As, Cr, Cu, Co and Ni drinking water concentrations were lower than the recommended limits while Pb and Zn had higher values than the recommended limits. These

high concentrations of toxic heavy metals might be attributed to elevated levels of acid mine drainage from the study [Winde et al., 2004].

4.4.2 Toxic heavy metal concentrations in soil samples

The mean toxic heavy metal concentrations from soils in the vicinity of the power station in mg/kg are presented in Table 4-9. These mean concentrations were also used to determine the mean daily intakes for residents in the study area resulting in carcinogenic and non-carcinogenic risk valuation for individual public members. The mean concentration of heavy metals in soil samples from the surroundings of the power station are presented in the descending order Cr > Ni > Cu > Zn > Co > Pb > As > Cd > Hg. The ranges of these heavy metals in mg/kg were: Cr (39.190 to 112.600 with an average of 67.688); Ni (11.950 to 31.930 with an average of 17.863); Cu (8.055 to 31.800 with an average of 15.129); Zn (4.744 to 27.33 with an average of 11.176); Co (2.548 to 13.410 with an average of 6.416); Pb (2.454 to 7.814 with an average of 4.335); As (0.355 to 1.045, averaging 0.588); Cd (0.067 to 0.107, averaging 0.080); Hg (0.024 to 0.035, averaging 0.027) respectively. This observation is captured in Figure 4-9. The results also showed that soils in the vicinity of the power station generally have higher heavy metal concentrations as compared to water samples from the same area. The measured results were compared with soils worldwide as depicted in Table 4-10. Cr and Ni had the highest heavy metal values in this study.

Table 4 - 9: Mean of heavy metals concentration values in soil samples

Sample Code	**Toxic heavy metals concentration (mg/kg)**								
	As	**Pb**	**Hg**	**Cd**	**Cr**	**Cu**	**Zn**	**Co**	**Ni**
MS21	1.014	7.516	0.026	0.097	112.600	31.800	27.33	13.310	31.930
MS23	0.620	4.417	0.024	0.083	69.320	15.070	12.18	7.002	19.710
MS24	0.548	3.310	0.028	0.078	70.640	11.470	9.422	5.039	16.410
MS26	0.385	2.454	0.024	0.072	60.500	8.094	7.316	2.548	12.780
MS29	1.045	7.814	0.035	0.107	103.600	29.910	20.95	13.410	28.100
MS34	0.484	3.831	0.028	0.074	53.650	12.280	6.669	5.379	14.470
MS35	0.374	2.795	0.029	0.067	48.390	8.055	4.744	3.207	11.950
MS37	0.471	3.913	0.026	0.071	51.300	9.329	5.511	3.966	12.360
MS38	0.355	2.965	0.024	0.075	39.190	10.150	6.458	3.879	13.060
Average	0.588	4.335	0.027	0.080	67.688	15.129	11.176	6.416	17.863
Minimum	0.355	2.454	0.024	0.067	39.190	8.055	4.744	2.548	11.950
Maximum	1.045	7.814	0.035	0.107	112.600	31.800	27.33	13.410	31.930

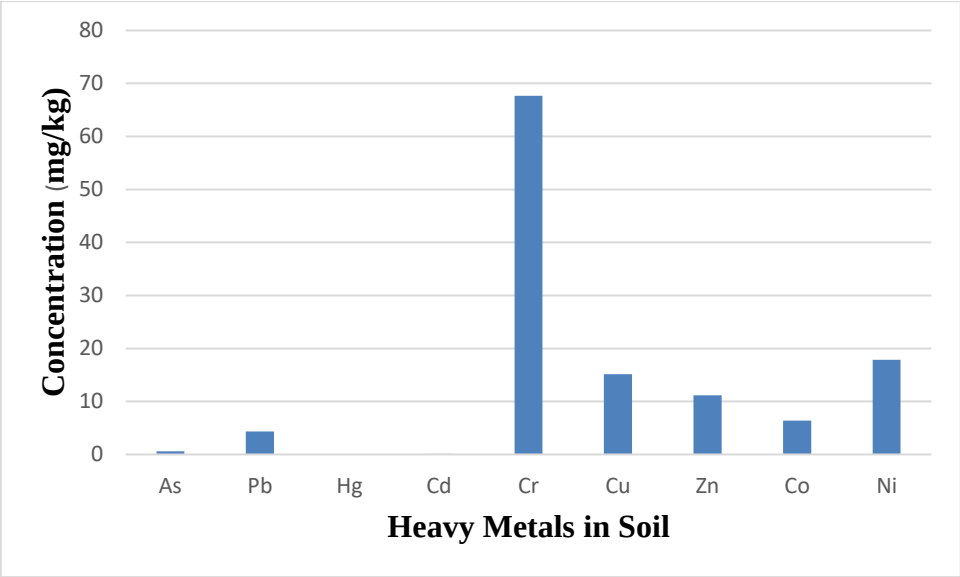

Fig. 4 - 9: Mean toxic heavy metals concentrations found in soil samples

Table 4 - 10: Worldwide values of soil heavy metal concentrations

Country	**Concentration limit (mg/kg)**									**Source**
	As	**Pb**	**Hg**	**Cd**	**Cr**	**Cu**	**Zn**	**Co**	**Ni**	
Germany	50.00	70.00	0.500	1.00	60.00	40.00	150.00	n.a	50.00	[Dar-Yuan Chia-Hsing, 2011]
Poland	n.a	100.00	n.a	3.00	100.00	100.00	300.00	50.00	100.00	[Mthunzi et al., 2015]
UK	32.00	450.00	10.00	10.00	130.00	n.a	n.a	n.a	130.00	[[CLEA, 2009]
Australia	20.00	300.00	1.00	3.00	50.00	100.00	200.00	n.a	60.00	[EPAA, 2012]
Taiwan	60.00	300.00	2.00	5.00	250.00	200.00	600.00	n.a	200.00	[Dar-Yuan Chia-Hsing, 2011]
Bulgaria	10.00	26.00	0.03	0.40	65.00	34.00	88.00	20.00	46.00	Atanassov, 2007]
Canada	20.00	200.00	0.80	3.00	250.00	150.00	500.00	n.a	100.00	[CME, 2009]
China	30.00	80.00	0.70	0.50	200.00	100.00	250.00	n.a	50.00	[EPMC, 2015]
Tanzania	1.00	200.00	2.00	1.00	100.00	200.00	150.00	n.a	100.00	[He et al., 2015]
FAO/WHO Guidelines	20.00	100.00	n.a	3.00	100.00	100.00	300.00	50.00	50.00	[Chiroma et al., 2014]
EU Guidelines	n.a	300.00	n.a	3.00	150.00	140.00	300.00	n.a	75.00	[EU, 2002]
South Africa	5.80	20.00	0.93	7.50	6.50	16.00	240.00	300.00	91.00	[DEA, 2010]

n.a: not available

4.4.3 Toxic heavy metal concentrations in coal samples

The mean concentrations of toxic heavy metals in coal from within the power station in mg/kg are presented in Table 4-11. These mean concentrations were used to compute the mean daily intakes for residents in the study area resulting in carcinogenic and non-carcinogenic risk valuation for individual public members.

Table 4 - 11: Toxic heavy metal concentration values in coal samples

Sample Code	**Toxic heavy metal concentration (mg/kg)**								
	As	**Pb**	**Hg**	**Cd**	**Cr**	**Cu**	**Zn**	**Co**	**Ni**
COAL 1	0.705	11.190	0.102	0.197	111.500	20.970	19.520	4.096	114.800
COAL 2	0.717	12.810	0.088	0.169	98.890	23.160	19.550	3.929	35.070
COAL 3	0.610	11.930	0.136	0.165	76.320	21.590	18.030	4.569	26.960
COAL 4	0.567	10.800	0.057	0.145	87.460	17.830	11.450	3.219	20.510
COAL 5	1.781	13.230	0.140	0.151	84.350	21.400	11.350	4.119	21.800
COAL 6	0.551	11.630	0.062	0.153	83.060	22.120	13.340	3.646	20.710
COAL 7	0.593	11.020	0.059	0.154	94.790	21.160	14.900	3.314	18.960
COAL 8	0.677	11.800	0.086	0.157	80.180	20.140	13.240	3.341	18.790
COAL 9	0.577	9.740	0.080	0.105	60.180	14.150	9.882	2.431	13.470
Average	0.753	11.572	0.090	0.155	86.303	20.280	14.585	3.629	32.341
Minimum	0.551	9.740	0.057	0.105	60.180	14.150	9.882	2.431	13.470
Maximum	1.781	13.230	0.140	0.197	111.500	23.160	19.550	4.569	114.800

The mean concentration of heavy metals in coal samples are presented in descending order such that Cr > Ni > Cu > Zn > Pb > Co > As > Cd > Hg. This observation is captured in Figure 4-10. The ranges of these heavy metals in mg/kg were as follows: Cr (60.180 to 111.500 with an average of 86.303); Ni (13.470 to 114.800 with an average of 32.341); Cu (14.150 to 23.160 with an average of 20.280); Zn (9.882 to 19.550 with an average of 14.585); Pb (9.740 to 13.230 with an average of 11.572); Co (2.431 to 4.569 with an average of 3.629); As (0.551 to 1.781, averaging 0.753); Cd (0.105 to 0.197, averaging 0.155); Hg (0.057 to 0.140, averaging 0.090. These results showed coal samples from the power station generally have higher heavy metal concentrations as compared to soil and water samples from the surrounding area.

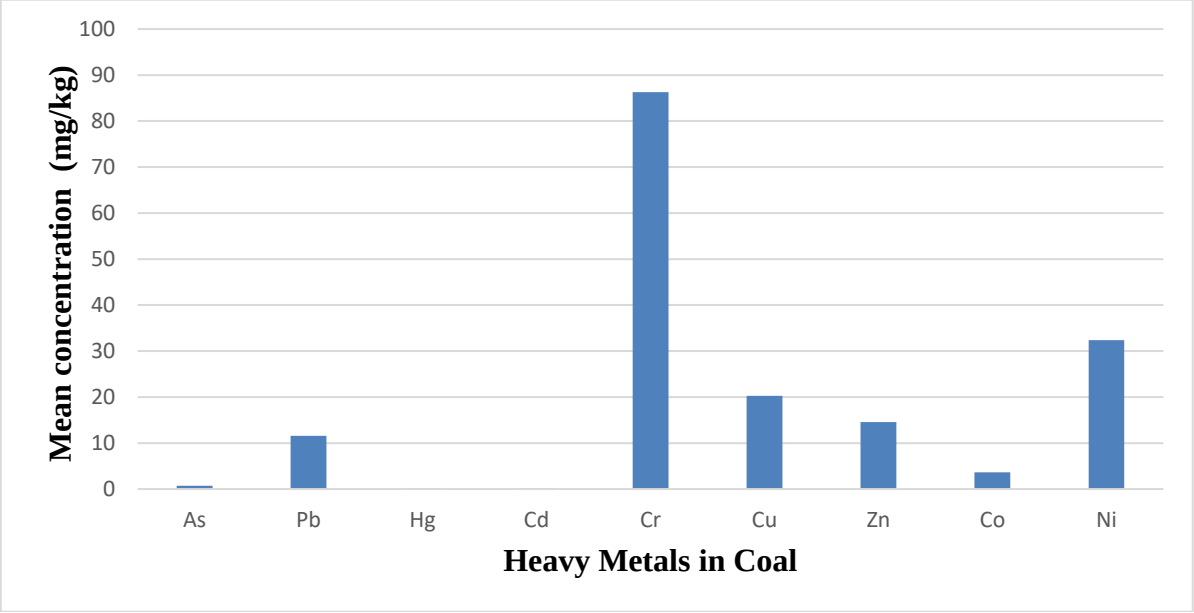

Fig. 4 - 10: Comparison of heavy metals from coal samples

The results were compared with the most common maximum and minimum concentrations of heavy metals in British, USA, Australian and Chinese [Xu et al., 2003] coals that are presented in Table 4-12. Cr and Ni were the highest in the current study, such that the measured value of Cr was larger than its respective maximum value in Table 4-12, while the measured value of Ni was lower than its respective maximum value in the same. The presence of elevated concentrations of the toxic elements such Cr and Ni could be detrimental to human beings and aquatic life since most toxic elements attack the proteins such as enzymes. The elevated concentrations of Cr and Ni could be attributed to seasonal variations in sampling results [Adaikpoh, Nwajei and Ogala, 2005]. All other measured heavy metal elemental concentrations from the study were found to be lower than their respective maximum values from Table 4-12.

Table 4 - 12: Worldwide values of heavy metal concentration in coal [Xu et al., 2003]

Heavy metal element	**Concentration (mg/kg)**	
	Min	**Max**
Cr	0.50	60.00
Co	0.50	30.00
Cu	5.00	50.00
Pb	0.50	80.00
Mn	5.00	300.00
Ni	0.20	50.00
Zn	0.20	300.00
Hg	0.50	1.00
Ag	0.50	2.00
As	0.50	80.00

4.4.4 Heavy metal concentration in bottom ash samples

The mean heavy metal concentrations in bottom ash from within the power station are presented in Table 4-13. These mean concentrations were used to compute the mean daily intakes for residents in the study area giving rise to the carcinogenic as well as non-carcinogenic risk assessment on individual public members.

Table 4 - 13: Mean of heavy metals concentration values in bottom ash samples

Sample Code	Toxic heavy metal concentration (mg/kg)								
	As	**Pb**	**Hg**	**Cd**	**Cr**	**Cu**	**Zn**	**Co**	**Ni**
BA01	5.143	16.200	0.035	0.461	106.200	20.010	21.510	11.350	60.850
BA03	5.574	16.420	0.037	0.505	130.700	28.060	22.860	13.280	59.560
BA04	5.867	17.520	0.037	0.514	130.800	28.830	24.030	13.600	60.210
BA05	5.241	15.320	0.039	0.484	122.100	26.850	21.790	12.150	56.940
BA06	5.452	17.470	0.034	0.548	132.000	29.260	24.760	13.980	64.070
BA07	5.531	11.240	0.045	0.415	95.110	21.260	21.570	9.408	53.870
BA08	5.921	15.380	0.045	0.459	108.200	21.310	23.840	11.130	61.960
BA09	4.947	13.910	0.037	0.400	90.750	21.470	19.630	9.006	55.970
BA10	5.450	14.470	0.040	0.445	102.700	22.220	23.670	10.370	58.380
Average	5.458	15.326	0.039	0.470	113.173	24.363	22.629	11.586	59.090
Minimum	4.947	11.240	0.034	0.400	90.750	20.010	19.630	9.006	53.870
Maximum	5.921	17.520	0.045	0.548	132.000	29.260	24.760	13.980	64.070

The mean heavy metal concentrations for bottom ash samples are presented in descending order such that Cr > Ni > Cu > Zn > Pb > Co > As > Cd > Hg. This observation is captured in Figure 4-11. These heavy metals ranged as follows in mg/kg: Cr (90.750 to 132.000 with an average of 113.173); Ni (53.870 to 64.070 with an average of 59.090); Cu (20.010 to 29.260 with an average of 24.363); Zn (19.630 to 24.760 with an average of 22.629); Pb (11.240 to 17.520 with an average of 15.326); Co (9.006 to 13.980 with an average of 11.586); As (4.947 to 5.921 with an average of 5.458); Cd (0.400 to 0.548 with an average of 0.470); Hg (0.034 to 0.045 with an average of 0.039) respectively. The results showed bottom ash samples from the power station generally have higher heavy metal concentrations as compared to coal and soil samples from the study area. This could be attributed to volatilization as well as enrichment of inorganic heavy metals which ultimately gives rise to a loss or decrease in the quantity of organic components [Savic et al., 2018]. The measured results are comparable with bottom ash heavy metal concentrations determined in Serbia, Finland and other worldwide heavy metal concentrations of bottom ash as revealed in Table 4-14. The mean heavy metal concentrations of Cr and Ni were found to be the highest in the current study. The presence of elevated concentrations of the toxic elements such Cr and

Ni could be detrimental to human beings and aquatic life since most toxic elements attack the proteins such as enzymes. The elevated concentrations of Cr and Ni could be attributed to seasonal variations in sampling results [Adaikpoh, Nwajei and Ogala, 2005].

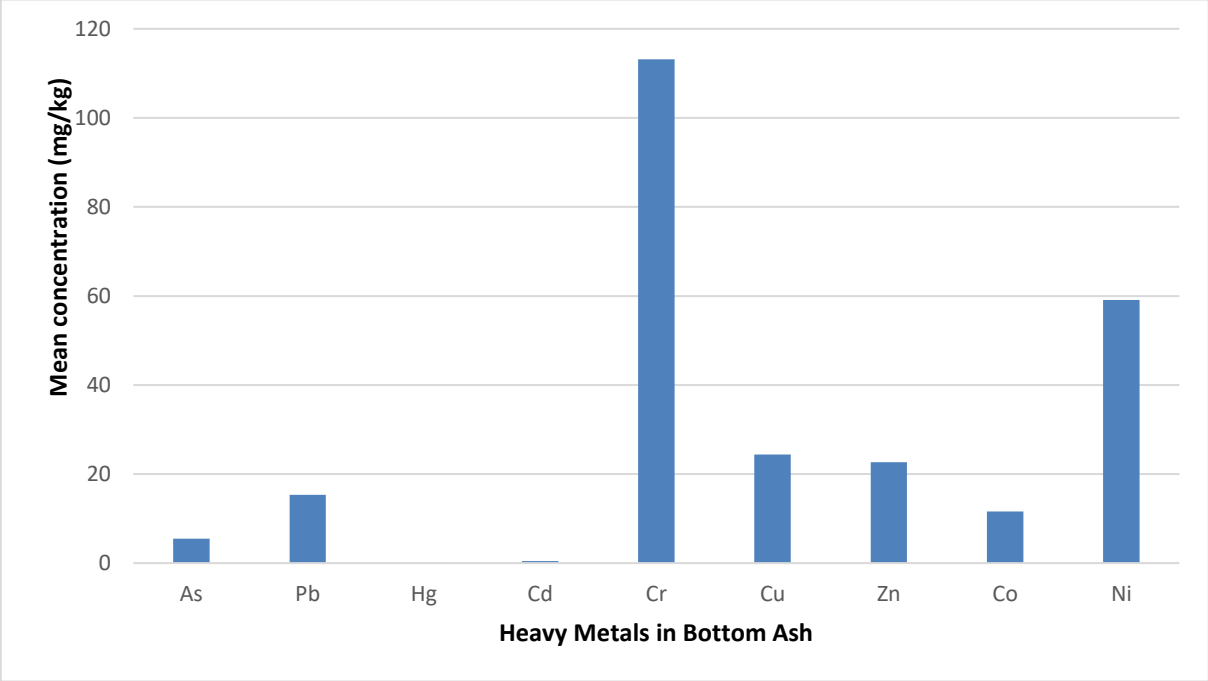

Fig. 4 - 11: Comparison of heavy metals from bottom ash sample

Table 4 - 14: Worldwide values of heavy metal concentration in bottom ash

Country	Concentration (mg/kg)								Source
	Cu	**Pb**	**Cd**	**Zn**	**Hg**	**As**	**Cr**	**Ni**	
Serbia (Kostolac)	281	45	0.87	189	1.3	141.2	428.3	219	[Savic et al., 2018]
Serbia (Gacko)	550.3	56.5	5.9	374	0.2	94	482.1	505.2	[Savic et al., 2018]
Finland	16.9	< 3.0	< 3.0	256.0	n.a	3.9	10.9	6.3	[Manskinen and Pöykiö, 2011]
Worldwide	n.a	35	< 250	950	< 4	4000	270	700	[Savic et al., 2018]

n.a: not available

4.4.5 Toxic heavy metal concentration in fly ash

The mean concentrations of heavy metals in fly ash from within the power station in mg/kg are presented in Table 4-15. These mean concentrations were also used to compute the mean daily intakes for residents in the study area resulting in carcinogenic and non-carcinogenic risk assessment for individual members of the public.

Table 4 - 15: Mean of heavy metals concentration values in fly ash samples

Sample Code	Heavy metals concentration (mg/kg)								
	As	**Pb**	**Hg**	**Cd**	**Cr**	**Cu**	**Zn**	**Co**	**Ni**
FA01	4.872	27.130	0.142	0.382	109.900	32.600	27.150	12.070	44.970
FA02	3.971	30.150	0.513	0.304	96.940	32.850	21.570	10.880	44.860
FA03	4.330	34.250	0.305	0.340	106.000	37.540	22.880	12.020	49.190
FA04	4.766	26.750	0.150	0.392	103.000	32.580	29.690	12.290	45.460
FA05	3.764	27.710	0.294	0.291	77.730	32.040	21.300	10.110	40.620
FA06	4.934	23.860	0.147	0.347	88.300	24.900	29.790	9.847	43.170
FA07	4.282	27.610	0.275	0.285	82.370	27.430	24.440	9.396	44.340
FA08	4.223	28.100	0.271	0.288	84.700	27.380	22.430	9.543	45.460
FA09	4.211	28.050	0.285	0.285	85.270	28.090	21.960	9.668	44.720
Average	4.373	28.179	0.265	0.324	92.690	30.601	24.579	10.647	44.754
Minimum	3.764	23.860	0.142	0.285	77.730	24.900	21.300	9.396	40.620
Maximum	4.934	34.250	0.513	0.392	109.900	37.540	29.790	12.290	49.190

The mean concentration of heavy metals in fly ash samples are presented in descending order such that Cr > Ni > Cu > Pb > Zn > Co > As > Cd > Hg. This observation is captured in Figure 4-12. The ranges of these heavy metals in mg/kg were as follows: Cr (77.730 to 109.900 with an average of 92.690); Ni (40.620 to 49.190 with an average of 44.754); Cu (24.900 to 37.540 with an average of 30.601); Pb (23.860 to 34.250 with an average of 28.179); Zn (21.300 to 29.790 with an average of 24.579); Co (9.396 to 12.290 with an average of 10.647); As (3.764 to 4.934 with an average of 4.373); Cd (0.285 to 0.392 with an average of 0.324); Hg (0.142 to 0.513 with an average of 0.265). The results showed that fly ash samples from the power station generally have relatively higher heavy metal concentrations as compared to bottom ash and coal samples. This could be attributed to volatilization as well as concentration of inorganic heavy metals which ultimately gives rise to a loss or decrease in the quantity of organic components [Savic et al., 2018]. The measured results generally fall within the fly ash concentrations of heavy metals in Greece, Spain and UK as presented in Table 4-16. Average heavy metal concentrations of Cr and Ni were found to be the highest. The presence of elevated concentrations

of the toxic elements such Cr and Ni could be detrimental to human beings and aquatic life since most toxic elements attack the proteins such as enzymes. The elevated concentrations of Cr and Ni could be attributed to seasonal variations in sampling results and to the fact that the elemental components of fly ash are not entirely bound to the particles [Adaikpoh, Nwajei and Ogala, 2005]. All elements that were determined quantitatively in this research have the potential of leaching from the fly ash to a variable extent [Llorens et al., 2001; Querol et al., 2001].

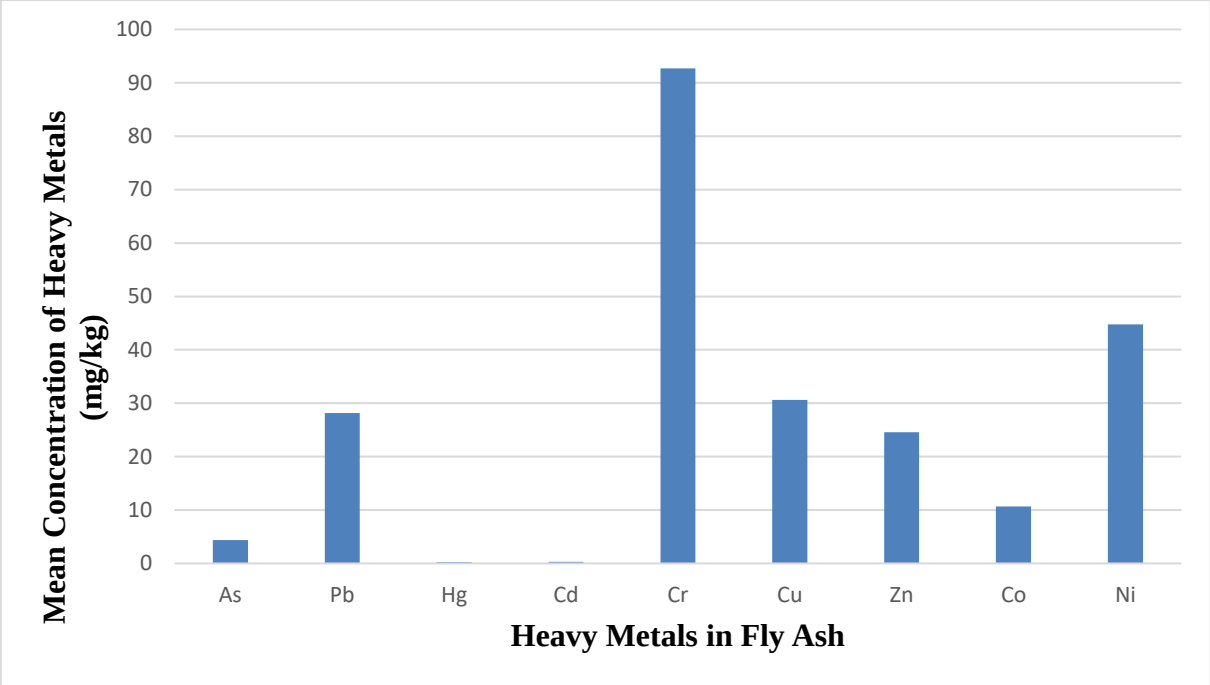

Fig. 4 - 12: Toxic heavy metal concentrations in fly ash

Table 4 - 16: Worldwide heavy metal concentrations in fly ash

Country	**Concentration (mg/kg)**											**Source**
	As	**Cd**	**Ca**	**Cr**	**Co**	**Cu**	**Pb**	**Mn**	**Hg**	**Ni**	**Zn**	
Greece	n.a	11.6-14.4	n.a	110-160	n.a	31.8-62.8	123-143	213-330	n.a	n.a	59.6-86.9	Fytianos and Tsaniklidi 1998
Spain	60	1.3	39700	134.2	29.2	71.8	52.0	324.6	0.01	87.9	221.3	Llorens et al. 2001
UK	40-205 (105)	0.13-0.82 (0.30)	n.a	n.a	n.a	n.a	17-176 (59)	n.a	n.a	n.a	n.a	Wedge et al. 1986
Botswana	3.76-4.93 (4.37)	0.29-0.39 (0.32)	48400-69870 (53990)	77.73-109.90 (92.69)	9.40-12.29 (10.65)	24.90-37.54 (30.60)	23.86-34.25 (28.18)	512.10-868.10 (625.47)	0.14-0.51 (0.27)	40.62-49.19 (44.75)	21.30-29.79 (24.58)	This study

n.a: not available

4.5 Non-carcinogenic risk assessment for toxic heavy metals due to soil and water exposure routes

The calculated average daily intakes (ADI) of different metals as well as the reference doses (RfD) from Table 3-3 were useful in computing the non-carcinogenic risk to members of the public due to heavy metals. The computed values were also tabulated as the hazard quotient (HQ) as well as hazards index (HI) for dermal, inhalation and ingestion pathways by means of equations 3.17 and 3.18.

4.5.1 Non-carcinogenic risk assessment due to toxic heavy metals in soil

In the case of non-carcinogenic risk calculations due to heavy metals in soil, ADI values shown in Table 4-17 were used. The ADI values were calculated by means of equations 3.13, 3.14 and 3.16 presented in Chapter 3. HQ and HI values are essential parameters for quantifying non-carcinogenic risk of heavy metals. If both HI and HQ are below one, then there is no significant risk on individual members of the public. If both values are above one, then there is a possibility for non-carcinogenic effects [Durowoju et al., 2018]. Table 4-18 gives HQ and HI values due to heavy metals from soil. The results show that the total HQ value is 0.42, which is less than one and therefore potentially not harmful. The dermal exposure route is the main source of the non-carcinogenic effect, trailed by the ingestion exposure route having values of 0.384 and 0.0379 respectively. The lowest contributor to the non-carcinogenic effect was the inhalation exposure route with a value of 0.000714.

Table 4 - 17: ADI values for non-carcinogenic risk calculations in soil samples

Parameter	ADI values for toxic heavy metals (mg/kg/day)									Total
	As	Pb	Hg	Cd	Cr	Cu	Zn	Co	Ni	
Ingestion	8.05E-07	5.94E-06	3.70E-08	1.10E-07	9.27E-05	2.07E-05	1.53E-05	8.79E-06	2.45E-05	1.69E-04
Inhalation	1.24E-10	9.14E-10	5.69E-12	1.69E-11	1.43E-08	3.19E-09	2.36E-09	1.35E-09	3.76E-09	2.60E-08
Dermal	1.99E-07	1.47E-06	9.16E-09	2.71E-08	2.30E-05	5.13E-06	3.79E-06	2.18E-06	6.06E-06	4.18E-05
Total	1.01E-06	7.41E-06	4.62E-08	1.37E-07	1.16E-04	2.59E-05	1.91E-05	1.10E-05	3.05E-05	2.11E-04

Table 4 - 18: HQ and HI values for heavy metals in soils

Parameter	HQ values									Total (HI)
	As	Pb	Hg	Cd	Cr	Co	Ni	Cu	Zn	
Ingestion	2.68E-03	1.65E-03	1.23E-04	2.19E-04	3.09E-02	4.39E-04	1.22E-03	5.60E-04	5.10E-05	3.79E-02
Inhalation	4.13E-07	n.a	6.62E-08	2.96E-07	4.76E-04	2.37E-04	n.a	n.a	n.a	7.14E-04
Dermal	6.65E-04	n.a	3.05E-05	5.43E-05	n.a	3.82E-01	1.08E-03	2.14E-04	5.06E-05	3.84E-01
Total	3.35E-03	1.65E-03	1.54E-04	2.74E-04	3.14E-02	3.83E-01	2.31E-03	7.74E-04	1.02E-04	4.23E-01

n.a: not available

4.5.2 Non-carcinogenic risk assessment due to heavy metals in water

Only dermal and ingestion pathways were considered for the non-carcinogenic risk assessment for water. Table 4-19 gives the actual used ADI, while the HQ values are presented in Table 4-20. Equations 3.13 and 3.15 as given in Chapter 3, were used to determine the respective ADI values in water. Table 4-20 gives HQ and HI values due to heavy metal presence in water. The results presented show that the total HQ value is 0.009, which is less than one and therefore posing no significant risk to harmful effects. The dermal exposure route was the major cause of non-carcinogenic risk with a value of 9.41E-03, followed by the ingestion exposure route with a value of 8.80E-07.

Table 4 - 19: ADI values due to water samples from the study area

Parameter	ADI values for heavy metals from water							Total
	As	Pb	Cr	Cu	Zn	Co	Ni	
Ingestion	2.74E-11	7.95E-10	1.64E-10	1.24E-08	2.39E-08	5.48E-11	1.53E-09	3.88E-08
Dermal	2.38E-08	6.91E-07	1.43E-07	1.07E-05	2.08E-05	4.77E-08	1.33E-06	3.38E-05
Total	2.39E-08	6.92E-07	1.43E-07	1.08E-05	2.08E-05	4.77E-08	1.34E-06	3.38E-05

Table 4 - 20: HQ and HI values for heavy metals in water samples

Parameter	HQ values							Total (HI)
	As	Pb	Cr	Cu	Zn	Co	Ni	
RfD(ing)	3.00E-04	3.30E-03	3.00E-03	3.70E-02	3.00E-01	2.00E-02	2.00E-02	
RfD(der)	3.00E-04	0.00E+00	0.00E+00	2.40E-02	7.50E-02	5.70E-06	5.60E-03	
Ingestion	9.13E-08	2.41E-07	5.48E-08	3.34E-07	7.95E-08	2.74E-09	7.67E-08	8.80E-07
Dermal	7.95E-05	n.a	n.a	4.48E-04	2.77E-04	8.36E-03	2.38E-04	9.41E-03
Total	7.95E-05	2.41E-07	5.48E-08	4.48E-04	2.77E-04	8.36E-03	2.38E-04	9.41E-03

n.a: not available

4.5.3 Non-carcinogenic risk assessment synopsis for toxic heavy metals

Table 4-21 presents a summary of the non-carcinogenic risk assessment due to toxic heavy metals through different pathways in the study. The total HQ value, which is also the HI was found to be 0.432. This cumulative value is below one, potentially not posing risk to local residents. The total HI value for soil samples is 4.23×10^{-1} while that for water samples is 9.41E-03. This higher HI value for soil as compared to water implies that soil poses a greater non-carcinogenic risk compared to water in the area. The heavy metal Co was the major cause of the non-cancer risk, trailed by As, with Cr contributing the least.

Table 4 - 21: Summary of HQ and HI values for water and soil samples

Medium	Parameter	HQ values									Total (HI)
		As	Pb	Hg	Cd	Cr	Co	Ni	Cu	Zn	
Soil	**Ingestion**	2.68E-03	1.65E-03	1.23E-04	2.19E-04	3.09E-02	4.39E-04	1.22E-03	5.60E-04	5.10E-05	**3.79E-02**
	Inhalation	4.13E-07	n.a	6.62E-08	2.96E-07	4.76E-04	2.37E-04	n.a	n.a	n.a	**7.14E-04**
	Dermal	6.65E-04	n.a	3.05E-05	5.43E-05	n.a	3.82E-01	1.08E-03	2.14E-04	5.06E-05	**3.84E-01**
	Sub-total	**3.35E-03**	**n.a**	**1.54E-04**	**2.74E-04**	**n.a**	**3.83E-01**	**n.a**	**n.a**	**n.a**	**4.23E-01**
Water	**Ingestion**	9.13E-08	2.41E-07	-	-	5.48E-08	2.74E-09	7.67E-08	3.34E-07	7.95E-08	**8.80E-07**
	Dermal	7.95E-05	n.a	-	-	n.a	8.36E-03	2.38E-04	4.48E-04	2.77E-04	**9.41E-03**
	Sub-total	**7.95E-05**	**2.41E-07**	**-**	**-**	**5.48E-08**	**8.36E-03**	**2.38E-04**	**4.48E-04**	**2.77E-04**	**9.41E-03**
Total		**3.43E-03**	**2.41E-07**	**1.54E-04**	**2.74E-04**	**5.48E-08**	**3.91E-01**	**2.38E-04**	**4.48E-04**	**2.77E-04**	**4.32E-01**

n.a: not available

4.6 Carcinogenic risk assessment due to heavy metals in water and soil

Pb, As, Cr, Co and Cd were regarded as metals having the potential to induce carcinogenic risk. Cancer risk for individual public members were computed by utilizing the mean contributions from different toxic heavy metals in the environment through all the exposure pathways. Equations 3.13, 3.14, 3.15 and 3.16 from Chapter 3 were useful in computing the ADI values. Equations 3.19, 3.20 and 3.21, from the same chapter, were used in estimating the cancer risk.

4.6.1 Carcinogenic risk assessment for heavy metals due to soil

Soil carcinogenic risk magnitudes were calculated with reference to the average daily intake (ADI) values as presented in Table 4-22.

Table 4 - 22: ADI values for soil carcinogenic risk calculations

Parameter	**ADI values of toxic heavy metals (mg/kg/day)**					**Total**
	As	Pb	Cd	Cr	Co	
Ingestion	3.45E-07	2.55E-06	4.70E-08	3.97E-05	3.77E-06	4.64E-05
Inhalation	5.31E-11	3.92E-10	7.23E-12	6.11E-09	5.79E-10	7.14E-09
Dermal	8.55E-08	6.30E-07	1.16E-08	9.84E-06	9.33E-07	1.15E-05
Total	4.31E-07	3.18E-06	5.86E-08	4.96E-05	4.70E-06	5.80E-05

The total cancer risk for soil was 1.04 as depicted in Table 4-23. This risk was mainly driven by the inhalation exposure route with a cancer risk of 1.00, followed by the ingestion route with a cancer risk of 0.0369. The least was the dermal pathway with a cancer risk of 1.28×10^{-7}.

Table 4 - 23: Cancer risk values for individual public members due to heavy metals in soil

Parameter	**Cancer risk values**					**Total risk**
	As	Pb	Cd	Cr	Co	
Ingestion	5.18E-07	3.68E-02	-	1.99E-05	-	3.69E-02
Inhalation	7.97E-10	1.64E-11	4.55E-11	1.00E+00	5.68E-09	1.00E+00
Dermal	1.28E-07	-	-	-	-	1.28E-07
Total	6.47E-07	3.68E-02	4.55E-11	1.00E+00	5.68E-09	1.04E+00

4.6.2 Carcinogenic risk assessment for toxic heavy metals in water

Dermal and ingestion pathways were useful in the cancer risk estimation due to toxic heavy metals in water. Table 4-24 presents the ADI values for water, while Table 4-25 shows the individual cancer risk

values for the same. The cancer risk was not calculated for those metals whose cancer slope factors (CSF) are unknown. The total cancer risk from water samples from the study area was 1.54 x 10^{-8} mainly due to dermal contact. Table 4-24 shows that the total average daily intake (ADI) for heavy toxic metals from water was 3.99 x 10^{-7}, which was also mainly through dermal contact.

Table 4 - 24: ADI values for carcinogenic risk in water

Parameter	**ADI values for heavy metals**					**Total**
	As	**Pb**	**Cd**	**Cr**	**Co**	
Ingestion	1.17E-11	3.41E-10	1.17E-11	7.05E-11	2.35E-11	4.58E-10
Dermal	1.02E-08	2.96E-07	1.02E-08	6.13E-08	2.04E-08	3.98E-07
Total	1.02E-08	2.97E-07	1.02E-08	6.14E-08	2.05E-08	3.99E-07

Table 4 - 25: Cancer risk values for toxic heavy toxic metals in water

Parameter	**Cancer risk values**					**Total risk**
	As	**Pb**	**Cd**	**Cr**	**Co**	
Ingestion	1.76E-11	2.89E-12	-	3.52E-11	-	5.57E-11
Dermal	1.53E-08	-	-	-	-	1.53E-08
Total	1.53E-08	2.89E-12	-	3.52E-11	-	1.54E-08

4.6.3 Carcinogenic risk assessment synopsis for toxic heavy metals

Table 4-26 shows a summary of the cancer risks from soil as well as water in the study area. The total carcinogenic risk from soil and water was found to be 1.04. Based on this table, the contribution of heavy metals to total cancer risk is such that Cr > Pb > As > Co > Cd. It was clearly observed from Table 4-26 that soil contributed the most to the total cancer risk with a total of 1.04, while water had the lowest contribution of 1.54 x 10^{-8}. The elevated concentration of the toxic heavy metal Cr might pose an increased risk of stomach, buccal, cavity, respiratory, pharynx and prostate cancers to people in the study area [Deng et al., 2019].

Table 4 - 26: Cancer risk values due to heavy metals in water and soil

Medium	Parameter	Cancer risk values					Total risk
		As	Pb	Cd	Cr	Co	
Soil	**Ingestion**	5.18E-07	3.68E-02	-	1.99E-05	-	**3.69E-02**
	Inhalation	7.97E-10	1.64E-11	4.55E-11	1.00E+00	5.68E-09	**1.00E+00**
	Dermal	1.28E-07	-	-	-	-	**1.28E-07**
	Sub-total	**6.47E-07**	**3.68E-02**	**4.55E-11**	**1.00E+00**	**5.68E-09**	**1.04E+00**
Water	**Ingestion**	1.76E-11	2.89E-12	-	3.52E-11	-	**5.57E-11**
	Dermal	1.53E-08	-	-	-	-	**1.53E-08**
	Sub-total	**1.53E-08**	**2.89E-12**	**-**	**3.52E-11**	**-**	**1.54E-08**
Total		**6.62E-07**	**3.68E-02**	**4.55E-11**	**1.00E+00**	**5.68E-09**	**1.04E+00**

4.7 Cancer risk using RESRAD-OFFSITE code

RESRAD-OFFSITE software was utilized to estimate the cancer risk for residents and other public members in the vicinity of the power station. RESRAD input parameters from Table 3-1 were used as the basis for the calculations. Figure 4-13 presents the total cancer risk from all pathways over a period of 130 years. In the case of natural radionuclides ^{40}K, ^{232}Th and ^{238}U, the maximum cancer risk (from RESRAD code) with all pathways summed was found to be 0.003 from year 25. This maximum cancer risk is ten times higher than the recommended WHO limit. The minimum cancer risk was found to be 0.002 at year 0, which is 6.7 times higher than the recommended WHO limit. Based on Figure 4-16, it was concluded that ^{232}Th was the key contributor to the cancer risk, tailed by ^{40}K and ^{238}U. The allowable cancer risk for regulatory functions falls in the range of 1×10^{-6} to 1×10^{-4} [USEPA, 1989]. However, the Republic of South Africa has set a cancer risk limit for members of the public at 5×10^{-6} [Government Gazette, 2006]. This implies that the total cancer risk from year 0 to year 130 was higher than acceptable values according to South African and USEPA risk limits. The cancer risk from RESRAD model are higher than the risk assessment based on the radiological risk hazards D, AEDE, Ra_{eq} and H_{ext}. This may be attributed to the fact that RESRAD model takes into account more parameters and sophisticated environmental transport models, while the radiological assessment only takes into account a fewer number of parameters [King and Keil, 2006]. The radiological hazard indices also tend to look at a single exposure pathway, while RESRAD considers all possible pathways of exposure and presents a much more realistic estimation of the radiological risk.

.

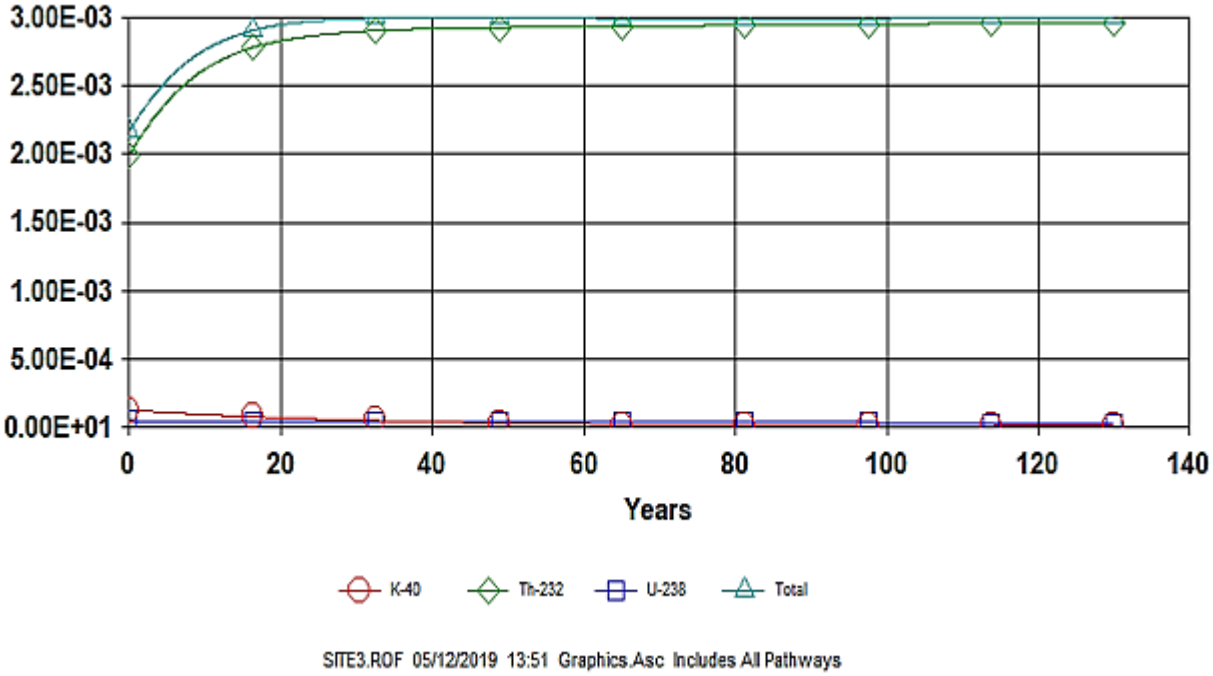

Fig. 4 - 13: Individual cancer risk from ^{238}U, ^{232}Th and ^{40}K through all pathways added over 130 years

Figure 4-14 shows that the total peak dose at time t = 0 year is 0.3 ± 0.1 mSv/y for all pathways summed and is lower than the basic radiation dose limit of 1 mSv/y for members of the public. It then increases to a value of 1.4 ± 0.1 mSv/y at year 40, a value which is greater than the basic radiation dose limit of 1 mSv/y for members of the public.

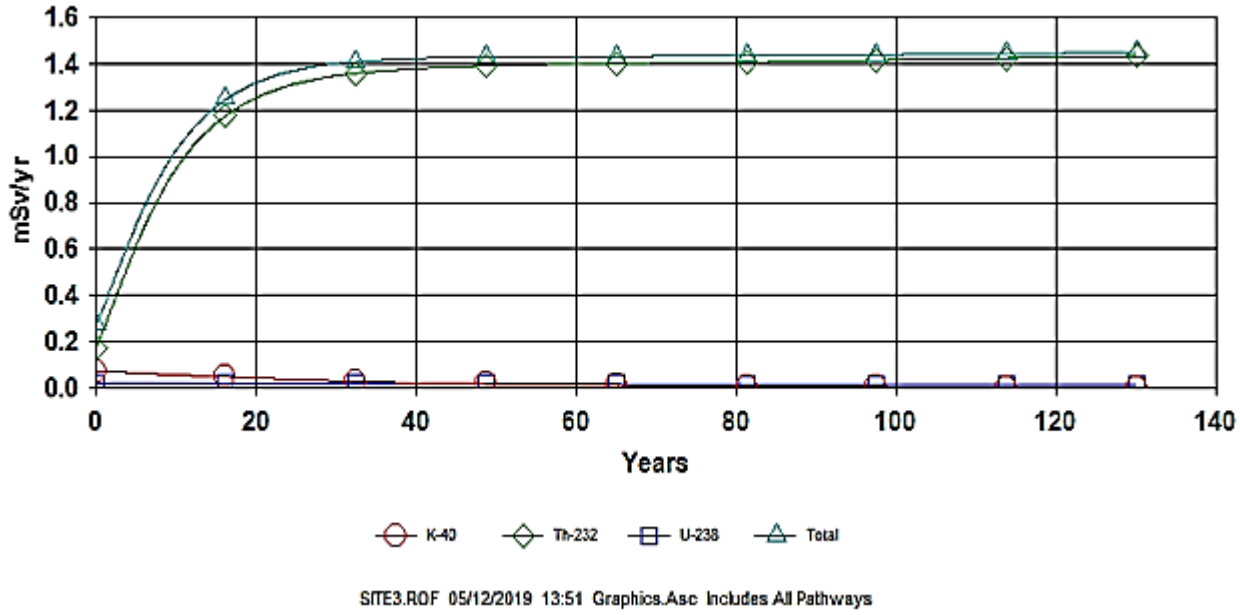

Fig. 4 - 14: Summed total dose due to all nuclides and all pathways

4.8 Summary of cancer risk from natural radionuclides and toxic heavy metals

For regulatory purposes, the allowable cancer risk varies from 10^{-6} to 10^{-4} [USEPA, 1989]. However, the Republic of South Africa has set a cancer risk limit for members of the public at 5×10^{-6} [Government Gazette, 2006]. In the case of natural radionuclides ^{40}K, ^{238}U and ^{232}Th, the maximum cancer risk (from RESRAD code) with all pathways summed was found to be 0.003. As a recap, the overall cancer risk from heavy toxic metals was found to be 1.04. Hence the total cancer risk owing to both heavy toxic metals and the natural radionuclides ^{232}Th, ^{40}K and ^{238}U was found to be 1.043. This value is higher than the acceptable values according to both the South African (5×10^{-6}) and USEPA (10^{-6} to 10^{-4}) standards.

Chapter 5: Summary, conclusion and recommendations

5.1 Summary and conclusions

The aim of the study was to determine the naturally occurring radioactivity and their variations with respect to time around the Morupule-B Coal Power Station using the RESRAD radiation code. The study was inspired by the fact that no previous studies had been carried out to determine and radioecologically model the natural radioactivity as well as the possible risks posed to public members by these contaminants. Soil, water, coal, bottom ash as well as fly ash samples were collected from the study area. Gamma spectrometry was utilized to determine the activity concentrations of natural radionuclides from soil, coal, bottom ash as well as fly ash samples. ICP-MS was used to measure the concentrations of heavy metals in water, soil, coal, bottom ash and fly ash samples.

The first objective was to determine the radiological risk due to the natural radioactive elements. A radiological hazard assessment was performed for soil, coal, bottom ash and fly ash in this study. From Table 4-8, the estimated absorbed dose rates (D) for soil ranged from 12.817 ± 1.716 nGy/h to 49.095 ± 1.187 nGy/h, with a mean of 25.549 ± 9.026 nGy/h. These values are lower than the worldwide average absorbed dose rate of 57 nGy/h [Santawamaitre, 2012]. Table 4-8 shows that the estimated annual effective dose equivalent (AEDE) for soil ranged from 15.719 ± 2.105 µSv/y to 60.210 ± 1.456 µSv/y with a mean of 31.333 ± 11.070 µSv/y. These values of annual effective dose equivalent (AEDE) are within the worldwide mean value of 70 µSv/y [Santawamaitre, 2012]. From Table 4-8, the radium equivalent activity (Ra_{eq}) for soil ranged from 27.217 ± 3.736 Bq/kg to 104.263 ± 2.567 Bq/kg, with a mean of 54.435 ± 19.464 Bq/kg. These values are below the recommended limit of 370 Bq/kg [Faanu, 2011]. From Table 4-8, the external hazard index (H_{ext}) ranges from 0.073 ± 0.010 to 0.282 ± 0.007, with a mean of 0.147 ± 0.053. The average H_{ext} value is less than one, meaning that there is insignificant external exposure risk due to NORMs in the soil [Ademola and Onyema, 2014].

From Table 4-9, the estimated absorbed dose rates (D) for coal ranged from 36.188 ± 2.199 nGy/h to 50.947 ± 2.144 nGy/h, with a mean of 42.519 ± 5.288 nGy/h. These values are all lower than the worldwide mean absorbed dose rate of 60 nGy/h [UNSCEAR, 2000; Faanu, 2011]. Table 4-9 shows that the estimated annual effective dose equivalent (AEDE) for coal ranged from 44.381 ± 2.697 µSv/y to 62.481 ± 2.629 µSv/y with a mean of 52.146 ± 6.480 µSv/y. These values of annual effective dose equivalent (AEDE) are within the worldwide mean value of 460 µSv/y [Pandit, Sahu and Puranik, 2011]. Table 4-9 further shows that the radium equivalent activity (Ra_{eq}) for coal ranged from 81.186 ± 4.773

Bq/kg to 113.635 ± 4.656 Bq/kg, with a mean of 95.156 ± 11.482 Bq/kg. These values are below the recommended limit of 370 Bq/kg [Faanu, 2011]. Table 4-9 also shows that the external hazard index (H_{ext}) for coal ranged from 0.219 ± 0.013 to 0.307 ± 0.013, with a mean of 0.257 ± 0.031. The average H_{ext} is below one, implying that there is no significant external exposure risk due to the coal [Ademola and Onyema, 2014].

From Table 4-10, the estimated absorbed dose rates (D) for bottom ash ranged from 72.748 ± 2.914 nGy/h to 140.530 ± 3.004 nGy/h, with a mean of 95.859 ± 20.357 nGy/h. These values are higher than the worldwide absorbed dose rate of 60 nGy/h [Pandit, Sahu and Puranik, 2011; UNSCEAR, 2000]. Table 4-10 shows that the estimated annual effective dose equivalent (AEDE) for bottom ash ranged from 89.218 ± 3.573 µSv/y to 172.351 ± 3.684 µSv/y with a mean of 117.563 ± 24.967 µSv/y. These values of annual effective dose equivalent (AEDE) are lower than the worldwide value of 460 µSv/y [UNSCEAR, 1993]. The radium equivalent activity (Ra_{eq}) for bottom ash ranged from 165.026 ± 6.298 Bq/kg to 317.718 ± 6.528 Bq/kg, with a mean of 217.015 ± 46.052 Bq/kg. These values are below the recommended limit of 370 Bq/kg [Faanu, 2011]. Table 4-10 also shows that the external hazard index (H_{ext}) for bottom ash ranged from 0.446 ± 0.017 to 0.858 ± 0.018, with a mean of 0.586 ± 0.124. The average H_{ext} is below one, meaning that the area is safe for human occupation with insignificant risk due to external exposure from NORMs in the bottom ash [Ademola and Onyema, 2014].

From Table 4-11, the estimated absorbed dose rates (D) for fly ash ranged from 102.540 ± 4.025 nGy/h to 215.940 ± 4.210 nGy/h, with a mean of 142.763 ± 46.278 nGy/h. These values are lower than the worldwide absorbed dose rate of 60 nGy/h [UNSCEAR, 2000]. Table 4-11 shows that the estimated annual effective dose equivalent (AEDE) for fly ash ranged from 125.751 ± 4.937 µSv/y to 264.833 ± 5.163 µSv/y with a mean of 175.086 ± 56.756 µSv/y. The values of annual effective dose equivalent (AEDE) are lower than the worldwide value of 460 µSv/y [UNSCEAR, 1993]. Radium equivalent activity (Ra_{eq}) values for fly ash samples ranged from 231.062 ± 8.744 Bq/kg to 490.247 ± 9.136 Bq/kg, with a mean of 322.435 ± 104.923 Bq/kg. The mean value is less than the recommended acceptable limit of 370 Bq/kg [Faanu, 2011]. It is important to note that Ra_{eq} values that exceed 370 Bq/kg may increase radiation hazards [Ahmed, Mohammed and Abdaljalil, 2018]. Table 4-11 further shows that the external hazard index (H_{ext}) ranged from 0.624 ± 0.024 to 1.324 ± 0.025, with a mean of 0.871 ± 0.283. The average H_{ext} value is below one, indicating a low risk from external exposure from the NORMs in the fly ash [Ademola and Onyema, 2014]. There is a notable increase in these radiological hazard quantities

in fly ash relative to the normal soil fom the study area. There is therefore still an increased risk due to the fly ash, though it is not a significant risk. Due to the stochastic nature of ionizing radiation risk, any addition to the background radiation increases the risk [Thomas and Symonds, 2016].

All estimated values for D, AEDE, Ra_{eq}, and H_{ext} in this research were generally highest for fly ash, followed by bottom ash, coal and soil samples in descending order as shown in Figure 4-11. The relatively high fly ash and bottom ash values for D, AEDE, Ra_{eq}, and H_{ext} could be attributed to the reasoning that during the combustion of coal, most of the non-combustible material, including the natural radionuclides, concentrate in both the bottom ash as well as fly ash thus enhancing the D, AEDE, Ra_{eq}, and H_{ext} values [Penfold et al., 1998]. Results from this study illustrate that all calculated annual effective dose averages of the soil, bottom ash, coal and fly ash samples are below the acceptable value being 1 mSv per year for public members [UNSCEAR, 2000]. Basing on these findings,

i. Materials from the area under study can safely be used for building and construction.
ii. Radioactive elements monitoring at the Morupule-B Coal Power Station facility is not necessary, but may be done just for purposes of creating and maintaining a database of radioactive elements and their quantities for the power station.

The second objective was to determine the toxicological risk due to toxic heavy elements. Table 4-26 presents a summary of the non-carcinogenic risk assessment due to toxic heavy metals through different pathways in the study. The total HQ value, which is also the HI was found to be 0.432. This cumulative value is below one, potentially not posing risk to people residing in the area. The total HI value for soil samples is 4.23×10^{-1} while that for water samples is 9.41E-03. This higher HI value for soil as compared to water implies that soil poses a greater non-carcinogenic risk compared to water from the study. The heavy metal Co turned out to be the major contributor to the non-cancer risk, tailed by As, with Cr contributing the least.

Table 4-31 shows a summary of the cancer risks from soil as well as water in the study area. The total carcinogenic risk from soil and water was found to be 1.04. Based on this table, the contribution of heavy metals to total cancer risk is such that Cr > Pb > As > Co > Cd. It was clearly observed from Table 4-31 that soil contributed the most to the total cancer risk with a total of 1.04, while water had the lowest contribution of 1.54×10^{-8}. The elevated concentration of the toxic heavy metal Cr might pose an

increased risk of stomach, buccal, cavity, respiratory, pharynx and prostate cancers to people in the study area [Deng et al., 2019].

The third objective was to model public radiation doses due to these natural radionuclides using RESRAD. RESRAD-OFFSITE software was utilized to estimate the cancer risk for residents and other public members in the vicinity of the power station. For regulatory duties, the allowable cancer risk varies from 10^{-6} to 10^{-4} [USEPA, 1989]. However, the Republic of South Africa has set a cancer risk limit for members of the public at 5×10^{-6} [Government Gazette, 2006]. In the case of natural radionuclides ^{40}K, ^{238}U and ^{232}Th, the maximum cancer risk (from RESRAD code) with all pathways summed was found to be 0.003. As a recap, the overall cancer risk from heavy toxic metals was found to be 1.04. Hence the total cancer risk owing to both heavy toxic metals and the natural radionuclides ^{232}Th, ^{40}K and ^{238}U was found to be 1.043. This value is higher than the acceptable values according to both the South African (5×10^{-6}) and USEPA (10^{-6} to 10^{-4}) standards. Based on this, it implies that toxic heavy elements monitoring at the Morupule-B Coal Power Station facility is necessary.

5.2 Recommendations and future work

Based on the findings from this research, the following recommendations should be considered for future studies:

- The study was limited to only primordial natural radionuclides and some selected heavy metals, but other radionuclides and less hazardous heavy metals should also be considered.
- Liquid scintillation should also be used to determine gross alpha and beta concentrations in drinking water for future works.
- Future works should also include the collection of plant samples (e.g. grass, field crops, vegetables etc) since they are a potential ingestion exposure pathway to man. This would result in more comprehensive results.
- More water samples should be collected to give a more realistic representation of water from the study area.
- Sampling should cover different seasons so as to account for seasonal variation of results. Sampling was only done at two different times within the year. It should have been done three to four times, but this was not possible due to time and logistical constraints. Future works should address these issues.

- Physico-chemical parameters such as temperature, electrical conductivity, soil pH, may also affect the migration of heavy metals and radionuclides. These should be considered for future works.

5.3 Limitations

- Some RESRAD code parameters are preset and may not be customized for the specific site.
- The radiological and RESRAD cancer risk values differ significantly since RESRAD model takes into account more parameters and sophisticated environmental transport models, while the radiological assessment only takes into account a fewer number of parameters and a single exposure pathway [King and Keil, 2006].

References

Abdel-Rahman, M. A. E. and El-Mongy, S. A. (2017). Analysis of radioactivity levels and hazard assessment of black sand samples from Rashid area, Egypt, Nuclear Engineering and Technology, pp.1752 to 1757, 10.1016/j.net.2017.07.020.

Ali, F. A. (2008). Measurements of Naturally Occurring Radioactive Materials (NORM) in Environmental Samples, Faculty of Engineering and Physical Sciences, University of Surrey.

Adaikpoh, E. O., Nwajei, G. E. and Ogala, J. E. (2005). Heavy Metals Concentrations in Coal and Sediments from River Ekulu in Enugu, Coal City of Nigeria, J. Appl. Sci. Environ. Mgt. 2005, Vol. 9 (3), pp. 5 to 8.

Ademola, J. A. and Onyema, U. C. (2014). Assessment of Natural Radionuclides in Fly Ash Produced at Orji River Thermal Power Station, Nigeria and the Associated Radiological Impact, Natural Sciences Journal, Vol. 6, pp.752 to 759.

Ahmed, R. S., Mohammed, R. S. and Abdaljalil, R. O. (2018). The Activity Concentrations and Radium Equivalent Activity in Soil Samples Collected from the Eastern Part of Basrah Governorate in Southern Iraq, International Journal of Analytical Chemistry, Article ID 2541020, https://doi.org/10.1155/2018/2541020.

Alashrah, S. and El-Taher, A. (2016). Gamma spectroscopic analysis and associated radiation hazards parameters of cement used in Saudi Arabia, J Environ Sci Technol, pp.238 to 245.

ALNabhani, K., Khan, F.and Yang, M. (2015). Review technologically enhanced naturally occurring radioactive materials in oil and gas production. Journal Process Safety and Environmental Protection. (99), pp.237 to 247.

ARPANSA (2015). Radiation Protection of the Environment, Radiation Protection Series G-1

Atieh, M. A., Ji, Y. and Kochkodan, V. (2017). Metals in the Environment: Toxic Metals Removal, Bioinorganic Chemistry and Applications.

Atanassov, I. (2007). New Bulgarian Soil Pollution Standards, Bulgarian Journal of Agricultural Science, 14(1), pp. 68 to 75, Institute for Sustainable Development, BG – 1408 Sofia, Bulgaria.

ATSDR (2007). Guidance for the Preparation of a Twenty First Set Toxicological Profile.

Avila, R., Broed, R. and Pereira, A. (2003). Ecolego - a toolbox for radioecological risk assessment, https://www.researchgate.net/publication/237552326, Accessed 03 May 2019.

Avila, R. (2019). Models for safety assessment of disposal options for VLLW.

Bal, S. S., Karatepe, S., Kuluöztürk, M. F., Yilmaz, E. and Kurşat, M. (2018). The annual change of environmental gamma Radiation in Bitlis, Journal of Science and Technology, E-ISSN 2146-7706.

Barrera, M., Casas-Ruiz, M., Alonso, J. J. and Vidal, J. (2017). Precise determination of HPGe detector efficiency for gamma spectrometry measurements of environmental samples with variable geometry and density, Nukleonika, pp.47 to 59, DOI: 10.1515/nuka-2017-0007.

Baum, M., Knox, H. D. and Miller, T. R. (2002). Nuclides and Isotopes, Chart of the Nuclides, 16th edition, Lockheed Martin Co.

Beer, J., McCracken, K. and Steiger, R. (2012). Cosmogenic Radionuclides: Theory and Applications in the Terrestrial and Space Environments, ISSN 1610-1677, DOI 10.100/978-3-642-14651-0, Springer Heidelberg Dordrecht, New York.

Bell, S. (1999). Measurement Good Practice Guide No. 11 (2), A Beginner's Guide to Uncertainty of Measurement, Centre for Basic, Thermal and Length Metrology National Physical Laboratory.

Bello, S., Muhammad, B. G. and Bature, B. (2017). Total Excess Lifetime Cancer Risk Estimation from Enhanced Heavy Metals Concentrations Resulting from Tailings in Katsina Steel Rolling Mill, Nigeria, DOI:10.4172/2169-0022.1000338.

Beretka, J. and Mathew, P. J. (1985). Natural Radioactivity of Australian Building Materials, Industrial Wastes and By-products, Health Physics 48, pp.87 to 95.

Beringer, P. and Remington, J. P. (2005). Remington: The Science and Practice of Pharmacy, Sciences, 21st Edition, Philadelphia: Lippincott Williams Publisher.

Bevington, P. R. and Robinson, D. K. (2003). Data Reduction and Error Analysis for the Physical Sciences, Third Edition, London: McGraw-Hill Higher Education.

Bode, P. (1998). Detectors of radiation, Delft University of technology, Netherlands.

Bose, S. R., Mulder, R. U., Silvain, D., Sondhaus, C. A. and Wacks, M. E. (1997). Benchmark Environmental Radioactivity at a Research Reactor Site.

Brigden, K. and Santillo, D. (2002). Heavy metal and metalloid content of fly ash collected from the Sual, Mauban and Masinloc coal-fired power plants in the Philippines, Greenpeace Research Laboratories, Department of Biological Sciences, University of Exeter, Exeter, UK.

Cember, H. and Johnson, T. E. (2009). Introduction to Health Physics, 4th Edition, New York, McGraw-Hill Companies, Inc.

Chambers, D. B. (2013). Radiological protection in North American naturally occurring radioactive material industries.

Chang, B. U., Koh, S. M., Kim, Y. J., Seo, J. S., Yoon, Y. Y., Row, J. W. and Lee, D. M. (2008). Nationwide survey on the natural radionuclides in industrial raw minerals in South Korea, Journal of Environmental Radioactivity 99, pp.455 to 460.

Chiroma, T. M., Ebewele, R. O. and Hymore, F. K. (2014). Comparative Assessment of Heavy Metal Levels in Soil, Vegetables and Urban Grey Waste Water used for Irrigation in Yola and Kano, International Refered Journal of Engineering and Science, Volume 3, pp. 01 to 09.

Choppin, G. R., Liljenzin, J. and Rydberg, J. (2002). Radiochemistry and Nuclear Chemistry, Third Edition, Butterworth-Heinemann, ISBN-10:0-7506-7463-6.

Choudhary, S. (2018). Cancer Therapy & Oncology International Journal, ISSN: 2473-554X, Juniper Publishers.

Christodoulides, G., Christofides, S., Tzortzis, M. and Tsertos, H. (2003). Gamma radiation measurements and dose rates in commercially - used natural tiling rocks (granites), Department of Physics, University of Cyprus, Nicosia, Cyprus and Medical Physics Department, Nicosia General Hospital, Nicosia, Cyprus.

Cinelli, G., Gruber, V., De Felice, L., Bossew, P., Hernandez-Ceballos, M. A., Mundigl, T. T. S. and De Cort, M. (2017). European annual cosmic-ray dose: estimation of population exposure, Journal of Maps, 13:2, pp.812 to 821, DOI: 10.1080/17445647.2017.1384934.

CLEA (2009). Heavy Metal Guidelines in Soil, Assessment of Potentially Toxic Elements, Yara UK Limited, Technical Bulletin No.6, Contaminated Land Exposure Assessment.

CME (2009). Soil, Ground Water and Sediment Standards for Use under Part XV.1 of the Environmental Protection Act, Canadian Ministry of the Environment, Canada.

Currie, L. A. (1968). Limits for qualitative detection and quantitative determination, Application to Radiochemistry, 40 (3), pp. 586 to 593.

DAR-Yuan, L. and Chia-Hsing, L. (2011). Regulatory Standards of Heavy Metal Pollutants in Soil and Groundwater in Taiwan, SGWPR Act, National Taiwan University, Taiwan.

DEA (2010). The Framework for the Management of Contaminated Land, South Africa, http:sawic.environment.gov.za/documents/562.pdf, Accessed on 12 March 2019.

Deng, Y., Wang, M., Tian, T., Lin, S., Xu, P., Zhou, L., Dai, C., Hao, Q., Wu, Y., Zhai, Z., Zhu, Y., Zhuang, G. and Dai, Z. (2019). The Effect of Hexavalent Chromium on the Incidence

and Mortality of Human Cancers: A Meta-Analysis Based on Published Epidemiological Cohort Studies. Frontiers in oncology, 9, 24. DOI:10.3389/fonc.2019.00024.

Desouky, O., Ding, N. and Zhou, G. (2015). Targeted and non-targeted effects of ionizing radiation, Journal of Radiation Research and Applied Sciences, Volume 8, Issue 2, pp. 247 to 254, https://doi.org/10.1016/j.jrras.2015.03.003.

DOH (2004). Regulation Relating to Maximum levels for Metals in Foodstuffs, South Africa, http://web.capetown.gov.za/eDocuments/Regulations_Relating_to_Maximum_Levels_for_Metals_in_Foodstuffs_-_R_500_of_2004_95200519507_245.pdf , Accessed 24 April 2019.

Durowoju, O. S., Edokpayi, J. N., Popoola, O. E. and Odiyo, J. O. (2018). Health Risk Assessment of Heavy Metals on Primary School Learners from Dust and Soil within School Premises in Lagos State, Nigeria, DOI: 10.5772/intechopen.74741.

Ecosurv. (2016). Environmental and Social Impact Assessment Statement, Morupule B Phase II Units 5 & 6 ESIA.

Egemen, E. and Coskun, Y. (1996). Regulatory leaching tests for fly ash: A case study. Waste Management & Research, pp.43 to 50.

European Commission. (1996). Exposure of air crew to cosmic radiation, Radiation Protection 85, European Commission, Luxembourg, 1996. ISBN 92-827-7994-7.

EPAA (2012). Classification and management of of contaminated soil for disposal, Environmental Protection Authority of Australia, Information Bulletin 105, Hobart, TAS 7001, Australia.

EPMC (2015). Standards of soil environmental quality of agricultural land, Environmental Protection Ministry of China, Huangbanhang 69, Beijing, China.

EU (2002). Heavy Metals in Wastes, European Commission on Environment, http://ec.europa.eu/environment/waste/studies/pdf/heavymetalsreport.pdf, Accessed 12 May 2019.

Faanu, A. (2011). Assessment of Public Exposure to Naturally Occurring Radioactive Materials from Mining and Mineral Processing Activities of Tarkwa Goldmine in Ghana (PhD Dissertation, February, 2011).

Fungaro, D. A., Cardoso da Silva, P. S., Campello, F. A., Caio da Silva Miranda and Carvalho Izidoro, J. (2017). Evaluation of Radionuclide Contamination of Soil, Coal Ash and Zeolitic Materials from Figueira Thermoelectric Power Plant in Brazil.

Ghofrani, J. (2016). Conceptualization and Software Development of a Simulation Environment for Probabilistic Safety Assessments of Radioactive Waste Repositories, Doctoral Thesis (Dissertation), Clausthal University of Technology.

Gilmore, G. R. (2008). Practical Gamma-ray Spectrometry, Second Edition, Chichester: John Wiley & Sons Ltd.

Government Gazette. (2006). Regulation Gazette No. 8454, Vol 490, No. 28755, Pretoria, South Africa.

Gruber, V. (2009). Radiation Exposure by Natural Radionuclides in Drinking Water in Upper Austria. A Radioanalytical and Hydrogeological Research and Evaluation in an International Context. PhD Thesis, University of Natural Resources and Applied Life Sciences, Vienna.

Hall, E. J. and A. J. Giaccia, A. J. (2011). Radiobiology for the radiologist, Seventh Edition, Lippincott Williams and Wilkins, Philadelphia.

Harb, S., El-Kamel, A. H., El-Mageed, A. I. A., Abbady, A. and Rashed, W. (2008). Concentration of U-238, U-235, Ra-226, Th-232 and K-40 for some granite samples in eastern desert of Egypt.

He, Z., Shentu, J., Yang, X., Baligar, V. C., Zhang, T. and Stoffella, P. J. (2015). Heavy Metal Contamination of Soils: Sources, Indicators and Assessment, Journal of Environmental Indicators, 9, pp. 17 to 18.

Heidrich, C., Brown., S. and Collier., D. (2011). Naturally Occurring Radionuclides in Australian Coal Combustion Products (CCPs).

Helaluddin, A. B. M., Khalid, R. S., Alaama, M. and Abbas, S. A. (2016). Main Analytical Techniques Used for Elemental Analysis in Various Matrices, Tropical Journal of Pharmaceutical Research, 15 (2), pp.427 to 434.

Hossain, I., Sharip, N. and Viswanathan, K. K. (2012). Efficiency and resolution of HPGe and NaI(Tl) detectors using gamma-ray spectroscopy, Scientific Research and Essays Vol. 7(1), pp.86 to 89.

IAEA (1989). Measurement of Radionuclides in Food and the Environment, Technical Report Series No. 295, Vienna, Austria.

IAEA (2002). Natural and Induced Radioactivity in Food, IAEA-TECDOC-1287, Vienna.

IAEA (2003). Guidelines for radioelement mapping using gamma ray spectrometry data, IAEA-TECDOC-1363, Vienna.

IAEA (2004). Soil sampling for environmental contaminants, IAEA-TECDOC-1415.

IAEA (2004). Quantifying Uncertainty in Nuclear Analytical Measurements, IAEA-TECDOC-1401, Vienna.

IAEA (2005). Nuclear Analytical Methods for Platinum Group Elements, IAEA TECDOC 1443, Vienna, Austria.

IRIS (2007). Integrated Risk Information System, USEPA.

Jarvis, K. (2006). National Environmental Research Centre (NERC) Facility, Thermo Fisher Scientific, UK.

Johnson, G. E., Hadjar, O. and Laskin, J. J. (2011). American Society for Mass Spectrometry, pp.1388, doi.org/10.1007/s13361-011-0154-4.

Kabata, H. and Pendias, A. (1993). Trace Elements in Soil and Plants, Second Edition, Boca Raton FL, USA.

Kamunda, C., Mathuthu, M. and Madhuku, M. (2016). Health Risk Assessment of Heavy Metals in Soils from Witwatersrand Gold Mining Basin, South Africa, International Journal of Environmental Research and Public Health.

Kamunda, C., (2017). Human Health Risk Assessment of Environmental Radionuclides and Heavy Metals around a Gold Mining Area in Gauteng Province, South Africa, Doctor of Philosophy in Physics Thesis at North-West University, Mafikeng, South Africa.

Kantele, J. (1995). Handbook of Nuclear Spectrometry, London, Academic Press Limited.

Keyser, R. M. and Hensley, W. K. (2002). Efficiency and resolution of germanium detectors as a function of energy and incident geometry, IEEE Nuclear Science Symposium Conference Record, Norfolk, VA, USA, 2002, Vol.1, pp.375 to 381 DOI: 10.1109/NSSMIC.2002.1239336.

King, D. A. and Keil, K. (2006), Comparison of Standard Radiological Risk Models and Using RESRAD to Derive Generic Risk-Based Area Factors for Final Status Surveys. Risk Analysis, 26: 175-183, DOI:10.1111/j.1539-6924.2006.00711.x.

Koliabina, D., Pepin, S., Bugai, D. A. and Avila, R. (2018). Comparison of RESRAD-OFFSITE and NORMALYSA software tools for the Tessenderlo test case. MODARIA WG3 model inter-comparison exercise, DOI: 10.13140/RG.2.2.11232.94725/1.

Krane, K. S. (1988). Introductory Nuclear Physics, Chichester: John Wiley & Sons Inc.

Kshetri, R. (2012). From a single encapsulated detector to the spectrometer for integral satellite: predicting the peak-to-total ratio at high γ – energies, Nuclear Physics Division, Saha Institute of Nuclear Physics, Bidhannagar, Kolkata, India.

Lane, T. W. and Morel, F. M. (2009). A biological function for cadmium in marine diatoms. Proc National Academy of Science, pp.4627 to 4631.

L'Annunziata, M. F. (2007). Radioactivity: Introduction and History, Amsterdam, Elsevier, B. V.

L'Annunziata, M. F. 2012. Radiation Physics and Radionuclide Decay, Handbook of Radioactivity Analysis, Third Edition.

Lapp, R. E. and Andrews, H. L. (1972), Nuclear Radiation Physics, Fourth Edition, London: Sir Isaac Pitman and Sons Ltd.

Lilley, J. (2001). Nuclear Physics: Principles and Applications, Chichester: John Wiley & Sons, Ltd.

Llorens, J. F., Fernandez-Turiel, J. L. and Querol, X. (2001). The fate of trace elements in a large coal-fired power plant. Environmental Geology, pp.409 to 416.

Lockwood, J. A. (1960). On the long-term variation in the cosmic radiation, https://doi.org/10.1029/JZ065i001p00019.

Luca, A., Neacsu, B., Antohe, A. and Sahagia, M. (2012). Calibration of the high and low resolution gamma ray spectrometers, Romanian Reports in Physics, pp.968 to 976.

Luo, X. S., Ding, J. and Xu, B. (2012). Incorporating bioaccessibility into human health risk assessments of heavy metals in urban park soils, Sci Total Environ 424, pp. 88 to 96.

Magill, J. and Galy, J. (2005). Radioactivity Radionuclides Radiation, ISBN 978-3-540-26881-9, Karlsruhe, Germany.

Manskinen, K. and Pöykiö, R. (2011). Comparison of the total and fractionated heavy metal and sulphur concentrations in bottom ash and fly ash from a large-sized (120 MW) power plant of a fluting board mill, Chemija, pp.46 to 55.

Martin, P. and Hancock, G. (1992). Routine Analysis of Naturally Occuring Radionuclides in Environmental Samples by Alpha-Particle Spectroscopy, Australian Government Publishing Service.

Masarik, J. (2009). Chapter 1 Origin and Distribution of Radionuclides in the Continental Environment, Radioactivity in the Environment, Vol. 16, pp. 1 to 25.

Mathuthu, M., Kamunda, C. and Madhuku, M. (2016). Modelling of Radiological Health Risks from Gold Mine Tailings in Wonderfonteinspruit Catchment Area, South Africa, Int J Environ Res Public Health, pp.570.

Mihalić, I. B., Fazinić, S., Tadić, T., Cosic, D. and Jakšić, M. (2016). Study of ion beam induced chemical effects in silicon with a downsized high resolution X-ray spectrometer for use with focused ion beams, Journal of Analytical Atomic Spectrometry.

Miller, B. G. (2016). Clean Coal Engineering Technology, Second Edition, 9780128113653, Butterworth-Heinemann Publishers.

Moazzem, S., Rasul M.G. and Khan M.M.K., (2015). A Review on Technologies for Reducing CO2 Emission from Coal Fired Power Plants, Intech Journal, DOI 10.5772/31876

Mohammed, N. H. (2014). Investigation of Uranium-238 Level in Phosphate Rock Samples from Kurun Mountain in Eastern Nuba Mountains in the state of Kordofan (Western Sudan), University of Khartoum.

Mouchel, D. and Wordel, R. (2000). A low-energy HPGE detector dedicated to radioactivity measurements far below environmental levels, Applied Radiation and Isotopes, Volume 47, Issues 9–10, pp.1033 to 1041.

Moulton-Meissner, H., Noble-Wang, J., Gupta, N., Hocevar, S., Kallen, A., and Arduino, M. (2015). Laboratory replication of filtration procedures associated with Serratia marcescens bloodstream infections in patients receiving compounded amino acid solutions, American journal of health-system pharmacy: AJHP : official journal of the American Society of Health-System Pharmacists, 72(15), pp.1285 to 1291. DOI:10.2146/ajhp150141.

Mouandza, S. Y. L., Moubissi, A.B., Abiama, P. E., Ekogo, T. B. and Ben-Bolie, G. H. (2018). Study of natural radioactivity to Assess of radiation hazards from soil samples collected from Mounana in south-east of Gabon, International Journal of Radiation Research, Vol. 16, No 4.

Mtunzi, F. M., Dikio, E. D. and Moja, S. J. (2015). Evaluation of Heavy Metal Pollution on Soil in Vaderbijlpark, South Africa, International Journal of Environmental Monitoring and Analysis, 3(2), pp. 44 to 49.

Murty, V.R.K. and Karunakara, N. (2008). Natural radioactivity in the soil samples of Botswana (a) Department of Physics, University of Botswana, Botswana (b) University Science Instrumentation Centre, Mangalore University, India, Radiation Measurements 43, pp.1541 to 1545.

Ndontchueng, M. M., Nguelem, E. J. M., Simo, A., Njinga, R. L., and Joël, G. S. C. (2014). Gamma emitting radionuclides in soils from selected areas in Douala-Bassa zone, littoral region of Cameroon. ISRN Spectroscopy, 2014, pp.1 to 8, DOI: 10.1155/2014/245125.

Neetu, K., Ankit, G., Ruchi, T., Ajay, B., Beniwal, P. S. G. L. and Bihani, S. D. (2012). A Review on Mass Spectrometry Detectors, International Research Journal of Pharmacy.

Nelson, G. and Reilly, D. (1991). Gamma-Ray Interactions with Matter, in Passive Nondestructive Analysis of Nuclear Materials, Los Alamos National Laboratory, pp. 27 to 42.

Nguelem, E. J. M, Ndontchueng, M. M. and Motapon, O. (2016). Determination of Ra-226, Th-232, K-40, U-235 and U-238 activity concentration and public dose assessment in soil

samples from bauxite core deposits in Western Cameroon, Springerplus 5(1), pp.1253, DOI: 10.1186/s40064-016-2895-9.

NNR (2013). RG-002 Safety assessment to radiation hazards to members of the public from NORM activities, South Africa.

NRC (1990). Committee on the Biological Effects of Ionizing Radiation (BEIR V), Health Effects of Exposure to Low Levels of Ionizing Radiation: Beir V. Washington (DC): National Academies Press (US).

NRC (1999). Arsenic in drinking water. Washington, DC. pp.251 to 257.

Ogwuegbu, M. O. C. and Muhanga, W. (2005). Investigation of lead concentration in the blood of people in the copper belt province of Zambia. Journal of Environment, pp.66 to 75.

O'Sullivan, J. E., Watson, R. J and Butler, E. C. (2013). An ICP-MS procedure to determine Cd, Co, Cu, Ni, Pb and Zn in oceanic waters using in-line flow-injection with solid-phase extraction for preconcentration, US National Library of Medicine National Institutes of Health Search database, DOI: 10.1016/j.talanta.2013.06.054.

Pallavicini, N. (2011). Activity concentration and transfer factors of natural and artificial radionuclides in the Swedish counties of Uppsala and Jämtland, MSc Thesis in Environmental Science, Swedish University of Agricultural Sciences, Department of Soil and Environment.

Pandit, G. G., Sahu, S. K. and Puranik, V. D. (2011). Natural radionuclides from coal fired thermal power plants – estimation of atmospheric release and inhalation risk. Radioprotection Vol. 46: pp.173 to 179.

Parks, J. E., (2015). The Compton Effect -- Compton Scattering and Gamma Ray Spectroscopy, Department of Physics and Astronomy, The University of Tennessee Knoxville, Tennessee 37996-1200.

Patra, A.C., Sahoo, S.K., Tripathi, R.M. & Puranik, V.D. (2013). Distribution of radionuclides in surface soils, Singhbhum Shear Zone, India and associated dose, Environ Monit Assess (2013) 185:7833–7843, DOI 10.1007/s10661-013-3138-y.

Penfold, J. S. S., Smith, K. R., Harvey, M. P. and Mobbs, S. F. (1998). Assessment of the radiological impact of coal-fired power stations in the United Kingdom, Didcot, Oxfordshire, pp.67 to 71.

Plebani, M. (2012). Quality indicators to detect pre-analytical errors in laboratory testing. The Clinical biochemist, pp.85 to 88.

Podgoršak, E. B. (2014). Kinetics of Radioactive Decay. In: Compendium to Radiation Physics for Medical Physicists. Springer, Berlin, Heidelberg.

Pressyanov, D. (2002). Short solution of radioactive decay chain equations, American Journal of Physics 70(4):444-445, DOI: 10.1119/1.1427084

Prince, J. H. (1979). "Comments on Equilibrium, Transient Equilibrium, and Secular Equilibrium in Serial Radioactive Decay", Juornal of Nuclear Medicine 20, pp. 162 to 164.

Querol, X., Umana, J. C., Alastuey, A., Ayora, C., Lopez-Soler, A. and Plana, F. (2001). Extraction of soluble major and trace elements from fly ash in open and closed leaching systems, Fuel, pp.801 to 813.

Rahman, M. M., Naher, N., Ghosh, S. and Islam, M. M. (2014). Efficiency Calibration of Gamma Spectrometry for Powdered Milk Sample Using Cylindrical Geometry, Journal of Nuclear and Particle Physics, Vol. 4, pp. 171 to 175.

Reguigui, N. (2006). Gamma Ray Spectrometry – Practical Infromation, A compilation, International Journal of Science and Technology, Vol. 3, No. 10.

Saha, G. B. (2010). Fundamentals of Nuclear Pharmacy, DOI 10.1007/978-1-4419-5860-0_2, # Springer Science + Business Media, LLC 2010.

Sandelin, K. and Backman, R. (2001). Trace elements in two pulverized coal-fired power stations, Environmental Science and Technology, pp.826 to 834.

Santawamaitre, T. (2012). An Evaluation of the Level of Naturally Occuring Radioactive Materials in Soil Samples along the Chao Phraya River Basin (Phd Thesis, May, 2012). University of Surrey, Department of Physics.

Savic, D., Nisic, D., Malic, N., Dragosavljevic, Z. and Medenica, D. (2018). Research on Power Plant Ash Impact on the Quality of Soil in Kostolac and Gacko Coal Basins, Minerals, DOI:10.3390/min8020054.

Shumba Energy. (2017). Morupule South PFS Mining section of the pre-feasibility study.

Singh, J. S. (1993). Restoration of Degraded Land: Concept & Strategies, Rastogi Publishers, ISBN: 8171331637, 9788171331635.

Stratton, G. (2011). Comparison of a High Purity Germanium Gamma Ray Spectrometer and a Multidimensional NaI (Tl) Scintillation Gamma Ray Spectrometer, A Senior Project presented to the Faculty of the Departments of Aerospace Engineering and Physics, California Polytechnic State University, San Luis Obispo.

Tchounwou, P. B., Yedjou, C. G., Patlolla, A. K. and Sutton, D. J. (2012). Heavy metal toxicity and the environment. Experientia, pp.133 to 164, DOI:10.1007/978-3-7643-8340-4_6.

Thomas, G. A., and Symonds, P. (2016). Radiation Exposure and Health Effects - is it Time to Reassess the Real Consequences? Clinical oncology (Royal College of Radiologists (Great Britain)), 28(4), pp. 231 to 236. DOI:10.1016/j.clon.2016.01.007.

Thorne, M. C. (2003). Background radiation: natural and man-made, Journal of Radiological Protection, Volume 23, Number 1.

Turner, J. E. (2007). Atoms, Radiation and Radiation Protection, Third Edition, Weinheim: Wiley-VCH.

UNEP (2002). Global mercury assessment, United Nations.

UNSCEAR (1982). Sources and Biological Effects, 1982 Report to the General Assembly, with annexes, United Nations, New York.

UNSCEAR (1993). Exposure from natural sources of radiation, 1993 Report to General Assembly, United Nations, New York.

UNSCEAR (2000). Sources and Effects of Ionizing Radiation, UNSCEAR 2000 Report Vol.1 to the General Assembly, with scientific annexes, United Nations, New York.

UNSCEAR (2008). Sources and effects of ionizing radiation, Report to the General Assembly with Scientific Annexes Vol. 1, United Nations, New York.

USEIA (2010). U.S. Coal Supply and Demand 2009 Review, DOE/EIA-0121, Washington DC.

USEPA (1989). Risk assessment guidance for Superfund, Human health evaluation manual, Part A, Vol. 1, Washington, DC, Office of emergency and remedial response, EPA/540/1-89/002, USA, pp.142.

USEPA (1991). Human Health Evaluation Manual, Supplemental Guidance, Standard Default Exposure Factors, OSWER Directive 9285.6-03, USA.

USEPA (2001). Toxics Release Inventory, Public Data Release Report, USA.

USEPA (2004). Risk Assessment Guidance for Superfund Volume I: Human Health Evaluation Manual (Part E, Supplemental Guidance for Dermal Risk Assessment). [EPA/540/R/99/005, USA.

USEPA (2006). Coal-Fired Power Plant Emissions, EPA 402-F-06-028, Washington DC.

USEPA (2007). Framework for Determining a Mutagenic Mode of Action for Carcinogenicity, Review Draft, EPA 120/R-07/002, USA.

USEPA (2011a). Recommended Use of BW3/4 as the Default Method in Derivation of the Oral Reference Dose, EPA/100/R11/001, Office of the Science Advisor, USA.

USEPA (2011b). National Primary Drinking Water Regulations, http://water.epa.gov/drink/contaminants/index.cfm#List, Accessed 25 April 2019.

Wang, Y., Su, H., Gu, Y., Song, X., and Zhao, J. (2017). Carcinogenicity of chromium and chemoprevention: a brief update. OncoTargets and therapy, pp.4065 to 4079, DOI: 10.2147/OTT.S139262.

Winde, F., Wade, P. and Van der Walt, I. J. (2004). Gold tailings as a source of waterborne uranium contamination of streams ─ the Koekemoerspruit, Klerksdorp goldfield, South Africa as a case study, Part I: Uranium migration along the aqueous pathway, Water SA, pp.219 to 226.

Wadge, A., Hutton, M. and Peterson, P. J. (1986). The concentrations and particle size relationships of selected trace elements in fly ashes from U.K. coal-fired power plants and a refuse incinerator, Science Total Environment, pp.13 to 27.

Wahl, W. (2007), Radionuclide Handbook for Laboratory Workers in Spectrometry, Radiation Protection and Medicine, Germany, ISuS.

WHO (2008). Guidelines for drinking water quality, Third Edition, Incorporating 1st and 2nd addenda, Vol. 1 Recommendations, World Health Organization, Geneva.

Yang, S. Y., Lin, J. M., Lin, W. Y., and Chang, C. W. (2018). Cancer risk assessment for occupational exposure to chromium and nickel in welding fumes from pipeline construction, pressure container manufacturing, and shipyard building in Taiwan, Journal of occupational health, 60(6), pp.515 to 524, DOI:10.1539/joh.2018-0075-FS.

Yu, C., Loureiro, C., Cheng, J. J., Jones, L. G., Wang, Y. Y., Chia, Y. P. and Faillance, E. (1993). Data Collection Handbook to Support Modelling Impacts of Radioactive Material in Soil. Environmental Assessment and Information Sciences Division, Argonne National Laboratory, Argonne, Illinois.

Yu, C. and Gnanapragasam, E. (1996). RESRAD: Model description and evaluation of model performance International Nuclear Information System (INIS).

Xu, M., Yan, R., Zheng, C., Qiao, Y., Han, J. and Sheng, C. (2003). Status of trace element emission in a coal combustion process: a review, Fuel Processing Technology, pp.215 to 237.

Yücel, H., Karadeniz, H., Çetiner, M. A., Demirel, H. and Turhan, S. (2003). Measurement of absolute intensity of 1001 keV gamma-ray of 234mPa, Journal of Radioanalytical and Nuclear Chemistry, DOI: 10.1023/A:1026226930151.

http://www.world-nuclear.org/information-library/safety-and-security/radiation-and-health/nuclear-radiation-and-health-effects.aspx, Accessed March 31, 2019.

Appendices

Appendix 1: Calibration

Reliability as well quality of all analytical measurements rely on how properly the instrument is calibrated using standard materials [IAEA, 2003]. The high purity germanium detector (HPGe) used for was calibrated with respect to energy and efficiency using a Cal VasGeo standard. To calibrate the detector, standard radionuclides were used. This standard source was used in calibrating the system for the soil, coal, fly ash and bottom ash. Efficiency calibration was performed for quantification of ^{238}U, ^{232}Th and ^{40}K radionuclides. This efficiency calibration also depends on the geometry of the standard calibration source [Rahman, Naher, Ghosh and Islam, 2014]. The efficiency calibration curve is basically a smooth plot depicting Efficiency vs. Energy. Energy and efficiency calibration curves for detector using standard radionuclides are shown in Figure 3-9 and Figure 3-10. The energy calibration curve matches the energy of radionuclide to its corresponding channel number at the centroid of a full energy peak [Faanu, 2011]. The energy calibration plot is linear, while the efficiency calibration curve is a power series thus indicating that the detector is functioning well. The following series and energies of interest were utilized in the activity concentration analysis for ^{238}U, ^{40}K and ^{232}Th.

Series and energy lines of interest

Series	Radionuclide	Peak energy (keV)	Emission probability (% decay)
^{238}U	^{234}Th	63.20	3.70
	^{234}Th	92.60	2.59
	^{234m}Pa	1001.03	0.83
^{226}Ra	^{214}Pb	351.93	37.60
	^{214}Pb	295.22	19.30
	^{214}Bi	609.31	46.10
	^{214}Bi	1120.29	14.91
	^{214}Bi	1764.49	15.10
^{210}Pb	^{210}Pb	46.54	4.25
^{232}Th	^{228}Ac	338.32	11.30
	^{228}Ac	911.20	25.80
	^{212}Pb	238.63	43.30
^{212}Bi	^{212}Bi	727.33	6.65
	^{212}Bi	1620.74	1.51
^{208}Tl	^{208}Tl	583.19	84.50
	^{208}Tl	2614.51	99.79
Non-series	^{40}K	1460.63	10.70

Appendix 2: Mean monthly rainfall for Morupule area from 1989 to 2006 [Ecosurv, 2009]

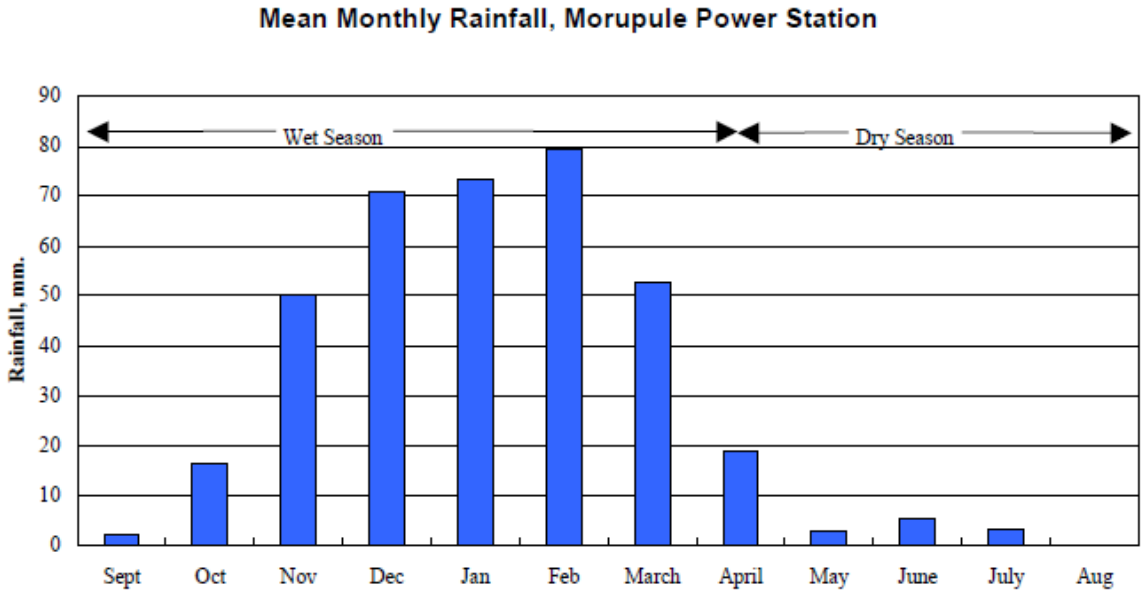

Appendix 3: Soil sampling points from surroundings of Morupule-B Coal Thermal Power Station

No.	Sample Code	Longitude	Latitude	Sample mass (kg)	Description of sampling location
1	MS01	27.016897	-22.5281	1.32400	Soil sample surrounding the power station
2	MS02	27.011433	-22.5204	1.11700	Soil sample surrounding the power station
3	MS03	27.002646	-22.5061	1.19300	Soil sample surrounding the power station
4	MS04	27.010527	-22.5001	1.21000	Soil sample surrounding the power station
5	MS05	27.017888	-22.4943	1.19200	Soil sample surrounding the power station
6	MS06	27.025321	-22.4887	1.27100	Soil sample surrounding the power station
7	MS07	27.033041	-22.4831	1.20600	Soil sample surrounding the power station
8	MS08	27.041855	-22.4869	1.28000	Soil sample surrounding the power station
9	MS09	27.050786	-22.4906	1.46095	Soil sample surrounding the power station
10	MS10	27.059376	-22.4943	1.12900	Soil sample surrounding the power station
11	MS11	27.064539	-22.4967	1.63600	Soil sample surrounding the power station
12	MS12	27.06012	-22.5000	1.59523	Soil sample surrounding the power station
13	MS13	27.060563	-22.5092	1.6500	Soil sample surrounding the power station
14	MS14	27.062737	-22.5177	1.61852	Soil sample surrounding the power station
15	MS15	27.067557	-22.5254	1.70065	Soil sample surrounding the power station
16	MS16	27.082964	-22.5486	1.30400	Soil sample along A1 road, on bank of Lotsane river
17	MS17	27.001697	-22.5256	1.47039	Soil sample along A14 road, on bank of Morupule river
18	MS18	27.001289	-22.5266	1.21862	Soil sample along bank of Morupule river

Appendix 3 Continued

No.	Sample Code	Longitude	Latitude	Sample mass (kg)	Description of sampling location
19	MS19	27.001146	-22.5270	1.497950	Soil sample along bank of Morupule river
20	MS20	27.001615	-22.5279	1.242490	Soil sample along bank of Morupule river
21	MS21	27.081123	-22.5476	0.517391	Soil sample along bank of Lotsane river
22	MS22	27.081486	-22.5477	0.557494	Soil sample along bank of Lotsane river
23	MS23	27.082958	-22.5480	0.559496	Soil sample along bank of Lotsane river
24	MS24	27.082663	-22.5479	0.578788	Soil sample along bank of Lotsane river
25	MS25	27.082429	-22.5479	0.570056	Soil sample along bank of Lotsane river
26	MS26	27.080557	-22.5477	0.634168	Soil sample along bank of Lotsane river
27	MS27	27.079559	-22.5477	0.522611	Soil sample along bank of Lotsane river
28	MS28	27.078771	-22.5473	0.567988	Soil sample along bank of Lotsane river
29	MS29	27.079516	-22.5481	0.543371	Soil sample along bank of Lotsane river
30	MS30	27.079865	-22.5486	0.594196	Soil sample along bank of Lotsane river
31	MS31	27.080217	-22.5487	0.593462	Soil sample along bank of Lotsane river
32	MS32	27.080069	-22.5491	0.596947	Soil sample along bank of Lotsane river
33	MS33	27.082249	-22.5477	0.481530	Soil sample along bank of Lotsane river
34	MS34	27.079976	-22.5497	0.611363	Soil sample along bank of Lotsane river
35	MS35	27.079773	-22.5500	0.684286	Soil sample along bank of Lotsane river
36	MS36	27.079024	-22.5498	0.657187	Soil sample along bank of Lotsane river

Appendix 3 Continued

No.	Sample Code	Longitude	Latitude	Sample mass (kg)	Description of sampling location
37	MS37	27.080581	-22.5495	0.625391	Soil sample along bank of Lotsane river
38	MS38	27.081093	-22.5491	0.616765	Soil sample along bank of Lotsane river
39	MS39	27.081894	-22.5494	0.638083	Soil sample along bank of Lotsane river
40	MS40	27.127500	-22.5401	0.707660	Soil sample in Palapye residential area
41	MS41	27.003200	-22.5246	0.658377	Soil sample along bank of Morupule river
42	MS42	27.003230	-22.5246	0.566864	Soil sample along bank of Morupule river
43	MS43	27.003169	-22.5240	0.567655	Soil sample along bank of Morupule river
44	MS44	27.001296	-22.5215	0.567165	Soil sample along bank of Morupule river
45	MS45	27.002253	-22.5211	0.580835	Soil sample along bank of Morupule river
46	MS46	27.002853	-22.5220	0.572353	Soil sample along bank of Morupule river
47	MS47	27.000810	-22.5219	0.558538	Soil sample along bank of Morupule river
48	MS48	27.001256	-22.5207	0.567466	Soil sample along bank of Morupule river
49	MS49	27.002854	-22.5231	0.620895	Soil sample along bank of Morupule river
50	MS50	27.002344	-22.5229	0.504088	Soil sample along bank of Morupule river
51	MS51	27.001784	-22.5203	0.549710	Soil sample along bank of Morupule river
52	MS52	27.000927	-22.5195	0.686609	Soil sample along bank of Morupule river
53	MS53	27.000556	-22.5189	0.691746	Soil sample along bank of Morupule river
54	MS54	27.000000	-22.5187	0.622688	Soil sample along bank of Morupule river
55	MS55	26.999444	-22.5188	0.531149	Soil sample along bank of Morupule river

Appendix 4: Sampling points from coal storage area of Morupule-B Coal Thermal Power Station

No.	Sample Code	Longitude	Latitude	Sample mass (kg)	Description of sampling location
56	COAL1	27.04750	-22.5223	0.424565	Coal storage area
57	COAL2	27.04750	-22.5230	0.417922	Coal storage area
58	COAL3	27.04750	-22.5238	0.430278	Coal storage area
59	COAL4	27.04750	-22.5247	0.438135	Coal storage area
60	COAL5	27.04611	-22.5222	0.404132	Coal storage area
61	COAL6	27.04583	-22.5231	0.419121	Coal storage area
62	COAL7	27.04583	-22.5241	0.422850	Coal storage area
63	COAL8	27.04583	-22.5249	0.419515	Coal storage area
64	COAL9	27.04611	-22.5249	0.433419	Coal storage area
65	COAL10	27.04611	-22.5236	0.437181	Coal storage area
66	COAL11	27.04611	-22.5243	0.426641	Coal storage area
67	COAL12	27.04722	-22.5243	0.414688	Coal storage area

Appendix 5: Sampling points from bottom ash storage area of Morupule-B Coal Thermal Power Station

No.	Sample Code	Longitude	Latitude	Sample mass (kg)	Description of sampling location
68	BA01	27.04861	-22.5215	0.692690	Bottom ash storage
69	BA02	27.04889	-22.5218	1.462260	Bottom ash storage
70	BA03	27.04889	-22.5220	0.695504	Bottom ash storage
71	BA04	27.04889	-22.5222	0.701556	Bottom ash storage
72	BA05	27.04889	-22.5224	0.709615	Bottom ash storage
73	BA06	27.04889	-22.5226	0.709975	Bottom ash storage
74	BA07	27.04861	-22.5228	0.688615	Bottom ash storage
75	BA08	27.04889	-22.5231	0.697814	Bottom ash storage
76	BA09	27.04889	-22.5218	0.699849	Bottom ash storage
77	BA10	27.04861	-22.5219	0.727250	Bottom ash storage
78	BA11	27.04889	-22.5228	0.697259	Bottom ash storage
79	BA12	27.04861	-22.5228	0.693989	Bottom ash storage

Appendix 6: Sampling points from fly ash storage area of Morupule-B Coal Thermal Power Station

No.	Sample Code	Longitude	Latitude	Sample mass (kg)	Description of sampling location
80	FA01	27.04889	-22.5217	0.389324	Fly ash storage area
81	FA02	27.04889	-22.5221	0.301447	Fly ash storage area
82	FA03	27.04889	-22.5225	0.614850	Fly ash storage area
83	FA04	27.04889	-22.5230	0.598750	Fly ash storage area
84	FA05	27.04944	-22.5232	0.567700	Fly ash storage area
85	FA06	27.04889	-22.5219	0.462956	Fly ash storage area
86	FA07	27.04861	-22.5228	0.273814	Fly ash storage area
87	FA08	27.04778	-22.5173	0.287000	Fly ash storage area
88	FA09	27.04778	-22.5174	0.296442	Fly ash storage area
89	FA10	27.04778	-22.5177	0.300069	Fly ash storage area
90	FA11	27.04861	-22.5220	0.278339	Fly ash storage area
91	FA12	27.04861	-22.5229	0.394511	Fly ash storage area

Appendix 7: Water Sampling points

No.	Sample Code	Longitude	Latitude	Description of sampling location
92	MW01	27.082957	-22.5486	Water from Lotsane river
93	MW02	27.083612	-22.5489	Water from Lotsane river
94	MW03	26.93318	-22.4915	Borehole water from farm near A14 road between Serowe and Palapye villages
95	MW04	27.045781	-22.5389	Borehole water from farm opposite Morupule-B Coal Thermal Power Station
96	MW05	27.083542	-22.5488	Water from Lotsane river
97	MW06	27.083012	-22.5486	Water from Lotsane river
98	MW07	27.081439	-22.5477	Water from Lotsane river
99	MW08	27.080669	-22.5476	Water from Lotsane river

Appendix 8: ^{226}Ra activity concentrations in soil samples

Activity Concentration (Bq/kg)					
Sample name	^{226}Ra				Weighted mean (Bq/kg)
	^{214}Pb (Bq/kg) 295.224keV	^{214}Pb (Bq/kg) 351.932keV	^{214}Bi (Bq/kg) 609.312keV	^{214}Bi (Bq/kg) 1120.287keV	^{214}Bi (Bq/kg) 1764.494keV	
MS01	9.327 ± 0.266	9.42 ± 0.33	9.802 ± 0.226	9.128 ± 0.521	10.840 ± 0.706	9.583 ± 0.144
MS02	9.836 ± 0.307	11.03 ± 0.36	11.030 ± 0.415	10.700 ± 1.193	11.220 ± 0.769	10.554 ± 0.194
MS03	8.950 ± 0.281	8.80 ± 0.33	9.269 ± 0.333	10.020 ± 1.127	9.165 ± 0.847	9.030 ± 0.174
MS04	9.496 ± 0.284	10.18 ± 0.34	10.160 ± 0.371	8.313 ± 1.137	10.500 ± 0.697	9.876 ± 0.180
MS05	9.765 ± 0.291	9.62 ± 0.72	9.812 ± 0.385	8.883 ± 1.300	10.770 ± 0.609	9.859 ± 0.205
MS06	8.691 ± 0.271	8.87 ± 0.33	9.014 ± 0.368	6.856 ± 1.295	9.485 ± 0.718	8.827 ± 0.174
MS07	8.642 ± 0.280	9.51 ± 0.30	8.887 ± 0.370	10.850 ± 1.134	10.160 ± 0.771	9.111 ± 0.172
MS08	15.340 ± 0.490	15.85 ± 0.64	15.902 ± 0.653	13.916 ± 1.810	16.593 ± 1.438	15.621 ± 0.321
MS09	6.876 ± 0.223	6.93 ± 0.30	7.045 ± 0.269	6.326 ± 0.441	7.935 ± 0.531	6.948 ± 0.136
MS10	10.260 ± 0.308	9.91 ± 0.39	10.550 ± 0.394	9.539 ± 1.096	10.080 ± 1.029	10.211 ± 0.198
MS11	7.174 ± 0.213	7.39 ± 0.26	6.957 ± 0.292	7.544 ± 0.780	7.713 ± 0.580	7.228 ± 0.137
MS12	7.452 ± 0.306	7.78 ± 0.48	6.903 ± 0.204	7.892 ± 0.681	7.902 ± 0.538	7.244 ± 0.150
MS13	7.097 ± 0.216	7.61 ± 0.34	7.484 ± 0.300	6.208 ± 0.727	7.010 ± 0.666	7.247 ± 0.149
MS14	6.541 ± 0.208	6.90 ± 0.25	7.078 ± 0.286	7.472 ± 0.821	6.834 ± 0.587	6.804 ± 0.133
MS15	7.059 ± 0.209	7.58 ± 0.26	7.602 ± 0.279	7.412 ± 0.834	7.642 ± 0.559	7.371 ± 0.134
MS16	19.240 ± 0.423	20.56 ± 0.48	19.980 ± 0.533	21.950 ± 1.325	18.490 ± 1.015	19.852 ± 0.258
MS17	5.564 ± 0.195	5.45 ± 0.25	5.783 ± 0.269	3.415 ± 1.496	5.350 ± 0.580	5.557 ± 0.130
MS18	10.700 ± 0.302	11.48 ± 0.33	10.900 ± 0.413	9.016 ± 1.219	9.063 ± 1.018	10.863 ± 0.197
MS19	6.693 ± 0.211	6.38 ± 0.25	6.536 ± 0.271	5.972 ± 0.987	7.797 ± 0.551	6.616 ± 0.133
MS20	8.351 ± 0.264	8.64 ± 0.33	8.025 ± 0.352	7.927 ± 0.959	8.758 ± 0.811	8.355 ± 0.171

Appendix 8 (continued)

Activity Concentration (Bq/kg)												
Sample name	^{226}Ra										Weighted mean (Bq/kg)	
	^{214}Pb (Bq/kg) 295.224keV		^{214}Pb (Bq/kg) 351.932keV		^{214}Bi (Bq/kg) 609.312keV		^{214}Bi (Bq/kg) 1120.287keV		^{214}Bi (Bq/kg) 1764.494keV			
MS21	6.092	± 0.206	7.02	± 0.25	6.955	± 0.282	4.687	± 1.116	8.241	± 0.562	6.649	± 0.134
MS22	8.549	± 0.408	8.30	± 0.55	8.391	± 0.512	6.806	± 1.973	9.855	± 1.161	8.485	± 0.266
MS23	10.700	± 0.441	8.92	± 0.62	11.400	± 0.644	7.727	± 2.193	12.320	± 1.323	10.458	± 0.302
MS24	13.110	± 0.374	14.64	± 0.39	13.780	± 0.443	10.190	± 1.540	8.825	± 1.360	13.613	± 0.225
MS25	7.570	± 0.409	8.16	± 0.58	8.276	± 0.525	6.942	± 0.820	10.690	± 1.069	7.978	± 0.259
MS26	9.483	± 0.308	9.63	± 0.32	10.070	± 0.378	5.074	± 1.006	9.825	± 0.891	9.536	± 0.184
MS27	10.800	± 0.476	12.08	± 0.58	12.970	± 0.731	13.140	± 0.967	14.750	± 1.346	11.954	± 0.303
MS28	15.330	± 0.405	15.71	± 0.39	16.410	± 0.477	17.520	± 1.278	10.650	± 2.089	15.749	± 0.236
MS29	11.750	± 0.470	10.97	± 0.63	12.230	± 0.609	8.396	± 1.724	13.390	± 1.464	11.651	± 0.308
MS30	10.460	± 0.333	11.23	± 0.35	10.880	± 0.386	8.857	± 1.036	8.703	± 1.940	10.741	± 0.200
MS31	11.610	± 0.347	11.98	± 0.36	11.130	± 0.381	12.090	± 1.105	11.800	± 0.795	11.619	± 0.199
MS32	6.195	± 0.364	7.84	± 0.50	8.565	± 0.587	4.958	± 0.778	8.765	± 1.457	6.958	± 0.245
MS33	14.056	± 1.542	15.94	± 0.93	12.164	± 0.981	11.472	± 2.942	14.669	± 2.152	14.076	± 0.581
MS34	7.096	± 0.382	8.50	± 0.53	8.802	± 0.553	9.866	± 1.916	9.777	± 1.187	7.998	± 0.261
MS35	7.370	± 0.346	7.48	± 0.41	7.588	± 0.514	6.850	± 1.593	7.238	± 1.198	7.431	± 0.228
MS36	12.010	± 0.427	11.31	± 0.93	11.770	± 0.996	14.580	± 2.642	14.980	± 1.901	12.027	± 0.352
MS37	6.676	± 0.357	6.61	± 0.50	8.222	± 0.502	7.846	± 1.689	7.554	± 1.329	7.080	± 0.244
MS38	14.990	± 1.514	15.24	± 0.83	12.040	± 0.978	11.680	± 2.954	14.690	± 2.146	14.015	± 0.555
MS39	6.534	± 0.354	6.53	± 0.49	7.152	± 0.542	4.987	± 1.759	7.076	± 0.998	6.661	± 0.244
MS40	8.016	± 1.177	9.98	± 0.74	9.318	± 0.774	6.124	± 2.965	7.961	± 1.603	9.187	± 0.460

Appendix 8 (continued)

Activity Concentration (Bq/kg)												
Sample name	^{226}Ra										Weighted mean (Bq/kg)	
	^{214}Pb (Bq/kg)		^{214}Pb (Bq/kg)		^{214}Bi (Bq/kg)		^{214}Bi (Bq/kg)		^{214}Bi (Bq/kg)			
	295.224keV		351.932keV		609.312keV		1120.287keV		1764.494keV			
MS41	4.411	± 0.292	4.18	± 0.37	4.833	± 0.479	4.728	± 0.620	4.409	± 1.046	4.447	± 0.192
MS42	9.216	± 0.320	9.02	± 0.32	8.947	± 0.357	1.635	± 1.155	3.658	± 0.075	4.371	± 0.070
MS43	5.636	± 0.349	5.24	± 0.49	6.242	± 0.489	4.750	± 0.723	4.655	± 1.454	5.569	± 0.230
MS44	7.462	± 1.727	11.98	± 0.93	11.350	± 1.038	11.420	± 3.005	12.420	± 1.811	11.264	± 0.594
MS45	5.394	± 0.342	5.11	± 0.40	5.738	± 0.388	4.651	± 0.701	4.650	± 1.353	5.336	± 0.204
MS46	10.410	± 0.363	11.16	± 0.38	10.890	± 0.415	3.115	± 1.685	3.234	± 1.321	10.476	± 0.216
MS47	5.391	± 0.341	4.91	± 0.39	5.678	± 0.385	4.649	± 0.674	4.765	± 1.543	5.262	± 0.201
MS48	7.728	± 0.527	9.92	± 0.34	9.571	± 0.378	5.310	± 0.710	2.101	± 1.053	8.728	± 0.212
MS49	7.216	± 0.476	7.98	± 0.30	8.309	± 0.350	6.657	± 0.848	5.178	± 1.027	7.781	± 0.197
MS50	10.450	± 1.865	12.48	± 0.92	12.280	± 1.045	10.130	± 2.994	10.280	± 2.350	11.945	± 0.612
MS51	7.479	± 0.393	6.20	± 0.56	6.755	± 0.630	6.760	± 0.806	7.465	± 1.415	6.988	± 0.265
MS52	7.738	± 1.341	8.72	± 0.74	8.563	± 0.787	9.062	± 2.268	4.081	± 2.292	8.349	± 0.479
MS53	5.716	± 0.236	6.24	± 0.24	5.812	± 0.286	6.059	± 0.735	1.569	± 4.181	5.930	± 0.143
MS54	8.765	± 4.864	8.62	± 5.77	7.812	± 0.385	6.883	± 1.300	7.770	± 0.609	7.753	± 0.315
MS55	6.041	± 0.382	6.36	± 0.50	7.438	± 0.546	5.405	± 2.066	7.242	± 1.039	6.493	± 0.255

Appendix 9: ^{226}Ra activity concentrations in coal samples

Sample name	^{226}Ra					Weighted mean (Bq/kg)
	^{214}Pb (Bq/kg) 295.224keV	^{214}Pb (Bq/kg) 351.932keV	^{214}Bi (Bq/kg) 609.312keV	^{214}Bi (Bq/kg) 1120.287keV	^{214}Bi (Bq/kg) 1764.494keV	
COAL1	19.320 ± 0.447	17.34 ± 0.79	16.610 ± 0.778	15.550 ± 2.154	15.715 ± 1.713	18.220 ± 0.337
COAL2	19.020 ± 0.657	18.29 ± 0.84	19.050 ± 0.904	17.440 ± 1.984	22.170 ± 1.931	18.920 ± 0.428
COAL3	17.220 ± 0.644	21.26 ± 0.74	19.680 ± 0.888	18.940 ± 3.255	23.660 ± 1.863	19.349 ± 0.412
COAL4	16.660 ± 0.625	18.86 ± 0.80	21.010 ± 0.857	18.130 ± 2.210	20.070 ± 2.100	18.425 ± 0.410
COAL5	20.315 ± 0.470	19.48 ± 0.75	18.755 ± 0.805	17.870 ± 2.122	18.775 ± 1.711	19.726 ± 0.345
COAL6	19.065 ± 0.452	19.22 ± 0.70	17.675 ± 0.799	19.835 ± 1.885	16.795 ± 1.626	18.791 ± 0.331
COAL7	23.330 ± 0.477	19.93 ± 0.90	19.005 ± 0.929	17.829 ± 2.105	19.035 ± 1.767	21.716 ± 0.369
COAL8	19.475 ± 0.456	20.25 ± 0.72	18.155 ± 0.797	18.150 ± 2.188	16.585 ± 1.694	19.266 ± 0.335
COAL9	19.230 ± 0.444	19.04 ± 0.72	17.180 ± 0.827	14.240 ± 2.460	16.395 ± 2.084	18.683 ± 0.336
COAL10	18.640 ± 0.645	19.88 ± 0.78	20.700 ± 0.785	20.550 ± 2.177	22.340 ± 1.675	19.779 ± 0.400
COAL11	16.970 ± 0.860	21.35 ± 0.77	24.321 ± 0.893	19.593 ± 2.237	22.364 ± 2.144	20.854 ± 0.461
COAL12	18.731 ± 0.681	22.08 ± 1.26	19.213 ± 0.605	20.587 ± 2.191	23.449 ± 1.711	19.626 ± 0.406

Appendix 10: ^{226}Ra activity concentrations in bottom ash samples

Sample name	^{226}Ra					Weighted mean (Bq/kg)
	^{214}Pb (Bq/kg) 295.224keV	^{214}Pb (Bq/kg) 351.932keV	^{214}Bi (Bq/kg) 609.312keV	^{214}Bi (Bq/kg) 1120.287keV	^{214}Bi (Bq/kg) 1764.494keV	
BA01	52.893 ± 1.967	58.75 ± 1.20	59.657 ± 1.231	52.015 ± 2.093	61.967 ± 2.642	57.745 ± 0.710
BA02	45.990 ± 0.749	47.75 ± 0.65	46.250 ± 0.807	45.720 ± 1.050	42.970 ± 1.574	46.431 ± 0.378
BA03	51.940 ± 1.000	53.03 ± 0.98	54.490 ± 1.142	52.200 ± 2.621	54.610 ± 2.440	53.086 ± 0.566
BA04	84.630 ± 1.138	85.64 ± 0.73	85.080 ± 1.203	89.120 ± 1.915	87.740 ± 2.203	85.697 ± 0.513
BA05	52.340 ± 1.000	54.70 ± 1.01	55.340 ± 1.179	52.280 ± 2.569	58.360 ± 2.201	54.207 ± 0.571
BA06	52.780 ± 1.002	54.07 ± 0.98	56.180 ± 0.961	57.720 ± 2.691	55.640 ± 2.419	54.587 ± 0.540
BA07	53.590 ± 1.028	55.24 ± 1.01	57.240 ± 1.175	55.150 ± 2.542	60.070 ± 2.548	55.449 ± 0.582
BA08	86.480 ± 1.166	86.85 ± 0.73	83.420 ± 1.193	90.340 ± 2.357	98.590 ± 6.193	86.357 ± 0.531
BA09	53.252 ± 1.043	55.31 ± 0.99	57.271 ± 1.056	59.861 ± 2.716	58.936 ± 2.739	55.622 ± 0.567
BA10	48.960 ± 0.949	50.74 ± 0.99	53.630 ± 1.127	52.070 ± 2.245	56.670 ± 2.307	51.246 ± 0.549
BA11	52.330 ± 1.009	55.26 ± 1.00	57.470 ± 1.165	55.310 ± 2.547	62.230 ± 2.113	55.363 ± 0.568
BA12	46.240 ± 0.753	47.06 ± 0.66	47.190 ± 0.831	44.070 ± 1.489	45.680 ± 1.467	46.553 ± 0.395

Appendix 11: ^{226}Ra activity concentrations in fly ash samples

Sample name	^{226}Ra										Weighted mean (Bq/kg)
	^{214}Pb (Bq/kg) 295.224keV		^{214}Pb (Bq/kg) 351.932keV		^{214}B (Bq/kg) 609.312keV		^{214}B (Bq/kg) 1120.287keV		^{214}B (Bq/kg) 1764.494keV		
FA01	66.990	± 1.410	71.20	± 1.45	70.830	± 1.659	67.340	± 2.264	74.060	± 2.993	69.568 ± 0.779
FA02	135.000	± 2.116	138.30	± 1.84	134.800	± 2.275	131.400	± 4.074	132.400	± 4.173	135.683 ± 1.099
FA03	43.070	± 0.947	42.33	± 0.88	38.490	± 1.026	40.900	± 2.705	24.550	± 3.152	40.994 ± 0.527
FA04	45.731	± 0.993	45.97	± 1.35	41.693	± 1.372	40.701	± 2.846	27.890	± 3.241	43.862 ± 0.657
FA05	66.310	± 1.453	67.39	± 1.50	66.400	± 1.839	61.510	± 4.345	59.370	± 3.786	66.135 ± 0.865
FA06	63.410	± 1.277	62.87	± 1.22	66.270	± 1.513	56.210	± 3.876	66.490	± 3.064	63.799 ± 0.727
FA07	122.300	± 1.880	122.30	± 1.36	115.500	± 1.894	81.410	± 12.880	114.400	± 3.703	120.001 ± 0.920
FA08	69.810	± 1.605	71.87	± 1.73	74.230	± 1.953	69.880	± 4.843	70.050	± 4.105	71.527 ± 0.959
FA09	68.130	± 1.567	70.90	± 1.71	70.800	± 1.843	67.600	± 2.620	71.400	± 4.092	69.613 ± 0.895
FA10	116.100	± 1.765	117.20	± 1.26	109.800	± 1.796	114.500	± 3.688	67.810	± 5.714	114.009 ± 0.856
FA11	119.600	± 1.837	120.60	± 1.33	113.100	± 1.863	122.700	± 3.950	112.500	± 3.650	118.329 ± 0.880
FA12	52.870	± 1.200	54.29	± 1.27	54.050	± 1.439	51.650	± 6.990	47.250	± 3.524	53.384 ± 0.725

Appendix 12: ^{238}U activity concentrations in soil samples

Activity Concentration (Bq/kg)			
Sample name	^{238}U		Weighted mean (Bq/kg)
	^{234}Th (Bq/kg) 63.28keV	^{234}Th (Bq/kg) 92.6keV	^{234m}Pa (Bq/kg) 1001keV	
MS01	26.600 ± 9.676	16.690 ± 1.754	26.960 ± 11.830	17.213 ± 1.708
MS02	15.460 ± 8.467	34.820 ± 2.813	nd ± nd	17.213 ± 2.670
MS03	19.840 ± 8.017	15.870 ± 1.845	nd ± nd	32.896 ± 1.798
MS04	18.860 ± 8.931	20.050 ± 1.986	nd ± nd	16.070 ± 1.939
MS05	18.750 ± 8.945	15.970 ± 1.822	nd ± nd	19.994 ± 1.785
MS06	19.106 ± 8.980	26.780 ± 2.307	nd ± nd	16.081 ± 2.234
MS07	21.135 ± 9.134	14.770 ± 1.806	nd ± nd	26.305 ± 1.772
MS08	15.623 ± 2.029	32.416 ± 3.453	nd ± nd	15.009 ± 1.749
MS09	10.790 ± 6.592	12.150 ± 1.459	nd ± nd	19.933 ± 1.425
MS10	9.987 ± 6.123	18.600 ± 2.022	nd ± nd	12.086 ± 1.920
MS11	22.920 ± 7.390	11.130 ± 1.332	nd ± nd	17.753 ± 1.311
MS12	23.017 ± 7.037	10.968 ± 1.782	nd ± nd	11.501 ± 1.727
MS13	16.330 ± 7.013	12.270 ± 1.384	nd ± nd	11.694 ± 1.358
MS14	18.120 ± 6.968	13.280 ± 1.420	40.150 ± 12.000	12.422 ± 1.382
MS15	24.550 ± 7.865	10.910 ± 1.305	nd ± nd	13.827 ± 1.287
MS16	31.130 ± 11.930	32.390 ± 2.611	32.830 ± 13.110	32.351 ± 2.504
MS17	11.330 ± 5.715	11.140 ± 1.390	nd ± nd	11.151 ± 1.351
MS18	22.170 ± 9.295	18.410 ± 1.927	nd ± nd	18.565 ± 1.887
MS19	16.490 ± 6.107	9.229 ± 1.333	nd ± nd	9.559 ± 1.302
MS20	22.780 ± 8.763	14.280 ± 1.709	nd ± nd	14.591 ± 1.677

Note: 'nd' means the activity concentration of ^{234}Pa is not detectable

Appendix 12 (continued)

Activity Concentration (Bq/kg)			
Sample name	^{238}U		Weighted mean (Bq/kg)
	^{234}Th (Bq/kg) 63.28keV	^{234}Th (Bq/kg) 92.6keV	^{234m}Pa (Bq/kg) 1001keV	
MS21	15.350 ± 6.364	10.380 ± 1.311	nd ± nd	10.582 ± 1.284
MS22	46.260 ± 14.910	17.690 ± 3.206	nd ± nd	18.953 ± 3.134
MS23	27.160 ± 14.680	17.450 ± 3.209	nd ± nd	17.893 ± 3.135
MS24	19.370 ± 4.099	22.320 ± 1.517	nd ± nd	21.965 ± 1.423
MS25	42.720 ± 15.520	22.000 ± 3.264	nd ± nd	22.878 ± 3.194
MS26	6.238 ± 3.445	14.200 ± 1.071	nd ± nd	13.498 ± 1.023
MS27	43.765 ± 15.567	22.520 ± 3.517	88.330 ± 25.140	24.736 ± 3.399
MS28	15.640 ± 5.007	28.090 ± 1.807	nd ± nd	26.655 ± 1.700
MS29	57.190 ± 18.310	41.830 ± 4.247	nd ± nd	42.614 ± 4.137
MS30	19.570 ± 5.038	29.570 ± 1.850	nd ± nd	28.382 ± 1.737
MS31	16.370 ± 4.907	20.310 ± 1.411	nd ± nd	20.009 ± 1.356
MS32	33.290 ± 12.340	20.260 ± 3.101	nd ± nd	21.034 ± 3.007
MS33	25.610 ± 23.183	47.682 ± 3.635	nd ± nd	47.152 ± 3.591
MS34	23.250 ± 11.020	16.390 ± 2.974	nd ± nd	16.856 ± 2.871
MS35	20.880 ± 9.539	17.790 ± 2.717	nd ± nd	18.022 ± 2.613
MS36	25.820 ± 22.070	46.380 ± 3.601	nd ± nd	45.847 ± 3.554
MS37	45.370 ± 14.430	10.100 ± 2.736	nd ± nd	11.324 ± 2.688
MS38	25.675 ± 23.098	46.380 ± 3.631	nd ± nd	45.881 ± 3.587
MS39	27.400 ± 12.920	13.040 ± 2.755	26.510 ± 15.330	14.049 ± 2.654
MS40	18.000 ± 3.191	18.590 ± 1.896	nd ± nd	18.436 ± 1.630

Note: ‘nd’ means the activity concentration of ^{234}Pa is not detectable

Appendix 12 (continued)

(Bq/kg)									
Sample name	^{238}U						Weighted mean (Bq/kg)		
	^{234}Th (Bq/kg)			^{234}Th (Bq/kg)			^{234m}Pa (Bq/kg)		
	63.28keV			92.6keV			1001keV		
MS41	17.980	±	11.400	12.400	±	2.592	nd	± nd	12.674 ± 2.527
MS42	12.520	±	3.969	15.090	±	1.128	nd	± nd	14.898 ± 1.085
MS43	37.610	±	13.540	6.695	±	2.883	nd	± nd	8.036 ± 2.820
MS44	25.615	±	22.095	45.380	±	3.534	nd	± nd	44.887 ± 3.490
MS45	12.684	±	4.095	14.926	±	1.095	nd	± nd	14.776 ± 1.058
MS46	7.511	±	2.030	22.380	±	1.540	nd	± nd	16.949 ± 1.227
MS47	9.351	±	4.653	8.517	±	4.525	nd	± nd	8.922 ± 3.244
MS48	10.450	±	3.597	10.650	±	2.733	nd	± nd	10.577 ± 2.176
MS49	6.596	±	3.537	18.230	±	1.241	nd	± nd	16.955 ± 1.171
MS50	12.420	±	3.969	16.110	±	1.128	nd	± nd	15.834 ± 1.085
MS51	9.150	±	6.120	7.920	±	3.270	nd	± nd	8.193 ± 2.884
MS52	13.500	±	3.786	15.690	±	1.567	nd	± nd	15.370 ± 1.448
MS53	7.168	±	3.064	13.600	±	0.983	nd	± nd	13.000 ± 0.936
MS54	8.523	±	4.213	8.653	±	4.453	nd	± nd	8.584 ± 3.060
MS55	8.550	±	4.112	7.260	±	4.291	nd	± nd	7.932 ± 2.969

Note: ‘nd’ means the activity concentration of ^{234}Pa is not detectable

Appendix 13: ^{238}U activity concentrations in coal samples

Sample name	^{238}U						Weighted mean (Bq/kg)		
	^{234}Th (Bq/kg) 63.28keV			^{234}Th (Bq/kg) 92.6keV			^{234m}Pa (Bq/kg) 1001keV		
COAL1	54.350	±	22.750	53.000	±	3.724	nd	±	nd	53.035	±	3.675
COAL2	41.980	±	19.940	40.160	±	4.733	nd	±	nd	40.257	±	4.605
COAL3	44.840	±	22.470	43.800	±	4.864	nd	±	nd	43.847	±	4.754
COAL4	79.540	±	23.730	44.430	±	4.745	nd	±	nd	45.780	±	4.653
COAL5	68.400	±	22.280	63.250	±	4.368	nd	±	nd	63.441	±	4.286
COAL6	50.100	±	23.155	70.571	±	4.771	nd	±	nd	69.737	±	4.673
COAL7	69.770	±	21.865	67.072	±	3.873	nd	±	nd	67.154	±	3.814
COAL8	85.400	±	25.535	71.350	±	4.871	25.435	±	19.625	69.239	±	4.649
COAL9	76.400	±	25.990	60.500	±	4.180	nd	±	nd	60.901	±	4.127
COAL10	93.580	±	25.650	53.010	±	5.188	nd	±	nd	54.604	±	5.085
COAL11	45.751	±	22.462	41.831	±	4.624	nd	±	nd	41.990	±	4.529
COAL12	90.128	±	23.194	45.459	±	4.768	nd	±	nd	47.270	±	4.670

Appendix 14: ^{238}U activity concentrations in bottom ash samples

Sample name	^{238}U						Weighted mean (Bq/kg)		
	^{234}Th (Bq/kg) 63.28keV			^{234}Th (Bq/kg) 92.6keV			^{234m}Pa (Bq/kg) 1001keV		
BA01	80.047	±	22.938	105.127	±	6.593	77.854	±	26.800	101.871	±	6.166
BA02	54.140	±	15.400	79.660	±	5.280	49.870	±	15.400	74.396	±	4.751
BA03	110.500	±	30.250	96.260	±	6.869	80.730	±	28.610	96.115	±	6.522
BA04	77.500	±	28.950	163.100	±	8.940	99.700	±	16.660	144.001	±	7.601
BA05	78.620	±	23.890	102.200	±	7.179	67.950	±	25.800	98.106	±	6.643
BA06	68.320	±	24.260	91.290	±	6.573	nd	±	nd	89.719	±	6.344
BA07	79.830	±	26.030	94.180	±	6.781	88.330	±	25.140	92.953	±	6.349
BA08	111.800	±	21.920	134.700	±	7.247	106.500	±	18.060	129.155	±	6.430
BA09	79.952	±	23.963	103.739	±	7.125	89.520	±	25.157	100.964	±	6.591
BA10	122.200	±	29.170	73.090	±	5.481	95.410	±	29.680	75.423	±	5.300
BA11	62.110	±	25.440	99.770	±	7.064	nd	±	nd	97.074	±	6.806
BA12	56.680	±	15.680	69.260	±	4.647	63.660	±	17.190	67.956	±	4.313

Appendix 15: ^{238}U activity concentrations in fly ash samples

Sample name	^{238}U						Weighted mean (Bq/kg)		
	^{234}Th (Bq/kg) 63.28keV			^{234}Th (Bq/kg) 92.6keV			^{234m}Pa (Bq/kg) 1001keV					
FA01	174.700	±	45.190	111.000	±	8.630	nd	±	nd	113.241	±	8.477
FA02	158.400	±	43.230	204.700	±	13.490	208.900	±	48.420	201.140	±	12.445
FA03	104.100	±	21.560	110.000	±	6.354	nd	±	nd	109.529	±	6.095
FA04	110.285	±	22.629	112.027	±	7.804	nd	±	nd	111.842	±	7.378
FA05	78.900	±	38.700	115.700	±	9.187	nd	±	nd	113.737	±	8.939
FA06	145.000	±	39.620	127.100	±	9.192	94.050	±	27.600	124.780	±	8.517
FA07	191.000	±	37.910	248.900	±	13.760	120.600	±	28.580	221.495	±	11.784
FA08	177.900	±	49.710	145.100	±	11.310	109.400	±	66.660	145.720	±	10.880
FA09	223.600	±	54.460	140.600	±	10.980	nd	±	nd	143.842	±	10.763
FA10	166.300	±	33.230	218.700	±	12.120	106.200	±	27.000	196.490	±	10.492
FA11	181.300	±	36.060	232.900	±	12.910	121.600	±	30.400	212.506	±	11.286
FA12	159.800	±	40.030	109.000	±	8.410	107.100	±	43.490	111.008	±	8.087

Appendix 16: ^{232}Th activity concentrations in soil samples

Activity Concentration (Bq/kg)			
Sample name	^{232}Th		Weighted mean (Bq/kg)
	^{228}Ac (Bq/kg) 338.320keV	^{228}Ac (Bq/kg) 911.204keV	^{212}Pb (Bq/kg) 238.632keV	
MS01	11.480 ± 0.759	13.490 ± 0.658	13.390 ± 0.457	13.041 ± 0.336
MS02	13.470 ± 1.124	16.700 ± 0.753	17.460 ± 0.620	16.588 ± 0.440
MS03	11.190 ± 0.953	12.700 ± 0.623	13.370 ± 0.442	12.901 ± 0.337
MS04	10.880 ± 0.848	12.000 ± 0.730	13.300 ± 0.480	12.537 ± 0.363
MS05	11.210 ± 0.787	13.960 ± 0.689	12.890 ± 0.490	12.832 ± 73.700
MS06	12.300 ± 0.907	13.100 ± 1.275	14.020 ± 0.452	13.625 ± 0.386
MS07	11.450 ± 0.846	12.700 ± 0.781	12.080 ± 0.231	12.086 ± 0.214
MS08	16.982 ± 1.974	24.522 ± 1.333	26.351 ± 0.864	24.761 ± 0.681
MS09	8.558 ± 0.781	10.410 ± 0.609	10.680 ± 0.366	10.324 ± 0.291
MS10	12.340 ± 1.160	16.190 ± 0.770	15.940 ± 0.486	15.602 ± 0.387
MS11	8.500 ± 0.650	11.060 ± 0.477	11.030 ± 0.333	10.659 ± 0.252
MS12	8.261 ± 0.542	13.490 ± 0.518	10.730 ± 0.518	10.115 ± 0.303
MS13	10.780 ± 0.810	11.570 ± 0.544	11.800 ± 0.368	11.610 ± 0.285
MS14	8.769 ± 0.776	10.410 ± 0.532	10.530 ± 0.353	10.277 ± 0.275
MS15	8.496 ± 0.380	10.380 ± 0.487	10.210 ± 0.586	9.416 ± 0.267
MS16	6.603 ± 1.411	33.190 ± 1.692	34.180 ± 0.729	33.105 ± 0.605
MS17	13.220 ± 0.788	7.004 ± 0.456	7.881 ± 0.321	7.492 ± 0.249
MS18	9.040 ± 1.065	15.820 ± 0.730	13.510 ± 0.270	13.758 ± 0.246
MS19	11.480 ± 0.781	9.030 ± 0.554	9.452 ± 0.349	9.296 ± 0.276
MS20	11.480 ± 1.044	12.460 ± 0.659	13.530 ± 0.431	13.025 ± 0.341

Appendix 16 (continued)

Activity Concentration (Bq/kg)												
Sample name	^{232}Th									Weighted mean (Bq/kg)		
	^{228}Ac (Bq/kg) 338.320keV			^{228}Ac (Bq/kg) 911.204keV			^{212}Pb (Bq/kg) 238.632keV					
MS21	7.366	±	0.711	9.297	±	0.569	10.140	±	0.345	9.539	±	0.272
MS22	14.780	±	1.669	14.060	±	1.166	14.790	±	0.664	14.629	±	0.545
MS23	17.450	±	1.869	17.050	±	1.219	14.380	±	0.779	15.406	±	0.619
MS24	17.210	±	1.009	21.290	±	0.802	19.480	±	0.292	19.521	±	0.265
MS25	9.981	±	1.843	14.490	±	1.132	13.400	±	0.756	13.345	±	0.595
MS26	12.990	±	0.890	15.480	±	0.669	13.860	±	0.228	13.971	±	0.210
MS27	15.600	±	1.787	19.000	±	1.257	18.320	±	0.849	18.139	±	0.655
MS28	19.910	±	1.264	24.060	±	0.896	22.630	±	0.326	22.637	±	0.298
MS29	15.180	±	1.633	21.120	±	1.356	21.650	±	0.792	20.570	±	0.631
MS30	17.240	±	0.642	20.120	±	0.777	18.670	±	0.282	18.606	±	0.245
MS31	14.990	±	1.093	19.460	±	0.774	16.850	±	0.265	17.017	±	0.244
MS32	10.160	±	1.613	12.240	±	1.127	11.080	±	0.672	11.245	±	0.543
MS33	22.017	±	2.627	20.352	±	1.950	20.036	±	1.201	20.372	±	0.953
MS34	11.650	±	1.692	9.850	±	0.802	14.610	±	0.690	13.918	±	0.619
MS35	9.356	±	1.432	11.410	±	1.090	9.937	±	0.294	10.011	±	0.278
MS36	11.840	±	2.641	21.720	±	1.762	22.980	±	0.999	21.615	±	0.825
MS37	10.530	±	1.536	11.020	±	1.078	9.550	±	0.308	9.692	±	0.291
MS38	21.210	±	2.676	21.550	±	1.846	22.040	±	1.137	21.825	±	0.910
MS39	10.360	±	1.475	12.970	±	0.576	11.580	±	0.638	12.192	±	0.411
MS40	11.240	±	2.165	14.260	±	1.448	11.040	±	0.726	11.650	±	0.622

Appendix 16 (continued)

Activity Concentration (Bq/kg)			
Sample name	^{232}Th		Weighted mean (Bq/kg)
	^{228}Ac (Bq/kg) 338.320keV	^{228}Ac (Bq/kg) 911.204keV	^{212}Pb (Bq/kg) 238.632keV	
MS41	5.992 ± 1.321	6.496 ± 1.024	5.278 ± 0.249	5.367 ± 0.238
MS42	12.140 ± 1.011	12.580 ± 2.161	14.370 ± 0.241	14.231 ± 0.233
MS43	7.529 ± 1.554	8.414 ± 0.937	7.990 ± 0.656	8.065 ± 0.508
MS44	17.540 ± 3.337	19.360 ± 1.894	23.800 ± 1.021	22.445 ± 0.868
MS45	7.527 ± 1.549	8.412 ± 0.935	7.876 ± 0.559	7.974 ± 0.458
MS46	17.260 ± 1.178	12.210 ± 1.586	17.920 ± 0.288	17.712 ± 0.276
MS47	8.453 ± 1.679	8.456 ± 0.956	7.886 ± 0.612	8.086 ± 0.493
MS48	12.840 ± 0.994	15.250 ± 0.734	13.520 ± 0.234	13.639 ± 0.218
MS49	10.310 ± 0.910	11.900 ± 0.623	12.570 ± 0.214	12.396 ± 0.198
MS50	19.370 ± 3.136	21.420 ± 1.885	23.250 ± 1.087	22.510 ± 0.902
MS51	10.620 ± 1.694	13.080 ± 1.268	11.840 ± 0.637	11.941 ± 0.540
MS52	9.233 ± 2.351	11.930 ± 1.552	14.090 ± 0.769	13.314 ± 0.661
MS53	7.018 ± 0.699	9.007 ± 0.522	7.595 ± 0.168	7.692 ± 0.156
MS54	11.210 ± 0.787	13.960 ± 0.689	12.890 ± 0.490	12.832 ± 0.356
MS55	10.580 ± 1.638	10.970 ± 1.148	11.130 ± 0.642	11.038 ± 0.530

Appendix 17: ^{232}Th activity concentrations in coal samples

Sample name	^{232}Th						Weighted mean (Bq/kg)
	^{228}Ac (Bq/kg)		^{228}Ac (Bq/kg)		^{212}Pb (Bq/kg)		
	338.320keV		911.204keV		238.632keV		
COAL1	23.250	± 2.448	22.510	± 1.393	29.590	± 0.860	27.276 ± 0.701
COAL2	24.220	± 2.256	27.550	± 1.576	30.340	± 1.096	28.715 ± 0.836
COAL3	22.690	± 1.169	27.980	± 1.617	25.430	± 0.586	25.174 ± 0.498
COAL4	30.030	± 2.523	27.150	± 1.652	28.860	± 1.097	28.533 ± 0.859
COAL5	23.045	± 2.293	26.835	± 1.352	30.930	± 0.936	28.939 ± 0.730
COAL6	21.380	± 2.327	25.195	± 1.371	21.950	± 0.804	22.666 ± 0.665
COAL7	22.515	± 2.262	26.075	± 1.326	29.930	± 0.899	28.111 ± 0.707
COAL8	24.925	± 2.250	25.780	± 1.720	31.630	± 0.876	29.834 ± 0.737
COAL9	23.025	± 2.466	22.550	± 1.422	29.970	± 0.877	27.514 ± 0.714
COAL10	23.410	± 2.514	25.330	± 1.637	30.430	± 1.001	28.459 ± 0.809
COAL11	30.724	± 1.349	25.466	± 1.641	26.561	± 1.021	27.561 ± 0.729
COAL12	22.671	± 1.097	26.976	± 1.642	25.765	± 0.754	25.048 ± 0.581

Appendix 18: ^{232}Th activity concentrations in bottom ash samples

Sample name	^{232}Th						Weighted mean (Bq/kg)
	^{228}Ac (Bq/kg)		^{228}Ac (Bq/kg)		^{212}Pb (Bq/kg)		
	338.320keV		911.204keV		238.632keV		
BA01	21.753	± 2.718	76.740	± 1.971	83.001	± 1.487	71.283 ± 1.088
BA02	61.260	± 1.796	62.970	± 1.261	72.180	± 1.187	66.613 ± 0.779
BA03	63.290	± 3.145	75.630	± 2.068	81.820	± 1.591	77.271 ± 1.170
BA04	105.200	± 3.310	121.000	± 2.228	118.500	± 1.210	117.772 ± 1.012
BA05	61.630	± 2.027	78.640	± 1.709	81.550	± 1.581	75.621 ± 1.007
BA06	65.430	± 2.904	76.500	± 1.674	79.380	± 1.569	76.338 ± 1.065
BA07	68.480	± 2.188	79.660	± 1.739	83.990	± 1.618	78.921 ± 1.042
BA08	103.600	± 3.192	120.500	± 2.218	118.200	± 1.207	117.223 ± 1.006
BA09	69.735	± 2.265	81.840	± 1.905	84.859	± 1.628	80.400 ± 1.086
BA10	63.300	± 2.889	75.680	± 1.650	76.700	± 1.523	74.544 ± 1.044
BA11	63.820	± 2.937	77.000	± 3.192	83.440	± 1.601	78.629 ± 1.286
BA12	56.850	± 1.691	64.540	± 1.282	71.250	± 1.179	65.814 ± 0.772

Appendix 19: ^{232}Th activity concentrations in fly ash samples

Sample name	^{232}Th						Weighted mean (Bq/kg)
	^{228}Ac (Bq/kg)		^{228}Ac (Bq/kg)		^{212}Pb (Bq/kg)		
	338.320keV		911.204keV		238.632keV		
FA01	81.230	± 2.820	91.820	± 2.240	107.100	± 2.215	95.191 ± 1.375
FA02	170.300	± 4.943	187.000	± 3.635	223.400	± 3.804	196.864 ± 2.320
FA03	79.290	± 3.206	85.760	± 2.334	80.900	± 0.982	81.458 ± 0.871
FA04	85.037	± 3.496	88.846	± 2.738	83.129	± 1.707	84.774 ± 1.338
FA05	78.580	± 4.493	91.330	± 3.234	83.380	± 1.440	84.213 ± 1.262
FA06	73.450	± 4.026	90.000	± 2.093	98.660	± 1.966	92.223 ± 1.350
FA07	151.800	± 5.188	168.500	± 3.453	98.660	± 1.865	169.867 ± 1.565
FA08	86.830	± 5.291	108.900	± 3.391	91.470	± 1.604	94.110 ± 1.398
FA09	93.400	± 5.129	102.600	± 3.243	110.700	± 2.436	105.966 ± 1.821
FA10	143.500	± 4.878	162.100	± 3.270	157.800	± 1.704	157.386 ± 1.443
FA11	145.600	± 4.297	158.700	± 3.579	162.900	± 1.768	160.103 ± 1.487
FA12	66.850	± 3.908	74.660	± 1.911	83.390	± 1.833	77.937 ± 1.253

Appendix 20: ^{40}K, ^{210}Pb, ^{212}Bi and ^{208}Tl activity concentrations in soil samples

Sample name	^{40}K (Bq/kg) 1460.81keV	^{210}Pb (Bq/kg) 46.54keV	^{212}Bi (Bq/kg)	^{208}Tl (Bq/kg)
MS01	182.800 ± 3.483	0.000 ± 0.000	15.88 ± 1.524	3.956 ± 0.168
MS02	225.500 ± 4.148	50.930 ± 21.940	5.883 ± 0.735	4.099 ± 0.177
MS03	196.600 ± 3.860	0.000 ± 0.000	12.43 ± 2.082	3.913 ± 0.189
MS04	180.800 ± 3.507	0.000 ± 0.000	13.91 ± 1.397	4.03 ± 0.174
MS05	174.000 ± 4.072	0.000 ± 0.000	14.12 ± 1.483	4.381 ± 0.156
MS06	223.000 ± 4.030	0.000 ± 0.000	14.63 ± 1.264	4.433 ± 0.176
MS07	229.200 ± 4.179	0.000 ± 0.000	12.46 ± 1.386	4.487 ± 0.171
MS08	275.763 ± 4.782	0.000 ± 0.000	14.81 ± 1.869	4.333 ± 0.164
MS09	157.100 ± 3.132	0.000 ± 0.000	10.09 ± 1.345	3.159 ± 0.154
MS10	190.100 ± 3.778	0.000 ± 0.000	16.37 ± 1.376	4.791 ± 0.171
MS11	132.400 ± 2.707	0.000 ± 0.000	12.49 ± 1.168	3.318 ± 0.135
MS12	137.694 ± 2.848	0.000 ± 0.000	12.1 ± 1.041	3.137 ± 0.153
MS13	153.200 ± 2.788	0.000 ± 0.000	13.7 ± 1.489	3.309 ± 0.139
MS14	125.100 ± 2.518	0.000 ± 0.000	6.985 ± 1.15	2.969 ± 0.126
MS15	133.500 ± 2.601	0.000 ± 0.000	9.429 ± 1.135	3.253 ± 0.116
MS16	271.900 ± 4.633	0.000 ± 0.000	34.38 ± 2.511	10.57 ± 0.271
MS17	88.150 ± 2.241	0.000 ± 0.000	8.979 ± 0.991	2.19 ± 0.119
MS18	198.200 ± 3.923	0.000 ± 0.000	20.01 ± 2.103	4.873 ± 0.204
MS19	133.900 ± 2.667	30.100 ± 16.250	8.715 ± 1.092	2.67 ± 0.135
MS20	188.900 ± 3.576	0.000 ± 0.000	102.1 ± 10.3	33.56 ± 1.518

Appendix 20 (continued)

Sample name	^{40}K (Bq/kg) 1460.81keV	^{210}Pb (Bq/kg) 46.54keV	^{212}Bi (Bq/kg)	^{208}Tl (Bq/kg)
MS21	180.900 ± 3.207	0.000 ± 0.000	11.63 ± 1.302	3.014 ± 0.129
MS22	136.800 ± 4.652	0.000 ± 0.000	15.88 ± 1.912	4.749 ± 0.261
MS23	167.600 ± 5.143	0.000 ± 0.000	16.27 ± 2.36	4.918 ± 0.288
MS24	282.700 ± 4.859	18.840 ± 4.157	21.98 ± 1.484	5.68 ± 0.134
MS25	158.300 ± 5.072	0.000 ± 0.000	20.57 ± 3.953	4.341 ± 0.306
MS26	250.400 ± 4.335	26.630 ± 3.881	16.32 ± 1.214	4.433 ± 0.12
MS27	174.000 ± 5.333	0.000 ± 0.000	19.92 ± 2.815	5.905 ± 0.47
MS28	261.600 ± 4.621	25.510 ± 4.189	20.62 ± 1.345	7.401 ± 0.141
MS29	192.900 ± 5.471	0.000 ± 0.000	24.29 ± 3.801	7.098 ± 0.195
MS30	286.300 ± 4.823	18.570 ± 4.154	20.88 ± 1.401	5.335 ± 0.129
MS31	328.900 ± 5.319	24.110 ± 4.571	18.14 ± 1.391	4.852 ± 0.13
MS32	185.500 ± 5.079	0.000 ± 0.000	17.78 ± 2.126	3.667 ± 0.259
MS33	251.396 ± 6.274	0.000 ± 0.000	16.86 ± 2.065	3.714 ± 0.185
MS34	199.700 ± 5.162	0.000 ± 0.000	16.22 ± 1.57	4.417 ± 0.263
MS35	175.800 ± 4.839	0.000 ± 0.000	18.86 ± 2.138	3.961 ± 0.218
MS36	347.100 ± 6.908	0.000 ± 0.000	26.42 ± 3.773	6.057 ± 0.267
MS37	178.200 ± 4.897	0.000 ± 0.000	33.56 ± 1.518	3.826 ± 0.26
MS38	352.900 ± 7.397	0.000 ± 0.000	13.46 ± 4.917	6.324 ± 0.339
MS39	189.400 ± 5.029	0.000 ± 0.000	19.92 ± 2.815	5.905 ± 0.47
MS40	234.400 ± 5.503	46.530 ± 42.580	16 ± 3.219	4.015 ± 0.276

Appendix 20 (continued)

Sample name	^{40}K (Bq/kg) 1460.81keV	^{210}Pb (Bq/kg) 46.54keV	^{212}Bi (Bq/kg)	^{208}Tl (Bq/kg)
MS41	89.200 ± 3.753	0.000 ± 0.000	8.755 ± 1.888	2.137 ± 0.217
MS42	215.500 ± 4.050	19.910 ± 3.552	7.881 ± 0.886	4.465 ± 0.126
MS43	128.800 ± 4.620	0.000 ± 0.000	10.14 ± 1.489	2.753 ± 0.216
MS44	242.600 ± 6.392	0.000 ± 0.000	17.69 ± 5.531	6.538 ± 0.337
MS45	157.000 ± 4.751	0.000 ± 0.000	102.1 ± 10.3	26.77 ± 1.162
MS46	246.900 ± 4.588	0.000 ± 0.000	9.5 ± 1.809	5.791 ± 0.148
MS47	120.000 ± 3.215	0.000 ± 0.000	9.329 ± 1.54	5.356 ± 0.124
MS48	217.300 ± 4.066	0.000 ± 0.000	14.46 ± 1.294	4.568 ± 0.128
MS49	195.300 ± 3.689	20.010 ± 3.916	6.233 ± 0.555	3.889 ± 0.115
MS50	283.200 ± 6.779	0.000 ± 0.000	22.12 ± 3.97	6.059 ± 0.387
MS51	138.900 ± 4.922	0.000 ± 0.000	15.73 ± 2.699	4.43 ± 0.254
MS52	190.500 ± 5.039	0.000 ± 0.000	15.14 ± 2.724	4.403 ± 0.238
MS53	169.100 ± 3.213	14.920 ± 3.162	7.168 ± 0.945	2.934 ± 0.099
MS54	167.000 ± 4.054	0.000 ± 0.000	6.945 ± 0.73	2.667 ± 0.099
MS55	154.200 ± 5.043	0.000 ± 0.000	10.76 ± 2.237	3.384 ± 0.255

Appendix 21: ^{40}K, ^{210}Pb, ^{212}Bi and ^{208}Tl activity concentrations in coal samples

Sample name	^{40}K (Bq/kg) 1460.81keV	Weighted mean (Bq/kg)	^{210}Pb (Bq/kg) 46.54keV	Weighted mean (Bq/kg)	^{212}Bi (Bq/kg)	^{208}Tl (Bq/kg)
COAL1	18.245 ± 2.789	18.25 ± 2.789	151.200 ± 45.065	151.2 ± 45.065	60.94 ± 6.161	15.42 ± 0.526
COAL2	15.651 ± 3.745	15.65 ± 3.745	0.000 ± 0.000	0 ± 0.000	27.74 ± 3.692	9.312 ± 0.432
COAL3	17.410 ± 5.043	17.41 ± 5.043	0.000 ± 0.000	0 ± 0.000	24.32 ± 3.776	8.428 ± 0.399
COAL4	10.600 ± 4.298	10.6 ± 4.298	0.000 ± 0.000	0 ± 0.000	35.34 ± 3.083	9.239 ± 0.362
COAL5	15.625 ± 6.242	15.63 ± 6.242	0.000 ± 0.000	0 ± 0.000	50.49 ± 6.713	15.81 ± 0.608
COAL6	20.065 ± 2.742	20.07 ± 2.742	150.100 ± 48.020	150.1 ± 48.020	63.5 ± 5.933	15.75 ± 0.585
COAL7	15.817 ± 3.149	15.82 ± 3.149	0.000 ± 0.000	0 ± 0.000	68.58 ± 5.69	15.54 ± 0.624
COAL8	22.495 ± 2.799	22.5 ± 2.799	254.550 ± 50.550	254.55 ± 50.550	61.23 ± 7.17	15.99 ± 0.545
COAL9	25.670 ± 2.587	25.67 ± 2.587	199.250 ± 12.910	199.25 ± 12.910	47.36 ± 5.918	15.66 ± 0.553
COAL10	9.126 ± 4.442	9.126 ± 4.442	0.000 ± 0.000	0 ± 0.000	30.07 ± 3.548	9.42 ± 0.404
COAL11	18.268 ± 3.603	18.27 ± 3.603	0.000 ± 0.000	0 ± 0.000	44.48 ± 6.347	15.13 ± 0.559
COAL12	16.432 ± 4.534	16.43 ± 4.534	0.000 ± 0.000	0 ± 0.000	45.64 ± 6.367	17.61 ± 0.559

Appendix 22: ^{40}K, ^{210}Pb, ^{212}Bi and ^{208}Tl activity concentrations in bottom ash samples

Sample name	^{40}K (Bq/kg) 1460.81keV	Weighted mean (Bq/kg)	^{210}Pb (Bq/kg) 46.54keV	Weighted mean (Bq/kg)	^{212}Bi (Bq/kg)	^{208}Tl (Bq/kg)
BA01	31.837 ± 3.749	31.84 ± 3.749	172.012 ± 51.785	172.01 ± 51.785	330.7 ± 8.938	98.61 ± 1.516
BA02	32.660 ± 2.410	32.66 ± 2.41	42.160 ± 23.130	42.16 ± 23.130	68.97 ± 2.486	20.03 ± 0.372
BA03	40.960 ± 3.798	40.96 ± 3.798	0.000 ± 0.000	0 ± 0.000	69.29 ± 9.328	25.08 ± 0.557
BA04	68.860 ± 2.440	68.86 ± 2.44	40.040 ± 2.766	40.04 ± 2.766	126.4 ± 3.447	39.43 ± 0.362
BA05	30.490 ± 3.656	30.49 ± 3.656	176.900 ± 50.070	176.9 ± 50.070	92.38 ± 2.384	25.04 ± 0.549
BA06	30.190 ± 4.049	30.19 ± 4.049	0.000 ± 0.000	0 ± 0.000	79.79 ± 5.543	25.59 ± 0.557
BA07	36.060 ± 3.813	36.06 ± 3.813	0.000 ± 0.000	0 ± 0.000	84.42 ± 3.691	25.71 ± 0.582
BA08	35.720 ± 8.686	35.72 ± 8.686	17.550 ± 11.240	17.55 ± 11.240	128.9 ± 2.791	40.09 ± 0.361
BA09	37.095 ± 3.867	37.1 ± 3.867	0.000 ± 0.000	0 ± 0.000	18.45 ± 2.09	3.873 ± 0.213
BA10	27.870 ± 3.667	27.87 ± 3.667	0.000 ± 0.000	0 ± 0.000	78.35 ± 4.087	23.96 ± 0.539
BA11	37.060 ± 3.902	37.06 ± 3.902	0.000 ± 0.000	0 ± 0.000	84.31 ± 4.509	26.46 ± 0.53
BA12	38.380 ± 2.149	38.38 ± 2.149	0.000 ± 0.000	0 ± 0.000	64.91 ± 2.39	20.3 ± 0.36

Appendix 23: ^{40}K, ^{210}Pb, ^{212}Bi and ^{208}Tl activity concentrations in fly ash samples

Sample name	^{40}K (Bq/kg) 1460.81keV	Weighted mean (Bq/kg)	^{210}Pb (Bq/kg) 46.54keV	Weighted mean (Bq/kg)	^{212}Bi (Bq/kg)	^{208}Tl (Bq/kg)
FA01	43.190 ± 6.210	43.19 ± 6.21	0.000 ± 0.000	0 ± 0.000	210.4 ± 8.51	63.09 ± 1.072
FA02	98.580 ± 6.144	98.58 ± 6.144	0.000 ± 0.000	0 ± 0.000	201.9 ± 4.974	63.56 ± 0.744
FA03	65.567 ± 12.765	65.57 ± 12.77	0.000 ± 0.000	0 ± 0.000	79.69 ± 3.487	24.97 ± 0.38
FA04	67.904 ± 14.857	67.9 ± 14.86	0.000 ± 0.000	0 ± 0.000	78.58 ± 2.865	23.54 ± 0.372
FA05	40.730 ± 7.243	40.73 ± 7.243	0.000 ± 0.000	0 ± 0.000	92.42 ± 8.377	29.94 ± 0.79
FA06	46.060 ± 5.620	46.06 ± 5.62	0.000 ± 0.000	0 ± 0.000	93.85 ± 3.169	31.59 ± 0.724
FA07	123.900 ± 4.769	123.9 ± 4.769	172.100 ± 6.510	172.1 ± 6.510	162.5 ± 6.145	53.49 ± 0.601
FA08	50.830 ± 7.975	50.83 ± 7.975	188.900 ± 84.990	188.9 ± 84.990	104.2 ± 7.375	34.22 ± 0.919
FA09	50.970 ± 8.513	50.97 ± 8.513	215.700 ± 76.720	215.7 ± 76.720	91.34 ± 7.173	32.68 ± 0.938
FA10	64.960 ± 12.520	64.96 ± 12.52	141.700 ± 5.854	141.7 ± 5.854	155.2 ± 5.926	49.87 ± 0.561
FA11	112.300 ± 28.720	112.3 ± 28.72	152.700 ± 6.229	152.7 ± 6.229	155.6 ± 5.916	51.77 ± 0.585
FA12	37.170 ± 5.953	37.17 ± 5.953	0.000 ± 0.000	0 ± 0.000	67.52 ± 5.698	24.12 ± 0.693

Appendix 24: Screenshot of Genie 2000 user interface for soil sample

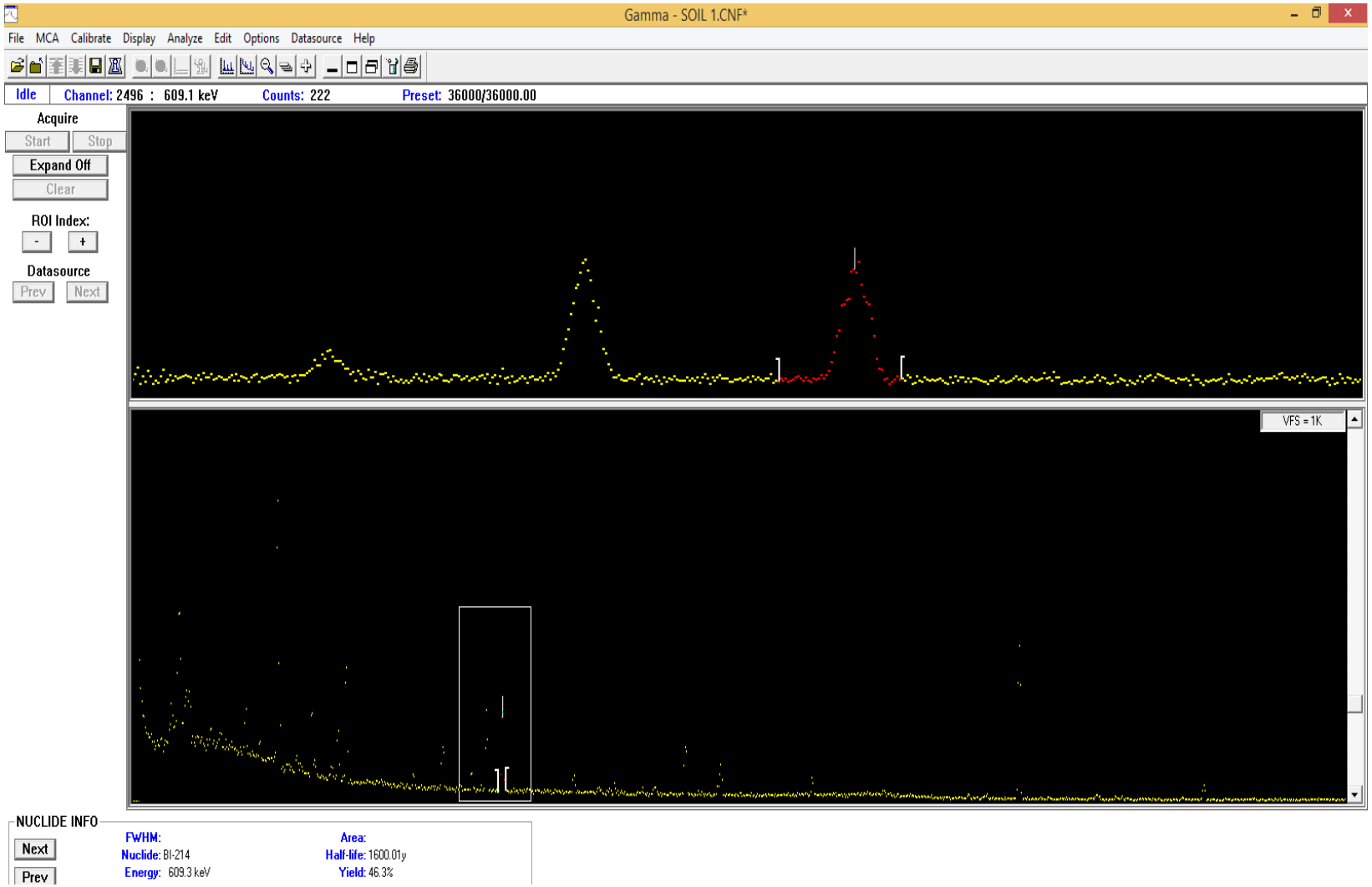

Appendix 25: Activity ratios for Th/U, K/U and K/Th in soil samples

Sample no.	Th/U	K/U	K/Th
MS01	0.757626031 ± 0.077669219	10.6200404 ± 1.07294116	14.0175231 ± 0.420184
MS02	0.963682308 ± 0.151631591	13.1007609 ± 2.04604102	13.5944811 ± 0.193029
MS03	0.392177178 ± 0.023760126	5.97649905 ± 0.34709906	15.2392831 ± 0.367782
MS04	0.780162011 ± 0.096785160	11.2509980 ± 1.37475263	14.4213610 ± 0.303044
MS05	0.641787890 ± 3.686564509	8.70264200 ± 0.80333949	13.5599972 ± 79.64896
MS06	0.847284649 ± 0.120148565	13.8675163 ± 1.94313910	16.3670100 ± 0.292581
MS07	0.459468252 ± 0.032000636	8.71321356 ± 0.60798048	18.9636901 ± 0.467255
MS08	1.649664614 ± 0.197541829	18.3725968 ± 2.16488834	11.1371710 ± 0.256137
MS09	0.517908013 ± 0.039789416	7.88136584 ± 0.58475045	15.2176943 ± 0.543156
MS10	1.290844856 ± 0.207548855	15.7283055 ± 2.51802045	12.1845049 ± 0.237188
MS11	0.600395468 ± 0.046545323	7.45785585 ± 0.57140370	12.4215725 ± 0.373993
MS12	0.879477170 ± 0.134709077	11.9723729 ± 1.81524628	13.6130570 ± 0.477412
MS13	0.992827520 ± 0.117830976	13.1006207 ± 1.53969387	13.1952635 ± 0.307928
MS14	0.827285363 ± 0.094672496	10.0706848 ± 1.13869049	12.1731693 ± 0.323328
MS15	0.681020868 ± 0.066278592	9.65510033 ± 0.91844086	14.1773928 ± 0.288969
MS16	1.023328661 ± 0.081374861	8.40480219 ± 0.66604561	8.21319925 ± 0.197504
MS17	0.671872634 ± 0.084389923	7.90539580 ± 0.97841001	11.7662119 ± 0.446771
MS18	0.741051694 ± 0.076478111	10.6760351 ± 1.10546028	14.4065996 ± 0.373883
MS19	0.972420765 ± 0.135595981	14.0074369 ± 1.92864591	14.4047077 ± 0.463102
MS20	0.892646407 ± 0.10524292	12.9459393 ± 1.50827825	14.5028750 ± 0.552210

Appendix 25 (continued)

Sample no.	Th/U	K/U	K/Th
MS21	0.901432202 ± 0.112367887	17.0945405 ± 2.09623822	18.9637562 ± 0.242660
MS22	0.771887947 ± 0.130856847	7.21802151 ± 1.21868519	9.35112608 ± 0.364203
MS23	0.861032016 ± 0.154779851	9.36688179 ± 1.66613630	10.8786684 ± 0.473713
MS24	0.888745668 ± 0.058814433	12.8706968 ± 0.86251395	14.4818672 ± 0.281801
MS25	0.583311388 ± 0.085492977	6.91942365 ± 0.99118769	11.8623154 ± 0.379920
MS26	1.035012639 ± 0.079943657	18.5504914 ± 1.44172789	17.9229612 ± 0.425077
MS27	0.733322931 ± 0.104185631	7.03430968 ± 0.99035860	9.59237655 ± 0.333062
MS28	0.849248527 ± 0.055292998	9.81417937 ± 0.64937784	11.5563102 ± 0.216139
MS29	0.482699795 ± 0.049144895	4.52666133 ± 0.45783653	9.37779832 ± 0.189084
MS30	0.655557531 ± 0.041030519	10.0874523 ± 0.64019331	15.3875927 ± 0.215693
MS31	0.850472250 ± 0.058917624	16.4375176 ± 1.14527656	19.3275179 ± 0.355501
MS32	0.534625206 ± 0.080690192	8.81906821 ± 1.28388492	16.4957958 ± 0.489840
MS33	0.432049171 ± 0.038615752	5.33156530 ± 0.42729680	12.3401818 ± 0.282671
MS34	0.825686633 ± 0.145361607	11.8476204 ± 2.04128107	14.3488097 ± 0.609233
MS35	0.555500054 ± 0.082012778	9.75481163 ± 1.43965328	17.5604153 ± 0.381712
MS36	0.47146246 ± 0.040741931	7.57085914 ± 0.60591912	16.0582438 ± 0.326042
MS37	0.855892668 ± 0.204790246	15.7365486 ± 3.76052686	18.3861238 ± 0.640259
MS38	0.475685494 ± 0.042151252	7.69169038 ± 0.62257359	16.1696972 ± 0.359067
MS39	0.867783032 ± 0.16649736	13.4809322 ± 2.57139258	15.5349110 ± 0.578178
MS40	0.631914146 ± 0.065256566	12.7142166 ± 1.16305482	20.1201645 ± 0.741212

Appendix 25 (continued)

Sample no.	Th/U	K/U	K/Th
MS41	0.423453095 ± 0.086507073	7.03787164 ± 1.43438167	16.6201918 ± 0.430208
MS42	0.955211108 ± 0.071306233	14.4650951 ± 1.08801652	15.1433489 ± 0.360590
MS43	1.003674216 ± 0.357818381	16.0282678 ± 5.65367750	15.9695921 ± 1.161572
MS44	0.500022983 ± 0.043415473	4.02789474 ± 0.34399889	8.05541921 ± 0.211027
MS45	0.539660323 ± 0.049543895	10.6250585 ± 0.82580639	19.6884189 ± 0.690136
MS46	1.045017752 ± 0.077375308	14.5675691 ± 1.08873211	13.9400207 ± 0.353025
MS47	0.906289812 ± 0.334101629	13.4493399 ± 4.90312520	14.8399990 ± 0.895252
MS48	1.289557544 ± 0.266115727	20.5449677 ± 4.24446441	15.9317960 ± 0.505131
MS49	0.731126694 ± 0.051823595	11.5188701 ± 0.82478758	15.7549576 ± 0.284682
MS50	1.421616023 ± 0.112844447	17.8853041 ± 1.29820477	12.5809669 ± 0.834727
MS51	1.457404213 ± 0.517237929	16.9531507 ± 5.99792702	11.6324288 ± 0.973519
MS52	0.866229509 ± 0.092248551	12.3945123 ± 1.21276463	14.3085778 ± 0.697448
MS53	0.591721665 ± 0.044260715	13.0079377 ± 0.96866089	21.9832035 ± 0.361365
MS54	1.494787910 ± 0.534509370	19.4538875 ± 6.95144076	13.0144801 ± 0.717273
MS55	1.391528856 ± 0.525079030	19.4390976 ± 7.30320177	13.9695972 ± 1.129555

Appendix 26: Activity ratios for Th/U, K/U and K/Th in coal samples

Sample no.	Th/U	K/U	K/Th
COAL1	0.514306776 ± 0.038011900	0.34401661 ± 0.05773862	0.66889380 ± 0.053326
COAL2	0.713300682 ± 0.084195062	0.38877642 ± 0.10311090	0.54503862 ± 0.093713
COAL3	0.574144107 ± 0.063278564	0.39706658 ± 0.12280771	0.69158000 ± 0.115283
COAL4	0.623267924 ± 0.066068655	0.23154298 ± 0.09678863	0.37149831 ± 0.094143
COAL5	0.456163447 ± 0.032896574	0.24629332 ± 0.09978855	0.53992339 ± 0.098587
COAL6	0.325021868 ± 0.023772649	0.28772265 ± 0.04379123	0.88524089 ± 0.040214
COAL7	0.418597373 ± 0.025997908	0.23553298 ± 0.04876255	0.56267191 ± 0.047265
COAL8	0.430884730 ± 0.030826953	0.32488691 ± 0.04593408	0.75399960 ± 0.041215
COAL9	0.451784308 ± 0.032785911	0.42150438 ± 0.05118903	0.93297702 ± 0.043866
COAL10	0.521191094 ± 0.050744627	0.16712917 ± 0.08282413	0.32066773 ± 0.081487
COAL11	0.656375435 ± 0.072895186	0.43505216 ± 0.09779799	0.66280993 ± 0.086574
COAL12	0.529898031 ± 0.053778643	0.34761904 ± 0.10188041	0.65601119 ± 0.096255

Appendix 27: Activity ratios for Th/U, K/U and K/Th in bottom ash samples

Sample no.	Th/U	K/U	K/Th
BA01	0.699736147 ± 0.043681879	0.31252397 ± 0.04137920	0.44663117 ± 0.037109
BA02	0.895390441 ± 0.058130666	0.43900291 ± 0.04284101	0.49029215 ± 0.032798
BA03	0.803942595 ± 0.055895960	0.42615663 ± 0.04896625	0.53008341 ± 0.040039
BA04	0.817853228 ± 0.043738983	0.47818971 ± 0.03040110	0.58468891 ± 0.017436
BA05	0.770817458 ± 0.053197613	0.31078761 ± 0.04279806	0.40319223 ± 0.037495
BA06	0.850856065 ± 0.061325962	0.33649459 ± 0.05101828	0.39547769 ± 0.045373
BA07	0.849037579 ± 0.059067360	0.38793770 ± 0.04883513	0.45691464 ± 0.041339
BA08	0.907611892 ± 0.045851141	0.27656672 ± 0.06864743	0.30471915 ± 0.067294
BA09	0.796331382 ± 0.053086212	0.36741000 ± 0.04519105	0.46137828 ± 0.038621
BA10	0.988338258 ± 0.070817489	0.36951539 ± 0.05511877	0.37387543 ± 0.048893
BA11	0.809993517 ± 0.058319413	0.38176989 ± 0.04829351	0.47132463 ± 0.040678
BA12	0.968489758 ± 0.062508235	0.56477966 ± 0.04780061	0.58315502 ± 0.032310

Appendix 28: Activity ratios for Th/U, K/U and K/Th in fly ash samples

Sample no.	Th/U	K/U	K/Th
FA01	0.840601100 ± 0.064085047	0.38139761 ± 0.06182533	0.45372010 ± 0.055115
FA02	0.978741344 ± 0.061645824	0.49010542 ± 0.04304163	0.50075071 ± 0.031087
FA03	0.743716051 ± 0.042142114	0.59862955 ± 0.12121215	0.80491681 ± 0.116721
FA04	0.757983488 ± 0.051411812	0.60714309 ± 0.13874544	0.80099778 ± 0.133185
FA05	0.740416116 ± 0.059238640	0.35810748 ± 0.06962385	0.48365706 ± 0.063908
FA06	0.739081550 ± 0.051594939	0.36913005 ± 0.05160787	0.49944427 ± 0.045362
FA07	0.766909287 ± 0.041407290	0.55938043 ± 0.03673168	0.72939583 ± 0.022139
FA08	0.645827199 ± 0.049166637	0.34881907 ± 0.06060940	0.54011208 ± 0.054973
FA09	0.736683762 ± 0.056559368	0.35434694 ± 0.06485116	0.48100279 ± 0.059495
FA10	0.800984887 ± 0.043394620	0.33060166 ± 0.06611816	0.41274394 ± 0.063790
FA11	0.753403416 ± 0.040619648	0.52845623 ± 0.13803262	0.70142532 ± 0.135238
FA12	0.702083140 ± 0.052376782	0.33484218 ± 0.05891408	0.47692667 ± 0.053897

Appendix 29: Weighted mean and error propagation calculation [Kamunda, 2017]

Weighted average

From the functions $b \pm \delta b$, $c \pm \delta c$ and $d \pm \delta d$, the weighted average (W_m) is calculated as:

$$W_m = \frac{\frac{b}{\delta b^2} + \frac{c}{\delta c^2} + \frac{d}{\delta d^2}}{\frac{1}{\delta b^2} + \frac{1}{\delta c^2} + \frac{1}{\delta d^2}}$$

Such that the corresponding propagated uncertainty is computed as:

$$\Delta W_m = \frac{1}{\sqrt{\frac{1}{\delta b^2} + \frac{1}{\delta c^2} + \frac{1}{\delta d^2}}}$$

Error propagation

The following are simplified formulae used in error propagation:

Function[1]	**Manipulation**	**Uncertainty**[2]
$y = a_1 x_1 - a_2 x_2$ or $y = a_1 x_1 + a_2 x_2$	Addition/subtraction	$s_y = \sqrt{a_1^{\,2} s_{x_1}^{\,2} + a_2^{\,2} s_{x_2}^{\,2}}$
$y = a_1 x_1 x_2$ or $y = a_1\left(\frac{x_1}{x_2}\right)$	Multiplication/division	$\frac{s_y}{y} = \sqrt{\left(\frac{s_{x_1}}{x_1}\right)^2 + \left(\frac{s_{x_2}}{x_2}\right)^2}$
$y = x^m$	Power of x	$\frac{s_y}{y} = \frac{m s_x}{x}$
$y = e^{-ax}$	Power of e	$\frac{s_y}{y} = a s_x$

Such that:

[1] a, a_1, a_2, a_3 and m are constants: x, x_1 and x_2 are some independent variables, with y being the dependent variable.

[2] s_i represents the estimated standard deviation for variable x_i.

Appendix 30: Radiological parameters for soil samples

Sample No.	D (nGy/h)			AEDE (µSv/y)			Ra_{eq} (Bq/kg)			H_{ext}		
MS01	23.452	±	0.828	28.761	±	1.015	49.936	±	1.794	0.135	±	0.005
MS02	27.375	±	1.273	33.572	±	1.562	58.297	±	2.761	0.157	±	0.007
MS03	31.188	±	0.870	38.249	±	1.067	66.482	±	1.885	0.180	±	0.005
MS04	22.536	±	0.934	27.638	±	1.145	47.919	±	2.025	0.129	±	0.005
MS05	24.243	±	44.520	29.732	±	54.600	51.741	±	105.410	0.139	±	0.285
MS06	24.958	±	1.072	30.608	±	1.314	52.735	±	2.322	0.142	±	0.006
MS07	29.011	±	0.847	35.579	±	1.039	61.237	±	1.827	0.165	±	0.005
MS08	33.389	±	0.928	40.948	±	1.139	71.651	±	2.035	0.193	±	0.005
MS09	21.996	±	0.694	26.975	±	0.851	46.792	±	1.504	0.126	±	0.004
MS10	22.935	±	0.931	28.127	±	1.142	49.035	±	2.019	0.132	±	0.005
MS11	20.161	±	0.635	24.725	±	0.778	43.190	±	1.375	0.117	±	0.004
MS12	17.165	±	0.827	21.051	±	1.015	36.568	±	1.795	0.099	±	0.005
MS13	18.804	±	0.661	23.061	±	0.810	40.093	±	1.434	0.108	±	0.004
MS14	17.163	±	0.649	21.049	±	0.795	36.751	±	1.407	0.099	±	0.004
MS15	17.642	±	0.899	21.637	±	1.103	37.572	±	1.943	0.101	±	0.005
MS16	46.280	±	0.634	56.758	±	0.778	100.627	±	1.376	0.272	±	0.004
MS17	13.352	±	0.816	16.376	±	1.000	28.651	±	1.768	0.077	±	0.005
MS18	25.152	±	0.630	30.846	±	0.773	53.499	±	1.364	0.144	±	0.004
MS19	15.615	±	1.498	19.150	±	1.837	33.162	±	3.249	0.090	±	0.009
MS20	22.485	±	1.511	27.576	±	1.853	47.763	±	3.282	0.129	±	0.009

Appendix 30 (continued)

Sample No.	D (nGy/h)			AEDE (µSv/y)			Ra_{eq} (Bq/kg)			H_{ext}		
MS21	18.194	±	0.706	22.314	±	0.866	38.153	±	1.519	0.103	±	0.004
MS22	23.297	±	1.533	28.571	±	1.881	50.406	±	3.329	0.136	±	0.009
MS23	24.561	±	0.522	30.121	±	0.640	52.829	±	1.117	0.142	±	0.003
MS24	33.727	±	1.635	41.363	±	2.005	71.648	±	3.549	0.194	±	0.010
MS25	25.231	±	0.828	30.943	±	1.016	54.149	±	1.788	0.146	±	0.005
MS26	25.116	±	1.962	30.803	±	2.407	52.757	±	4.255	0.142	±	0.012
MS27	29.640	±	0.840	36.351	±	1.031	64.073	±	1.810	0.173	±	0.005
MS28	36.896	±	0.681	45.250	±	0.835	79.169	±	1.459	0.214	±	0.004
MS29	40.156	±	1.443	49.247	±	1.770	86.882	±	3.131	0.235	±	0.008
MS30	36.289	±	1.775	44.505	±	2.177	77.033	±	3.871	0.208	±	0.010
MS31	33.238	±	1.395	40.763	±	1.711	69.669	±	3.031	0.188	±	0.008
MS32	24.245	±	1.235	29.734	±	1.515	51.398	±	2.669	0.139	±	0.007
MS33	44.572	±	1.740	54.664	±	2.134	95.642	±	3.783	0.258	±	0.010
MS34	24.521	±	1.271	30.073	±	1.558	52.135	±	2.746	0.141	±	0.007
MS35	21.704	±	1.773	26.617	±	2.174	45.874	±	3.858	0.124	±	0.010
MS36	48.711	±	1.268	59.739	±	1.555	103.483	±	2.745	0.280	±	0.007
MS37	18.517	±	0.872	22.709	±	1.070	38.905	±	1.904	0.105	±	0.005
MS38	49.095	±	1.187	60.210	±	1.456	104.263	±	2.567	0.282	±	0.007
MS39	21.753	±	0.547	26.678	±	0.671	46.068	±	1.177	0.124	±	0.003
MS40	25.329	±	1.352	31.063	±	1.658	53.144	±	2.934	0.143	±	0.008

Appendix 30 (continued)

Sample No.	D (nGy/h)			AEDE (µSv/y)			Ra_{eq} (Bq/kg)			H_{ext}		
MS41	12.817	±	1.716	15.719	±	2.105	27.217	±	3.736	0.073	±	0.010
MS42	24.465	±	0.596	30.003	±	0.730	51.841	±	1.297	0.140	±	0.004
MS43	13.955	±	0.621	17.114	±	0.762	29.487	±	1.336	0.080	±	0.004
MS44	41.834	±	1.534	51.305	±	1.881	90.904	±	3.329	0.246	±	0.009
MS45	18.190	±	1.028	22.308	±	1.261	38.269	±	2.220	0.103	±	0.006
MS46	28.824	±	0.575	35.350	±	0.705	61.287	±	1.238	0.166	±	0.003
MS47	14.010	±	0.792	17.182	±	0.972	29.726	±	1.764	0.080	±	0.005
MS48	22.186	±	1.387	27.209	±	1.701	46.813	±	3.009	0.126	±	0.008
MS49	23.464	±	0.807	28.777	±	0.99	49.719	±	1.772	0.134	±	0.005
MS50	32.721	±	0.462	40.129	±	0.567	69.830	±	0.994	0.189	±	0.003
MS51	16.790	±	1.440	20.591	±	1.766	35.964	±	3.118	0.097	±	0.008
MS52	23.086	±	1.424	28.313	±	1.747	49.077	±	3.089	0.133	±	0.008
MS53	17.703	±	1.754	21.712	±	2.151	37.020	±	3.815	0.100	±	0.010
MS54	18.680	±	2.192	22.910	±	2.688	39.793	±	4.766	0.107	±	0.013
MS55	16.762	±	2.227	20.557	±	2.731	35.591	±	4.823	0.096	±	0.013

Appendix 31: Radiological parameters for coal samples

Sample No.	D (nGy/h)			AEDE (µSv/y)			Ra_{eq} (Bq/kg)			H_{ext}		
COAL1	41.738	±	2.219	51.188	±	2.721	93.445	±	4.824	0.252	±	0.013
COAL2	36.596	±	2.045	44.881	±	2.508	82.525	±	4.438	0.223	±	0.012
COAL3	36.188	±	2.199	44.381	±	2.697	81.186	±	4.773	0.219	±	0.013
COAL4	38.826	±	1.818	47.617	±	2.229	87.398	±	3.953	0.236	±	0.011
COAL5	47.440	±	2.196	58.181	±	2.694	106.027	±	4.772	0.286	±	0.013
COAL6	46.746	±	1.958	57.329	±	2.401	103.695	±	4.256	0.280	±	0.012
COAL7	48.664	±	2.407	59.681	±	2.952	108.570	±	5.226	0.293	±	0.014
COAL8	50.947	±	2.144	62.481	±	2.629	113.635	±	4.656	0.307	±	0.013
COAL9	45.825	±	2.194	56.200	±	2.691	102.223	±	4.757	0.276	±	0.013
COAL10	42.797	±	2.928	52.487	±	3.591	96.004	±	6.366	0.259	±	0.017
COAL11	36.808	±	2.247	45.142	±	2.756	82.809	±	4.883	0.224	±	0.013
COAL12	37.653	±	3.099	46.178	±	3.801	84.355	±	6.739	0.228	±	0.018

Appendix 32: Radiological parameters for bottom ash samples

Sample No.	D (nGy/h)			AEDE (µSv/y)			Ra_{eq} (Bq/kg)			H_{ext}		
BA01	91.446	±	3.566	112.150	±	4.373	206.256	±	7.740	0.557	±	0.021
BA02	75.967	±	3.133	93.166	±	3.842	172.168	±	6.803	0.465	±	0.018
BA03	92.785	±	3.006	113.791	±	3.686	209.766	±	6.532	0.567	±	0.018
BA04	140.530	±	3.004	172.351	±	3.684	317.718	±	6.528	0.858	±	0.018
BA05	92.272	±	3.054	113.162	±	3.745	208.592	±	6.623	0.563	±	0.018
BA06	88.817	±	3.119	108.926	±	3.825	201.207	±	6.778	0.543	±	0.018
BA07	92.116	±	2.533	112.971	±	3.107	208.586	±	5.514	0.563	±	0.015
BA08	131.960	±	3.243	161.838	±	3.978	299.534	±	7.057	0.809	±	0.019
BA09	96.754	±	2.048	118.659	±	2.512	218.792	±	4.455	0.591	±	0.012
BA10	81.032	±	4.012	99.378	±	4.920	184.166	±	8.715	0.497	±	0.024
BA11	93.886	±	5.923	115.142	±	7.265	212.368	±	12.888	0.574	±	0.035
BA12	72.748	±	2.914	89.218	±	3.573	165.026	±	6.298	0.446	±	0.017

Appendix 33: Radiological parameters for fly ash samples

Sample No.	D (nGy/h)			AEDE (µSv/y)			Ra_{eq} (Bq/kg)			H_{ext}		
FA01	111.610	±	3.557	136.883	±	4.363	252.689	±	7.707	0.683	±	0.021
FA02	215.940	±	4.210	264.833	±	5.163	490.247	±	9.136	1.324	±	0.025
FA03	102.540	±	4.025	125.751	±	4.937	231.062	±	8.744	0.624	±	0.024
FA04	105.710	±	5.529	129.638	±	6.781	238.298	±	12.000	0.644	±	0.032
FA05	105.110	±	5.108	128.906	±	6.264	237.297	±	11.080	0.641	±	0.030
FA06	115.270	±	5.105	141.369	±	6.261	260.205	±	11.093	0.703	±	0.030
FA07	210.100	±	4.952	257.663	±	6.074	473.945	±	10.736	1.280	±	0.029
FA08	126.280	±	5.425	154.876	±	6.653	284.212	±	11.695	0.768	±	0.032
FA09	132.580	±	3.820	162.601	±	4.685	299.298	±	8.296	0.808	±	0.022
FA10	188.550	±	2.273	231.236	±	2.788	426.554	±	4.922	1.152	±	0.013
FA11	199.560	±	2.273	244.743	±	2.788	450.099	±	4.922	1.216	±	0.013
FA12	99.909	±	2.273	122.529	±	2.788	225.319	±	4.922	0.609	±	0.013